C 1

NATIONAL ADVISORY COMMITTEE FOR AERONAUTICS

TECHNICAL NOTE 3783

HANDBOOK OF STRUCTURAL STABILITY

PART III - BUCKLING OF CURVED PLATES AND SHELLS

By George Gerard and Herbert Becker

New York University

Washington
August 1957

TABLE OF CONTENTS

NATIONAL ADVISORY COMMITTEE FOR AERONAUTICS

TECHNICAL NOTE 3783

HANDBOOK OF STRUCTURAL STABILITY

PART III - BUCKLING OF CURVED PLATES AND SHELLS

By George Gerard and Herbert Becker

SUMMARY

Available theories and test data on buckling of curved plates and shells are reviewed. For torsion and external-pressure loadings, the test data are correlated in terms of linear buckling theories for both the elastic and inelastic ranges.

The cases which exhibit a marked disagreement between linear theory and test data include those of curved plates and cylinders under axial compression, cylinders under bending, and spherical plates under external pressure. These cases have been analyzed by a unified semiempirical approach for both the elastic and inelastic ranges which is satisfactory for analysis and design purposes.

The effects of internal pressure on buckling of elements under uniaxial loads are discussed and data on various combined loadings are presented in interaction form.

INTRODUCTION

In Part I ("Buckling of Flat Plates," ref. 1) and Part II ("Buckling of Composite Elements," ref. 2) of this Handbook the available theories and experimental data are in relatively good agreement. However, in the buckling of curved plates and shells, which is treated in the present report, there is considerable disagreement between theory and experiment in many cases. As a consequence, considerable reliance must be placed on semiempirical methods using theory as a guide. In order to minimize the use of differing semiempirical approaches which have appeared in the literature, a unified presentation of experimental and theoretical results on buckling of curved plates and shells is attempted.

The fundamentals of the buckling behavior of curved elements are described in the section "Physical Behavior of Curved Elements" and the linear and nonlinear theories relating to stability of curved elements follow in "Stability Theory of Curved Elements." The principles presented

in these introductory sections are referred to throughout the report. The unification attempted in the various sections utilizes the principles and theory of the above-named two sections as a guide in establishing semiempirical methods where theory is deficient.

Large discrepancies between linear theory and test data have long been known to exist for the buckling of axially compressed cylinders. In the section "Circular Cylinders Under Axial Compression," three basic concepts are used in an effort to resolve the discrepancies from a structural analysis and design standpoint. In the first, the relation between buckling stress and cylinder-wall curvature is shown to give correlation with the data when a semiempirical construction is utilized based on the limiting data for short and for long cylinders. The transition between these cases is guided by the results of linear theory. The second concept relates to the end effects on short cylinders which result in significant increases in the buckling-stress coefficient in the transition region.

The third concept, which applies to long cylinders, is based upon the use of the classical equation for axial-compressive-buckling stress of a circular cylinder utilizing a coefficient C which is a function of r/t. Test data lie in a range of large values of r/t, for the most part, whereas theory defines the relation between C and r/t for relatively small values of r/t. In this report the two are shown to coalesce, thereby providing a continuous dependence of C upon r/t. This permits correlation of inelastic-buckling data with theory for the pertinent plasticity-reduction factor and depicts the effect of initial imperfections upon buckling behavior.

These concepts also are used for correlation of buckling of curved plates in uniaxial compression and spherical plates under external pressure. In addition, the data on cylinders in bending are shown to permit unification with the semiempirical theory resulting from these concepts.

The behavior of circular and elliptic cylinders in bending is presented in the section "Cylinders in Bending," in which the concept of a gradient effect upon buckling stress is introduced. This is applied to the inelastic range as well as to the elastic range. In addition, the familiar modulus of rupture is resolved into its component elements, and instability in the inelastic range is explored in some detail.

The behavior of cylinders buckling in torsion is described in the section "Cylinders Under Torsion," in which test data on circular and elliptic cylinders and on D-tubes of semicircular and semielliptic cross section are shown to correlate reasonably well with linear theory. The effect of internal pressure is discussed.

Behavior of circular cylinders under external pressure is discussed in the section with that name. Buckling of circular cylinders under combined loadings is described in the following section, in which interaction curves and equations are presented for various load combinations.

The behavior of axially loaded plates curved in one direction is discussed in the section "Curved Plates Under Axial Compression." The approach used for axially compressed cylinders was applied here in an effort to correlate the data with empirical theory utilizing the various geometric parameters of the plates. The results of this approach are not so well defined as those for axially compressed cylinders although the trends are comparable. Data on the effects of plasticity are compared with inelastic-buckling theory for axially compressed cylinders. Also, the effect of internal pressure on axial compressive buckling is described.

The buckling of spherical plates under normal pressure is discussed in the section "Spherical Plates Under Normal Pressure." It is shown that the unified approach used for axially compressed circular cylinders and singly curved plates appears to form a realistic basis for analyzing the spherical-plate test data. An analysis of initial imperfections is presented based upon the measured geometric imperfections in the spherical plates from which buckling test data were obtained. The relation of C as a function of r/t was constructed from this information and is shown to give reasonable correlation with the test results.

The sections "Curved Plates Under Shear" and "Curved Plates Under Combined Shear and Longitudinal Compression" pertain to the buckling behavior of singly curved plates in shear and in combined shear and axial compression, respectively. The effects of internal pressure and plasticity are discussed. The appendix summarizes the results of importance in analysis and design in a convenient form.

This survey was conducted at New York University under the sponsorship and with the financial assistance of the National Advisory Committee for Aeronautics.

SYMBOLS

A_n	plasticity coefficients
a	semimajor axis of ellipse, in.
a_o	initial imperfection, fraction of sheet thickness

B	axial rigidity, $Et/\left(1 - \nu^2\right)$
b	semiminor axis of ellipse, in.; also, width of curved plate, in.
c	chord of circular-arc section, in.
C	compressive-buckling coefficient for long cylinders
C_b	bending-buckling coefficient for long cylinders
D	bending rigidity, $Et^3/\left[12\left(1 - \nu^2\right)\right]$, in-lb
d	diameter of spherical plate (chord width), in.
E	elastic (Young's) modulus, psi
E_s	secant modulus, psi
E_t	tangent modulus, psi
F	stress function for cylinders
g	exponent in expression for a_o
H	depth of circular-arc section, in.
K	constant in expression for a_o
k_b	buckling coefficient for cylinders in bending
k_c	buckling coefficient for axially loaded cylinders and singly curved plates
k_p	buckling coefficient for hydrostatic pressure
k_{pl}	buckling coefficient for flat plate, in general
k_s	buckling coefficient for singly curved plate in shear
k_t	buckling coefficient for cylinder or D-tube in torsion

k_y	buckling coefficient for radial pressure on cylinder
L	length of cylinder or curved plate, in.
L_1, L_2	wave length of buckle axially and circumferentially as used in expression for a_o, in.
M	bending moment, in-lb
m	wave number in axial direction of cylinders and singly curved plates
N_x, N_y, N_{xy}	axial, circumferential, and shear loads applied to cylinder
n	wave number in circumferential direction of cylinders and singly curved plates
p	pressure, psi
R_b	stress ratio for bending on cylinder
R_c	stress ratio for axial compression on cylinders and singly curved plates
R_p	pressure ratio for cylinders and singly curved plates
R_s	stress ratio for shear on singly curved plates
R_t	stress ratio for torsion on cylinders
R_x	stress ratio for axial loading, either tension or compression, on singly curved plate
r	radius, in.
$\bar{r}$	critical radius of curvature on section of elliptic cylinder in bending
S	sensitivity factor in expression for a_o
S_a	section modulus of circumscribed circle, $\pi a^2 t$
S_c	section modulus of circular cylinder, cu in.

S_e section modulus of elliptic cylinder, cu in.

t sheet, plate, or cylinder-wall thickness, in.

U, U_o unevenness factors in expressions for a_o

u, v, w displacements in x-, y-, and z-directions, in.

X dimensional factor in expression for a_o, in.

x, y, z coordinates for circular cylinders and singly curved plates, axial, tangential, and radial directions, respectively

y/a elliptic cylinder parameter (eq. (36))

Z general length-range parameter for cylinders, singly curved plates, and spherical plates

$$Z_L = L^2\left(1 - \nu_e^2\right)^{1/2}/rt$$

$$Z_b = b^2\left(1 - \nu_e^2\right)^{1/2}/rt$$

$$Z_d = d^2\left(1 - \nu_e^2\right)^{1/2}/rt$$

$$\alpha = \left(3/\sigma_i^2\right)\left[1 - \left(E_t/E_s\right)\right]$$

$$\beta = L/\lambda$$

γ gradient factor

γ_ϵ strain gradient factor

γ_σ stress gradient factor

ϵ strain, in./in.

η plasticity-reduction factor

λ buckle wave length, in.

μ	magnification factor, k_{exp}/k_{emp}
ν	Poisson's ratio, $\nu_p - (\nu_p - \nu_e)(E_s/E)$
ν_e	elastic Poisson's ratio, 0.3 in this report
ν_p	plastic Poisson's ratio, generally 0.5
ρ	shape factor for inelastic-bending-stress distribution
σ	normal stress, psi
σ_b	actual plastic stress at extreme fiber of cylinder in bending
σ_{cl}	classical buckling stress of sphere under external pressure
$\sigma_i = \left(\sigma_x^2 + \sigma_y^2 - \sigma_x\sigma_y + 3\tau^2\right)^{1/2}$	
σ_r	bending modulus of rupture, M/s_c
τ	shear stress, psi
θ	cylindrical coordinate
χ	curvature

Subscripts:

cr	critical (buckling stress)
emp	empirical
exp	experimental
e	edge; also, elliptic cylinder
o	initial
b	bending
c	compression; also, circular cylinder
x,y	in axial and tangential directions, respectively

PHYSICAL BEHAVIOR OF CURVED ELEMENTS

Correlation of Test Data and Linear Theory

In Part 1 of this Handbook (ref. 1) the buckling of flat plates was reviewed. The close correlation of experimental data on the elastic and plastic buckling of flat plates under various types of loadings and boundary conditions confirms the use of classical linear stability concepts in such problems. Furthermore, it suggests that small initial imperfections unavoidably present in practical structural elements are unimportant from an engineering standpoint.

In investigating the elastic buckling of thin-wall circular cylinders, curved plates, and thin-wall spheres, classical stability theory has been used also. In general, however, the close correlation between theory and test data observed for flat plates is not obtained for curved elements. The amount of agreement varies and depends upon the type of loading and the geometric parameters of the curved element.

The most complete test data are available for cylinders. These data were reviewed by Batdorf (ref. 3) and were compared with a simplified linear buckling analysis based on the use of Donnell's equations. This set of equations as well as others are discussed in the section entitled "Stability Theory of Curved Elements." For the purposes here, it will suffice to compare the results of the simplified analysis with available test data.

Representative elastic-buckling data for cylinders under axial compression, torsion, and lateral pressure are shown in figure 1. It can be observed that for compressive loading the best test data at failure are approximately one-half of the theoretical buckling values with some data as low as 10 percent of theory.

Furthermore, the scatter in the data is large, even on the logarithmic plots on which the results are shown because of the large numerical range of the parameters. Other test data on elastic buckling of curved plates under axial compression, spheres under hydrostatic pressure, and cylinders under bending all behave in the characteristic manner of axially compressed cylinders.

For torsion loads the test data on failure of the cylinders are in considerably better agreement with buckling theory than are those for compression. Here too, however, the test data are consistently below the theoretical values. In the case of buckling under lateral pressure, the relatively small amount of test data is in good agreement with theory.

The particularly poor agreement between linear theory and tests for axially compressed curved elements has motivated considerable theoretical

investigation to determine the cause of such behavior. Some investigators have maintained that such elements are particularly sensitive to initial imperfections which lead to premature failure. Others have abandoned classical buckling concepts. By use of large-deflection theory in conjunction with deflection functions corresponding to the experimentally observed diamond pattern, it was found that neighboring large-deflection equilibrium configurations exist at loads less than those of the linear theory. It has been suggested that the small amount of energy required to trigger the jump to the neighboring equilibrium configurations can be supplied by small vibrations in the testing machine. Thus, the compressed cylinder cannot reach the classical load and fails at a fraction of this value.

These approaches are discussed at some length in the sections "Stability Theory of Curved Elements" and "Circular Cylinders Under Axial Compression." At this point, however, it seems important to inquire for the reasons for the apparent failure of linear theory for compressive buckling of curved elements. In this case, large-deflection theory must be introduced, whereas for torsional buckling linear theory provides reasonable agreement with test data and for cylinders under lateral pressure good agreement is obtained.

Postbuckling Behavior

Some explanation on physical grounds is required to indicate when large-deflection effects may assume importance in particular buckling problems. For such an explanation, it is logical to consider the postbuckling behavior of various elements, since this is the region of large deflections.

A schematic representation of the postbuckling behavior of axially compressed columns, flat plates, and cylinders is shown in figure 2 for both theoretically perfect elements and those containing initial imperfections. It is assumed that all elements behave elastically.

For the perfect column, the postbuckling behavior is essentially horizontal in the range of Wave depth/Shell thickness values considered here (elastic effects are negligible) and buckling can follow either the right branch (0, 1, A+) or the left (0, 1, A-). The horizontal behavior can be attributed to the fact that, after buckling, no significant transverse-tension membrane stresses are developed to restrain the lateral motion and, therefore, the column is free to deflect laterally under the critical load.

The flat plate, however, does develop significant transverse-tension membrane stresses after buckling because of the restraint provided by the boundary conditions at the unloaded edges. These membrane stresses act

to restrain lateral motion and thus the flat plate is capable of carrying loads beyond buckling as indicated by the approximately parabolic character of the stress-deflection plot of figure 2. The flat plate also can follow either the right branch (0, 1, B+) or the left (0, 1 B-).

For the axially compressed curved plate, the effect of the curvature is to translate the flat-plate postbuckling parabola downward and toward the right, depending upon a width-radius parameter. For the complete long cylinder a considerable translation occurs. Note that by shifting the parabola to the right buckling would tend to follow the right branch only (0, 1, C) because of the lower loads involved, with the result that the inward type of buckling is observed for curved plates and cylinders. This inward buckling causes superimposed transverse membrane stresses of a compressive nature so that the buckle form itself is unstable.

As a consequence of the compressive membrane stresses, buckling of an axially compressed cylinder is coincident with failure and occurs suddenly (snap buckling, "oilcanning") accompanied by a considerable drop in load. This is in contrast with the behavior of a flat plate which, because of superimposed tension membrane stresses after elastic buckling, can support loads in excess of the buckling load.

From figure 2 it can be observed that the behavior of elements with small initial imperfections tends to follow closely that of the theoretically perfect elements except in the region where σ/σ_{cr} approaches 1.0. For columns and flat plates the data for the initially imperfect element asymptotically approach the theoretically perfect postbuckling curves for Wall depth/Shell thickness values at which failure occurs. Thus, small initial imperfections are relatively unimportant in these cases. For the cylinder, however, the divergence is greatest in the region where buckling and maximum load occur simultaneously. Consequently, initial imperfections can be expected to be of relatively great importance in this case as reflected by the low test data and its large scatter shown in figure 1.

From this discussion, it can be concluded that the nature of the transverse membrane stresses superimposed after buckling provides an important clue to the discovery of cases in which large-deflection effects are likely to be important in buckling problems.

By returning now to the data shown in figure 1, it is possible to understand the degree of correlation between test data and linear stability theory. As discussed above, poor agreement would be anticipated for the axially compressed cylinder since transverse compressive stresses are superimposed when buckling occurs. For the cylinder under torsion, the membrane stresses superimposed after buckling, transverse to the axes of the buckles, are tensile. Therefore, large-deflection effects would be relatively unimportant and good agreement between linear theory and test data would be expected.

When a cylinder buckles under lateral pressure, transverse tensile membrane stresses are superimposed along the generators of the cylinder and are resisted by the boundary restraints at the ends. In the case of very long cylinders, this effect would be negligible and the load-deflection characteristics would approach those of a column. Actually, under lateral pressure, the buckling of an infinitely long cylinder is equivalent to that of a ring. For shorter cylinders, the superimposed membrane stresses become progressively more important, approaching those of a flat plate as the length-radius ratio approaches zero.

The superimposed-transverse-membrane-stress states when buckling occurs for the cases considered above, as well as for several other cases, are summarized in table 1. From table 1 it can be observed that in all cases in which significant transverse compressive membrane stresses are superimposed when buckling occurs, there is unsatisfactory correlation of test data with linear stability theory. For such cases only large-deflection theory must be used. In all other cases, linear stability theory should be satisfactory.

STABILITY THEORY OF CURVED ELEMENTS

From the discussion presented in the section "Physical Behavior of Curved Elements" it is apparent that classical stability theory (linear, infinitesimal deflections) yields satisfactory correlation with test data when tensile (≥ 0) transverse membrane stresses are superimposed after buckling. In cases in which significant transverse compressive (< 0) membrane stresses develop, the buckle form itself tends to be unstable and nonlinear theory (finite deflections) has been used in the attempt to resolve the discrepancies between test data and classical buckling theory.

It is the purpose in this section to review the mathematical techniques available for the solution of linear and nonlinear problems associated with buckling of curved elements containing no initial imperfections. The theoretical buckling load is of importance because it closely coincides with the failure of cylinders, of wide plates of sharp curvature, and of spheres. For plates of small curvature, buckling marks the region in which continued application of load results in an accelerated growth of lateral deflections which ultimately leads to failure.

In small-deflection (linear) stability theory, the deflections are assumed to be infinitesimal. Thus, the strains are linear functions of the displacements and therefore the stresses are also linear in displacements. As a result, linear equilibrium differential equations in terms of displacements are obtained. In Timoshenko's book on stability theory (ref. 4), the solutions for a large number of curved-element elastic-buckling problems are presented. These solutions are based on a set of

three equilibrium equations which vary only in minor terms from those suggested by Flügge (ref. 5). The complex geometry involved in distortions of curved elements is responsible for widespread disagreement among investigators as to the proper minor terms to be included in the strain-displacement relationships and hence in the equilibrium equations.

By omitting terms which are of small magnitude when the circular cross section of a thin-wall cylindrical element is distorted, Donnell reduced the set of three equilibrium equations to a single eighth-order partial differential equation in the radial displacement w (ref. 6). For plastic buckling of cylindrical elements, Gerard utilized the simplified strain-displacement and equilibrium equations of Donnell and obtained a set of three equilibrium equations in the displacements (ref. 7). These equations reduce to Donnell's single eighth-order equilibrium equation in the elastic case.

In large-deflection (nonlinear) theory, the deflections are assumed to be finite though small. They are large, however, as compared with those of small-deflection theory. The strain-displacement relations now include nonlinear terms and therefore the equilibrium equations in terms of displacements are nonlinear. Donnell, in his approximate analysis of the effects of initial imperfections on the buckling behavior of compressed cylinders, derived a large-deflection equilibrium equation (ref. 8) which is an extension of that derived by Von Kármán for large deflections of flat plates (ref. 9). By use of a corresponding energy formulation, Von Kármán and Tsien investigated the postbuckling behavior of compressed circular cylinders (ref. 10). They discovered that neighboring large-deflection equilibrium configurations existed at loads considerably below those of classical stability theory. They formulated an energy criterion of buckling based on this behavior which yields buckling loads in reasonable agreement with test data.

Linear Stability Theory for Cylindrical Elements

Donnell's simplified equations for thin-wall circular cylinders (ref. 6) have been used with a considerable degree of success in buckling problems. The linear stability theory is based on the following relations between the displacement derivatives and the middle-surface strain variations and curvature changes that occur during buckling of circular cylindrical elements:

$$\left.\begin{aligned}
\epsilon_1 &= \partial u/\partial x \\
\epsilon_2 &= (\partial v/r\,\partial\theta) + (w/r) \\
\epsilon_3 &= \frac{1}{2}\left(\frac{\partial u}{r\,\partial\theta} + \frac{\partial v}{\partial x}\right) \\
\chi_1 &= \partial^2 w/\partial x^2 \\
\chi_2 &= \partial^2 w/r^2\partial\theta^2 \\
\chi_3 &= \partial^2 w/r\,\partial x\,\partial\theta
\end{aligned}\right\} \tag{1}$$

By use of appropriate stress-strain relations, equations relating the incremental forces and moments with the displacement derivatives can be derived. Upon substituting the latter into the simplified equilibrium equations, a set of three equations in terms of the displacements and their derivatives is obtained.

Using deformation plasticity theory, Gerard derived a set of equilibrium equations applicable to plastic buckling of thin-wall circular cylinders (ref. 7). In the interest of generality, these equations are presented in equations (2) to (4) and are then reduced to Donnell's eighth-order equation for elastic buckling.

$$A_1\frac{\partial^2 u}{\partial x^2} - \frac{A_{13}}{2}\frac{\partial^2 u}{r\,\partial x\,\partial\theta} + \frac{A_3}{4}\frac{\partial^2 u}{r^2\partial\theta^2} - \frac{A_{13}}{4}\frac{\partial^2 v}{\partial x^2} + \left(\frac{A_{12}}{2} + \frac{A_3}{4}\right)\frac{\partial^2 v}{r\,\partial x\,\partial\theta} -$$

$$\frac{A_{23}}{4}\frac{\partial^2 v}{r^2\partial\theta^2} + \frac{A_{12}}{2}\frac{\partial w}{r\,\partial x} - \frac{A_{23}}{4}\frac{\partial w}{r^2\partial\theta} = 0 \tag{2}$$

$$A_2 \frac{\partial^2 v}{r^2 \partial\theta^2} - \frac{A_{23}}{2} \frac{\partial^2 v}{r\, \partial x\, \partial\theta} + \frac{A_3}{4} \frac{\partial^2 v}{\partial x^2} - \frac{A_{13}}{4} \frac{\partial^2 u}{\partial x^2} + \left(\frac{A_{12}}{2} + \frac{A_3}{4}\right) \frac{\partial^2 u}{r\, \partial x\, \partial\theta} -$$

$$\frac{A_{23}}{4} \frac{\partial^2 u}{r^2 \partial\theta^2} + A_2 \frac{\partial w}{r^2 \partial\theta} - \frac{A_{23}}{4} \frac{\partial w}{r\, \partial x} = 0 \tag{3}$$

$$D\left[A_1 \frac{\partial^4 w}{\partial x^4} - A_{13} \frac{\partial^4 w}{r\, \partial x^3 \partial\theta} + \left(A_{12} + A_3\right) \frac{\partial^4 w}{r^2 \partial x^2 \partial\theta^2} - A_{23} \frac{\partial^4 w}{r^3 \partial x\, \partial\theta^3} + A_2 \frac{\partial^4 w}{r^4 \partial\theta^4}\right] +$$

$$\frac{B}{r}\left(\frac{A_{12}}{2} \frac{\partial u}{\partial x} - \frac{A_{23}}{4} \frac{\partial u}{r\, \partial\theta} - \frac{A_{23}}{4} \frac{\partial v}{\partial x} + A_2 \frac{\partial v}{r\, \partial\theta} + A_2 \frac{w}{r}\right) + N_x \frac{\partial^2 w}{\partial x^2} + 2N_{xy} \frac{\partial^2 w}{r\, \partial x\, \partial\theta} +$$

$$N_y \frac{\partial^2 w}{r^2 \partial\theta^2} + p = 0 \tag{4}$$

The plasticity coefficients are defined as follows:

$$A_1 = 1 - \left(\alpha \sigma_x{}^2 / 4\right)$$

$$A_2 = 1 - \left(\alpha \sigma_y{}^2 / 4\right)$$

$$A_3 = 1 - \alpha\tau^2$$

$$A_{21} = A_{12} = 1 - \left(\alpha \sigma_x \sigma_y / 2\right)$$

$$A_{31} = A_{13} = \alpha \sigma_x \tau$$

$$A_{32} = A_{23} = \alpha \sigma_y \tau$$

where:

$$\alpha = \left(3/\sigma_i^2\right)\left[1 - \left(E_t/E_s\right)\right]$$

$$\sigma_i = \left(\sigma_x^2 + \sigma_y^2 - \sigma_x\sigma_y + 3\tau^2\right)^{1/2}$$

The axial rigidity is:

$$B = 4E_s t/3 \tag{5}$$

The bending rigidity is:

$$D = E_s t^3/9 \tag{6}$$

In the elastic region, $\alpha = 0$ and, therefore, $A_1 = A_2 = A_3 = A_{12} = 1$ and $A_{13} = A_{23} = 0$. By replacing the definitions of equations (5) and (6), which are for a fully plastic plate, with $B = Et/\left(1 - \nu_e^2\right)$ and $D = Et^3/12\left(1 - \nu_e^2\right)$, respectively, and replacing the coefficient 1/2 by ν_e, equations (2) to (4) reduce to the following elastic relations:

$$\frac{\partial^2 u}{\partial x^2} + \frac{1 - \nu_e}{2}\frac{\partial^2 u}{r^2\partial\theta^2} + \frac{1 + \nu_e}{2}\frac{\partial^2 v}{r\,\partial x\,\partial\theta} + \frac{\nu_e}{r}\frac{\partial w}{\partial x} = 0 \tag{7}$$

$$\frac{\partial^2 v}{r^2\partial\theta^2} + \frac{1 - \nu_e}{2}\frac{\partial^2 v}{\partial x^2} + \frac{1 + \nu_e}{2}\frac{\partial^2 u}{r\,\partial x\,\partial\theta} + \frac{\partial w}{r^2\partial\theta} = 0 \tag{8}$$

$$D\nabla^4 w + \frac{B}{r}\left(\nu_e\frac{\partial u}{\partial x} + \frac{\partial v}{r\,\partial\theta} + \frac{w}{r}\right) + N_x\frac{\partial^2 w}{\partial x^2} + 2N_{xy}\frac{\partial^2 w}{r\,\partial x\,\partial\theta} + N_y\frac{\partial^2 w}{r^2\partial\theta^2} + p = 0 \tag{9}$$

By suitable manipulation of equations (7) to (9), Donnell was able to obtain the following single equation in terms of the radial displacement (ref. 6):

$$D\nabla^8 w + \frac{Et}{r^2}\frac{\partial^4 w}{\partial w^4} + \nabla^4\left(N_x \frac{\partial^2 w}{\partial x^2} + 2N_{xy}\frac{\partial^2 w}{r\,\partial x\,\partial\theta} + N_y \frac{\partial^2 w}{r^2\partial\theta^2} + p\right) = 0 \qquad (10)$$

The relationships among the other displacements are

$$\nabla^4 u = -\nu\frac{\partial^3 w}{r\,\partial x^3} + \frac{\partial^3 w}{r^3\partial x\,\partial\theta^2} \qquad (11)$$

$$\nabla^4 v = -(2+\nu)\frac{\partial^3 w}{r^2\partial x^2\partial\theta} - \frac{\partial^3 w}{r^4\partial\theta^3} \qquad (12)$$

It is to be noted that by letting $1/r = 0$ and replacing $r\,\partial\theta$ by ∂y, equations (4), (9), and (10) reduce to the governing equations for flat plates.

Boundary Conditions

The usual boundary conditions for flat plates discussed in Part 1 (ref. 1) apply directly to curved plates. However, a complete cylinder has only two boundaries (at the ends) instead of the four of a rectangular plate. Thus, for the cylinder, two of the four sets of boundary conditions are replaced by the condition that the displacements are cyclic functions of the angle θ with a cycle length of $2\pi r$.

For cylinders which can be classified as long, the boundary conditions at the ends have a negligible influence on the buckling stress. At the other limit, short cylinders approach flat plates in their behavior and, consequently, boundary conditions are of considerable importance in such cases.

Appropriate boundary conditions on the displacements, u, v, and w can be handled in a straightforward manner in cases in which equations (2) to (4) or (7) to (9) are used. However, boundary conditions on the displacements u and v cannot be handled directly when equation (10) is used since this equation is in terms of the displacement w only. This

situation is not serious, however, since certain conditions on u and v are implied which correspond to those often occurring in practical construction.

Donnell's eighth-order differential equation, equation (10), requires eight boundary conditions for a unique solution. The usual boundary conditions of simple support or clamping impose a total of only four boundary conditions (two at each end) on the displacement w. However, by use of equations (11) and (12), four additional boundary conditions on the displacements u and v are implied.

Batdorf has discussed this problem at some length (ref. 3) and has concluded that the substitution of a double-sine-series expansion for w into Donnell's equation corresponds to the following boundary conditions:

(a) Each edge of the cylinder or cylindrical plate is simply supported $\left(w_e = 0, \left(\partial^2 w/\partial y^2\right)_e = 0\right)$.

(b) Motion parallel to each edge during buckling is prevented entirely $(v_e = 0)$.

(c) Motion normal to each curved edge in the plane of the sheet occurs freely $(u_e \neq 0)$.

Such boundary conditions on u and v are appropriate to cylinders or cylindrical plates bounded by supporting members such as deep stiffeners or ribs. Such members are generally stiff in their own planes but may be readily warped out of their planes.

By comparing solutions using Donnell's equation with more exact solutions for which warping is not permitted $(u = 0)$, the effects of the implied boundary conditions can be evaluated. Batdorf has shown that generally the effect on the buckling stress of preventing free warping normal to the curved edges of a cylinder or cylindrical plate is negligible (ref. 11).

Solutions Based on Donnell's Equation

Although solutions based on sets of three equilibrium equations such as equations (7) to (9) were known, Batdorf demonstrated the simplicity of using Donnell's equation by rederiving several solutions for simply supported cylinders in a unified manner (ref. 3). The method of solution used in several of these problems is demonstrated below.

For more complicated boundary conditions, such as clamped edges, a slight modification of Donnell's equation permits solution by use of the Galerkin method. This procedure has been used by Batdorf and his collaborators to solve the compressive buckling of cylinders and curved plates with clamped circumferential edges and to analyze curved plates under shear and combined loading.

Case 1. Axially compressed cylinders and curved plates.- For a cylinder, a solution of equation (10) which satisfies the boundary conditions of simple support is

$$w = w_o \sin \frac{\pi y}{\lambda} \sin \frac{m\pi x}{L} \tag{13}$$

where $\lambda = \pi r/n$ and is the half-wave length of the buckles in the circumferential direction. Upon substituting equation (13) into equation (10) and letting $N_y = N_{xy} = 0$ for this case, the compressive-buckling coefficient is

$$k_c = \frac{\left(m^2 + \beta^2\right)^2}{m^2} + \frac{12Z_L{}^2m^2}{\pi^4\left(m^2 + \beta^2\right)^2} \tag{14}$$

where

$$\beta = L/\lambda$$

$$Z_L = \left(L^2/rt\right)\left[\left(1 - \nu_e{}^2\right)^{1/2}\right]$$

The compressive-buckling stress is

$$\sigma_{cr_c} = \frac{k_c\pi^2E}{12\left(1 - \nu_e{}^2\right)}\left(\frac{t}{L}\right)^2 \tag{15}$$

The critical value of k_c can be found by suitable minimizations of equation (14). For long cylinders

$$k_c = \frac{4(3)^{1/2}}{\pi^2} Z_L = 0.702 Z_L \tag{16}$$

For short cylinders ($Z_L < 2.85$), the critical value of k_c is determined by substituting the limiting values of $\beta = 0$ and $m = 1$ into equation (14). Such results are shown as the theoretical line in figure 1(a).

By substituting equation (16) into equation (15), the classical buckling stress for a long axially compressed cylinder is obtained:

$$\sigma_{cr_c} = 3\left(1 - \nu_e^2\right)^{-1/2} Et/r = 0.6E(t/r) \tag{17}$$

These results can be applied to the compressive buckling of a long simply supported cylindrical plate by a change in certain of the variables. For a long plate the unloaded-edge boundary conditions are of importance and consequently the compressive-buckling coefficient becomes

$$k_c = \frac{\left(n^2 + \beta^2\right)^2}{\beta^2} + \frac{12 Z_b^2 \beta^2}{\pi^4 \left(n^2 + \beta^2\right)^2} \tag{18}$$

where n replaces β in equation (14), $\beta = b/\lambda$ and replaces m, and

$$Z_b = \left(b^2/rt\right)\left(1 - \nu_e^2\right)^{1/2}$$

$$\sigma_{cr_c} = \frac{k_c \pi^2 E}{12\left(1 - \nu_e^2\right)}\left(\frac{t}{b}\right)^2$$

Upon minimizing equation (18), the solution given by equations (16) and (17) is obtained for wide, long, cylindrical plates. For narrow, long, curved plates, the critical value of k_c is obtained by substituting $n = 1$ into equation (18) and minimizing with respect to β.

For the limiting value of $Z_b = 0$, equation (14) reduces to the value corresponding to an infinitely wide plate column and equation (18) reduces to a long flat plate. For values of Z_b at which the element can be considered long, the buckling of the cylindrical plate and cylinder are identical according to linear theory.

Case 2. Cylinders under lateral and hydrostatic pressure.- For hydrostatic loading, $2N_x = N_y$ and $N_{xy} = 0$ in equation (10). Upon substituting equation (13) into equation (10), the following value for the buckling coefficient can be determined:

$$k_p = \frac{\left(m^2 + \beta^2\right)^2}{\frac{m^2}{2} + \beta^2} + \frac{12Z_L^2}{\pi^4} \frac{m^4}{\left(m^2 + \beta^2\right)^2\left(\frac{m^2}{2} + \beta^2\right)} \tag{19}$$

The terms β and Z_L are defined according to equation (14) and

$$\sigma_{cr_p} = \frac{k_p \pi^2 E}{12\left(1 - \nu_e^2\right)}\left(\frac{t}{L}\right)^2 \tag{20}$$

A minimum value for k_p is obtained when $m = 1$ and, therefore, equation (19) reduces to

$$k_p = \frac{\left(1 + \beta^2\right)^2}{\frac{1}{2} + \beta^2} + \frac{12Z_L^2}{\pi^4\left(1 + \beta^2\right)^2\left(\frac{1}{2} + \beta^2\right)} \tag{21}$$

The fraction 1/2 in the denominators of each term of equation (21) reflects the fact that the axial stress is one-half the circumferential stress in hydrostatic loading. For the case of lateral pressure only, the axial stress is zero and, therefore, equation (21) reduces to

$$k_y = \frac{\left(1 + \beta^2\right)^2}{\beta^2} + \frac{12Z_L^2}{\pi^4\beta^2\left(1 + \beta^2\right)^2} \tag{22}$$

The critical values of k_y as a function of Z_L are shown in figure 1(c).

Nonlinear Stability Theory for Cylindrical Elements

As discussed at the beginning of this section on the stability of curved elements, nonlinear theory has been used in attempts to resolve the large discrepancies between buckling loads based on linear stability theory and test data for certain cases. These cases include cylinders and cylindrical plates under axial compression and spheres and spherical plates under external pressure.

The difference between linear and nonlinear theory appears in the strain-displacement relations. By virtue of finite deflections, for nonlinear theory additional terms involving derivatives of the radial displacement w are included in the relations given by equations (1) for linear theory:

$$\left.\begin{aligned} \epsilon_1 &= (\partial u/\partial x) + \left[(\partial w/\partial x)^2/2\right] \\ \epsilon_2 &= (\partial v/r\,\partial\theta) + (w/r) + \left[(\partial w/r\,\partial\theta)^2/2\right] \\ \epsilon_3 &= \frac{1}{2}\left(\frac{\partial u}{r\,\partial\theta} + \frac{\partial v}{\partial x}\right) + \frac{1}{2}\frac{\partial w}{\partial x}\frac{\partial w}{r\,\partial\theta} \end{aligned}\right\} \tag{23}$$

The curvature relations remain the same as in the linear case and are given by equations (1). It is to be noted that equations (23) are valid for small finite deflections only. For larger deflections, additional terms are required in the strain and curvature relations.

By use of the stress-strain relations and equilibrium equations used previously in the linear theory, the following two governing equations in terms of a stress function F result:

$$\nabla^4 F/E = \left(\partial^2 w/\partial x\,\partial y\right)^2 - \left(\partial^2 w/\partial x^2\right)\left(\partial^2 w/\partial y^2\right) - (1/r)\left(\partial^2 w/\partial x^2\right) \tag{24}$$

The equilibrium equation for $p = 0$ is

$$\begin{aligned} D\nabla^4 w = {} & t\left(\partial^2 F/\partial y^2\right)\left(\partial^2 w/\partial x^2\right) - 2t\left(\partial^2 F/\partial x\,\partial y\right)\left(\partial^2 w/\partial x\,\partial y\right) + \\ & t\left(\partial^2 F/\partial x^2\right)\left[\left(\partial^2 w/\partial y^2\right) + (1/r)\right] \end{aligned} \tag{25}$$

It is extremely difficult to obtain an exact solution of equations (24) and (25). As an approximation, a function for w is chosen which contains undetermined parameters and which corresponds approximately to the wave form observed experimentally. By use of equation (24) the middle surface stresses may be determined. Finally, by use of suitable minimum-energy considerations, the undetermined parameters may be ascertained. It is to be noted that equation (25) is not used in this method of solution.

Energy Criterion of Buckling

Von Kármán and Tsien used nonlinear stability theory to investigate the large-deflection behavior of an axially compressed circular cylinder (ref. 10). As a result, they discovered finite-deflection equilibrium configurations at loads considerably below the classical buckling load of linear theory. It was postulated that before the classical buckling load based on infinitesimal disturbances could be reached, finite disturbances in the form of random impulses, unavoidably present during the loading processes, trigger the jump to the finite-deflection equilibrium configurations. Tsien further investigated the details of how this jump occurs and formulated the "energy criterion" of buckling or the existence of the "lower buckling load" as contrasted with the "upper buckling load" of classical theory (ref. 12).

The energy criterion of buckling depends to some extent on the type of loading system employed. As one limit, a controlled-deformation type of rigid testing machine can be considered in which the jump to finite deflections occurs at a constant value of end shortening. As the other limit, a dead-weight or controlled-load type of testing machine can be considered in which the jump occurs at a constant value of load. Most likely a jump pattern would lie between these two limits, depending upon the rigidity of the actual machine and the details of the loading system.

Consider now the large-deflection behavior of an axially compressed cylinder in a controlled-deformation type of testing machine. In figure 3 the results of a large-deflection analysis are shown schematically with both average stress and strain energy plotted as a function of the controlled variable end shortening. According to classical theory, the cylinder under loading follows the path OBA and buckles at A. From the strain-energy diagram, however, once point B has been reached, less strain energy is required to follow the path BD (the finite-deflection equilibrium configuration for the buckled cylinder) than to follow the path BA (unbuckled equilibrium configuration). Thus, Tsien contended that, because of finite disturbances, the jump to the large-deflection equilibrium configuration occurs along path BC at constant end shortening (ref. 12). The buckling load according to the energy criterion is thereby reduced to approximately one-half of the classical value.

In a controlled-load type of testing machine, the loading force can move during the buckling process and, therefore, the total potential energy of the system must be considered. In figure 3(b) the end shortening and total potential energy are shown schematically as a function of average stress for this case. At point B, less energy is required to follow the path BD than to follow the path BA. Therefore, the jump occurs at constant average stress along path BC and the buckling load determined by the energy criterion is approximately one-third of the classical value.

In both figures 3(a) and 3(b) the shaded areas ABE represent the small additional energy which is presumably supplied by the finite disturbance necessary to trigger the jump. The shaded areas EFC represent the energies released by the cylinder after passing point E so that the net change in energy is zero. It can be observed that the point F corresponds to the minimum value of end shortening or average stress at which a jump can occur.

CIRCULAR CYLINDERS UNDER AXIAL COMPRESSION

Certain of the general background material relating to the behavior and theory of the buckling of circular cylinders under axial compression have been presented in the sections entitled "Physical Behavior of Curved Elements" and "Stability Theory for Cylindrical Elements." This material forms an essential adjunct to the discussion presented in the present section.

Because of the essentially nonquantitative character of the available theories on buckling of circular cylinders and curved plates under axial compression, cylinders under bending, and spheres and spherical plates under pressure, a much greater reliance must be placed on the use of test data than is usual in buckling problems. By using the various theories as a guide, an approach toward a unified treatment of test data on the aforementioned elements has been attempted.

In the present section, circular cylinders under axial compression are treated. Semiempirical relations established for these cylinders are extended to cylinders under bending in the section "Cylinders Under Bending," to axially compressed curved plates in the section "Curved Plates Under Axial Compression," and to spherical plates under pressure in the section "Spherical Plates Under External Pressure."

Historical Background

In the period before 1934 theoretical investigations into the buckling stress of an axially compressed circular cylinder were limited to the use of linear theory. Attempts were made to obtain correlation of theory with the existing test data, primarily furnished by Robertson (ref. 13) and by Lundquist (ref. 14), by employing expressions for experimental buckle wave shapes in a theory derived in general form by Southwell (ref. 15). Details of this early work can be found in reports by Lundquist (ref. 14) and Donnell (ref. 8), and in the book by Timoshenko (ref. 4). In 1947, Batdorf, Schildcrout, and Stein employed linear theory as a guide and constructed empirical curves using the data of several of the early investigators (ref. 16). By this means they were able to accentuate the dependence of the buckling coefficient for long cylinders upon r/t, which was discussed in 1934 by Donnell (ref. 8).

In reference 8, Donnell postulated that initial imperfections were responsible for observed experimental buckling stresses which were low when compared with those from linear theory and derived the large-deflection compatibility equation for shells. Since then the classical linear approach to this problem has been virtually abandoned. An investigation of the postbuckling behavior was made by Von Kármán and Tsien (ref. 10), who derived a family of curves of stress as a function of end shortening by use of the large-deflection compatibility equation derived by Donnell together with equations for the energy of the shell and an assumed deflection function representing the diamond buckle pattern. In order to determine the buckling load, an energy criterion was used to replace the classical definition. In obtaining a solution to their equations they assumed values for some of the parameters of the system of equations, instead of minimizing the work energy with respect to all the parameters. This latter approach was made by Leggett and Jones (ref. 17), who found that the family of curves derived by Von Kármán and Tsien became a single curve unique for a specific material.

Through further investigation, Tsien developed the energy criterion of buckling which, for a long circular cylinder, leads to a specific value for the buckling coefficient C equal to 0.375 in the buckling-stress equation $\sigma_{cr} = CE\frac{t}{r}$ (ref. 12). Furthermore, by this approach, Tsien showed that this value applies to a specimen loaded in a perfect controlled-deformation type of testing machine. The buckling stress will be lower for actual machines or for a controlled-loading type of testing machine. Further work has been done by Michielsen (ref. 18) and Kempner (ref. 19) on the postbuckling behavior in an end-shortening range in which plasticity effects probably are of importance.

Donnell and Wan (ref. 20) more recently refined the initial-imperfection concept developed by Donnell (ref. 8). Their results indicated that the sensitivity of axially compressed cylinders to initial

imperfections is associated with the fact that these imperfections usually are of the same size as the relatively small buckles generated at critical load. They also defined, theoretically, the relationship between C and r/t in terms of an unevenness factor U which reflects the initial imperfections in the shell.

The theoretical work, for the most part, has been confined to the elastic range, as was a large portion of the experimental data. However, Osgood (ref. 21), Moore and Holt (ref. 22), and Moore and Clark (ref. 23) performed tests on compressed cylinders at stresses beyond the proportional limit. Bijlaard (ref. 24) and Gerard (ref. 7) derived plasticity-reduction factors to be used for such a case. Bijlaard extended his inelastic-flat-plate approach to cylinders, whereas Gerard rederived the cylinder equilibrium equations using the effects of plasticity in combination with an assumed buckling-stress coefficient of 0.6. In this manner he was able to obtain good correlation with test data.

Buckling Behavior

The buckling behavior of an axially compressed circular cylinder may be classified into four ranges of behavior, as shown in figure 4. "Short" cylinders tend to behave as wide plate columns with sinusoidal buckles, whereas "long" cylinders buckle in a characteristic diamond pattern. These two types of behavior define the limits of local buckling. For cylinders with lengths between these extremes, defined here as the "transition" range, there appears to be an interaction between the plate sine-wave buckle pattern and the cylinder diamond pattern. At the short limit, the effects of the supports and rotational restraints at the ends of the cylinders are most marked.

The buckle patterns for these ranges are shown in figure 5 together with a schematic cylinder-buckling curve covering the three regions mentioned above. The fourth region pertains to "very long" cylinders in which the ratio of length to radius is so large that primary instability, or Euler buckling, occurs unaccompanied by local buckling. The action of a column, which corresponds to very long cylinders, is well known; and flat-plate buckling, which corresponds to that of short cylinders, has been examined in reference 1. The investigations described in this section are confined to the transition and long ranges of the cylinder.

In an attempt to clarify the significance of the test data, and, correspondingly, to clarify cylinder buckling behavior under axial compression, the work of Batdorf, Schildcrout, and Stein (ref. 16) has been amplified in this report. By use of available theoretical data for long cylinders, the relationship between the buckling coefficient C and the parameter r/t has been extended to low values of r/t which are well

$R/t = 1,455$ (Wrong eqn.)

within the inelastic range. Furthermore, in the transition region where length effects are important, test data on k_c as a function of Z_L have been shown to exhibit cusps associated with integer wave forms according to expectations based upon theory.

Long-Cylinder Range

In the section "Physical Behavior of Curved Elements" a criterion was suggested for determining the applicability of linear theory to shell-buckling problems. Axial compression, which generates compressive membrane stresses in the cylinder after buckling, was shown to require consideration of large-deflection behavior. Such investigations have been confined to long cylinders because the diamond-buckle-pattern deflection functions which are assumed in the energy equations do not satisfy the end boundary conditions. Furthermore, test data show that for long cylinders the buckling stress is independent of the boundary conditions. The theory is discussed in the section "Stability Theory of Curved Elements," in which both the energy-criterion and the initial-imperfection approach are described.

The empirical correlation for long cylinders performed by Batdorf, Schildcrout, and Stein, in which k_c is plotted as a function of Z_L for various values of r/t (ref. 16), clearly depicts the dependence of C upon r/t in the transition and long ranges. This is a significant step in that it demonstrates the existence of order in the data where before there seemed to be nothing but wide scatter when it was interpreted from the standpoint of available theoretical data.

Empirical data on the values of C were obtained by drawing curves through the test points plotted in the form of k_c as a function of Z_L for the specific ranges of r/t shown in figure 6. At large values of Z_L these curves were virtually straight lines at unit slope when plotted on logarithmic plotting paper. Thus they defined an expression for buckling stress in this range equivalent to the classical equation, except for the dependence of C upon r/t as shown in figure 7 instead of a constant value of $C = 0.6$.

The empirically derived curve of C as a function of r/t for long cylinders is shown in figure 7 together with the theoretical curves of Donnell and Wan (ref. 20) for several values of the unevenness factor U. The latter is related to the initial imperfections of the cylinder. It may be seen that the curve for $U = 0.00025$ merges smoothly with the empirical curve of Batdorf, Schildcrout, and Stein (ref. 16), while all theoretical curves converge at a very low r/t value to a value that approaches the classical value of 0.6 as an upper limit.

It is evident that a cylinder with a low r/t value will probably buckle inelastically. The application of figure 7 to calculation of inelastic-buckling stresses is discussed below.

Transition Range

At the short-cylinder limit, the buckling stress under axial compression depends upon L/t, since only one-half wave forms in the axial direction. For long cylinders in which boundary conditions are unimportant, the effects of initial imperfections are considered to be solely a function of r/t although this is probably a considerable oversimplification. In the transition region where the number of integer wave forms changes as suggested in figure 5, the buckling stress is written in the functional form

$$\sigma_{cr} = f(Z_L, r/t, L/t) \tag{26}$$

Since Z_L is a function of length, and since linear theory predicts changes of wave number with length, there is a basis for expecting cusps in the empirical data as the wave number changes by integral values in the transition region. Since there appears to be little possibility of establishing a completely theoretical variation, a rather simple semiempirical approach has been adopted herein.

Two basic data are selected in this development; the flat-plate-buckling coefficient at $Z_L = 0$, and the straight line drawn through the logarithmic plot of k_c as a function of Z_L at large values of this parameter. A transition curve is then fitted to these data using linear theory as a guide. Several types of transition have been suggested by the results of investigations on the buckling of axially compressed curved plates. However, the simplest transition, which matches the linear theory in the special case of $C = 0.6$, is obtained (see section entitled "Stability Theory of Curved Elements") from the expression for k_c presented by Batdorf (ref. 3):

$$k_c = k_{pl} + \left(12Z_L^2/\pi^4 k_{pl}\right) \tag{27}$$

When this relation is modified to account for the effect of r/t,

$$k_c = k_{pl} + \left[\left(0.581CZ_L\right)^2/k_{pl}\right] \tag{28}$$

This becomes the flat-plate-buckling coefficient at $Z_L = 0$ and is tangent to the curve $k_c = 1.162CZ_L$. The complete buckling-coefficient curve is shown in figure 5.

One of these complete curves has been drawn for each value of r/t for which the data of Batdorf and his collaborators (ref. 16) apply (fig. 6), utilizing the values of C obtained from figure 7. It may be seen that the data rise above the curve in the region of the transition in each case. The magnification ratio μ of the test value of k_c to the theoretical value from the curve for the corresponding values of Z_L appears as a function of Z_L in figure 8. These individual curves were also plotted together in figure 9, in which the cusps are clearly evident. The highest peak occurs at $Z_L = 35$, approximately, with a second peak at about 650. The data indicate possible additional cusps at larger values of Z_L. However, the average of the data appears to fall below the unity line. The explanation for this may be found in figure 6 in which it is seen that the lines for $k_c = 1.162CZ_L$ lie above the test points in some cases.

The reason for the presence of the peaks presumably lies in the interaction between the sine-curve-deflection shape of the short plate and the diamond buckle pattern of the intermediate-length cylinder. The transition from one to the other as the cylinder length increases is shown in figure 5, in which both r and t are assumed to be constant. When the cylinder is short, the buckle pattern is that of a wide-plate column in agreement with theory. The diamond buckle pattern is known to prevail for long cylinders, as may be seen from photographs of buckled cylinders contained in the reports of Lundquist (ref. 14) and Donnell (ref. 8). In the transition range the competition between these wave forms is the most evident basis on which to explain the presence of the peaks. The cylinder is long enough to permit diamond buckles to form and yet is short enough for the end boundary conditions to influence the details of this pattern.

Numerical Values of Buckling Stress

The elastic-buckling stress for cylinders in the short, transition, and long ranges may be determined from the equation

$$\sigma_c = \frac{k_c \pi^2 E t^2}{12\left(1 - \nu_e^2\right)L^2} \tag{29}$$

using the value of k_c obtained from figure 6 for the appropriate values of r/t.

For long cylinders the modified form of the classical buckling-stress expression,

$$\sigma_{cr} = CEt/r \tag{30}$$

may be used, in which C is obtained from figure 7.

It should be noted that the buckling coefficient for $Z_L = 0$ applies to cylinders clamped along the edges. For any other value of edge restraint a new set of design curves may be drawn using the pertinent plate-buckling coefficient and the scheme depicted in figure 5, which is perfectly general and applies to any set of edge restraints. Construction of the cusps presents some problem, since all of the test data used to construct the curves of figure 6 pertain to clamped edges only.

Plasticity-Reduction Factor

As one aspect of a unified approach to the computation of inelastic-buckling stresses in cylinders, Gerard utilized the limiting value of $C = 0.6$ (ref. 7) in conjunction with the equilibrium equations of Donnell (ref. 8) and the inelastic approach used by Stowell for flat plates (ref. 25). It was found that the plasticity-reduction factor for axial compression in the local-buckling range is

$$\eta = \left(E_t/E_s\right)^{1/2}\left(E_s/E\right)\left[\left(1 - \nu_e^2\right)\Big/\left(1 - \nu^2\right)\right]^{1/2} \tag{31}$$

Although good agreement exists between this theory and test data, improved correlation occurs when C is obtained from figure 7 instead of using 0.6. The correspondence is shown in figure 10. For 7075-T6 aluminum alloy, the lack of agreement in the yield region indicates a need for more test data before a recommendation can be made for η in this range. The theory is seen to be adequate at stresses in the plastic range.

For analysis of long cylinders, plastic-buckling curves are presented in figure 11, in which

$$\epsilon_{cr} = Ct/r \tag{32}$$

In the initial-imperfection interpretation of cylinder behavior, the classical value of $C = 0.6$ is approached as an upper limit as shown in figure 7. Furthermore, a simple geometrical construction based upon the energy criterion also suggests that the classical buckling coefficient should be approached as an upper limit at large plastic strains. In addition, it is experimentally observed that axisymmetric buckle patterns form in cylinders with small values of r/t which buckled well in the inelastic range.

In figure 12, the large-deflection unloading curve, which is always elastic, has been attached, at a large strain, to the schematic stress-strain curve for a structural alloy. If the cylinder is assumed to be loaded in a rigid controlled-deformation type of testing machine, then the vertical line on the figure defines the energy balance on the elastic unloading curve.

It is seen from figure 12 that the vertical line intersects the loading curve at a stress only slightly less than that at which the unloading curve begins. The stress loss is closely proportional to the local tangent modulus to the stress-strain curve. Consequently, for a material with a sharp knee, C should be approximately equal to the classical value at a stress near the yield. In fact, C will approach 0.6 as E_t approaches zero.

Effect of Internal Pressure

Flügge (ref. 5) investigated the effect of internal pressure on the buckling of a circular cylinder under axial compression by using linear theory and found that no increase in buckling load is to be expected as a result of the pressurization. Lo, Crate, and Schwartz (ref. 26) analyzed the problem using large-deflection theory with the energy criterion of Von Kármán and Tsien (ref. 10) and found an increase from the theoretical value of $0.37Et/r$ to the classical value of $0.6Et/r$ as the pressure increases.

Lo, Crate, and Schwartz also tested a 2024-T3 aluminum-alloy cylinder under axial loading through a range of internal pressure and found that the theoretical increase in load with pressure was substantiated, although the actual buckling stress obtained experimentally was of the order of half the classical theoretical value at no pressure. The value of C for $p = 0$ was obtained from figure 7 and is in good agreement with these test data, which are closely fitted by a straight line as shown in figure 13.

The maximum pressure applied to the cylinder produced an axial tension stress in the wall equal to roughly half the compression stress at which the cylinder buckled with no internal pressure. The buckling stress in the cylinder at this pressure was twice the unpressurized buckling stress.

CYLINDERS IN BENDING

The buckling behavior of cylinders under bending loads corresponds to that of axially compressed cylinders and curved plates in two respects. First, linear theory predicts buckling stresses of the same order of magnitude for both these cases. Second, the test data are below the predictions of linear theory by approximately the same amount. Consequently, it seems reasonable to correlate test data on cylinders in bending in a manner similar to that used for axially compressed cylinders.

The buckling of cylinders subject to bending is influenced by several considerations beyond those encountered in the buckling of axially compressed cylinders:

(1) The linear variation of bending strain across the section results in a strain gradient and hence a stress gradient at any location on the cylinder surface. A "gradient factor" is introduced which permits calculation of the bending-buckling stress from the axial-compressive-buckling stress of a corresponding circular cylinder.

(2) For elliptic cylinders buckling may not occur at the extreme compression fiber of the section but at a location depending upon the axis ratio of the ellipse. The elliptic-cylinder geometry at this location must be used in the buckling-stress expression together with the section modulus for this location to permit a comparison of applied stress to allowable stress.

These two effects apply in both the elastic and inelastic ranges. In the latter range two additional effects occur:

(3) The nonlinear distribution of bending stress across the section leads to the well-known modulus of rupture effect.

(4) The reduction of local wall stiffness due to plasticity leads to the plasticity-reduction factor.

These factors are discussed in the present section, in which the bending behavior of cylinders of circular, elliptic, and circular-arc sections is examined. Figure 14 depicts the cross-section geometry for the various shapes.

Historical Background

Brazier calculated the stress at which a circular cylinder would become unstable as a result of flattening of the cross section (ref. 27). This type of instability is comparable with Euler buckling of a very long

axially compressed cylinder. Brazier instability can be observed in some of Osgood's tests on long, thick-wall cylinders that buckled in the inelastic range (ref. 21).

The stress at which local buckling occurs in circular cylinders under bending has often been assumed to be equal to the value for axial compressive buckling of the same cylinder. Flügge, however, performed calculations based upon linear theory that showed a 30-percent increase in bending-buckling stress over the classical axial value (ref. 28). Such an increase is in general agreement with the test results obtained by Lundquist on aluminum-alloy specimens (ref. 29) and by Donnell on steel and brass specimens (ref. 8).

Lundquist and Burke extended the experimental investigation to cylinders of elliptic cross section bending about the minor axis (ref. 30). Heck performed tests in which elliptic cylinders were bent about the major axis as well as about the minor axis (ref. 31). More recently, Frahlich, Mayers, and Reissner analyzed circular-arc cross sections (ref. 32), and Anderson, Pride, and Johnson conducted tests on specimens of this shape (ref. 33).

Inelastic-buckling data were obtained for circular cylinders in bending by Osgood (ref. 21), Moore and Holt (ref. 22), and Moore and Clark (ref. 23).

Behavior of Circular Cylinders in Bending

The local-buckling behavior of circular cylinders in pure bending may be divided into several ranges similar to those pertaining to axially compressed cylinders. In the short-cylinder range the buckling coefficient k_b approaches that of a wide compressed plate as a lower limit, for which the buckling stress is expressed in the form

$$\sigma_{cr} = \frac{k_b \pi^2 E}{12(1 - \nu_e^2)} \left(\frac{t}{L}\right)^2 \tag{33}$$

and

$$Z_L = \frac{L^2}{rt}\left(1 - \nu_e^2\right)^{1/2}$$

In the long-cylinder range the relation between buckling stress and the cylinder geometry is of the form $\sigma_{cr} = CEt/r$. In figure 15 the various ranges are shown for the data of Lundquist (ref. 29) and that of Donnell (ref. 8).

The two limits of the local-buckling region are connected by a transition curve, and throughout this entire region buckling occurs in the diamond pattern observed in axially compressed cylinders. When the cylinder is very long, the flattening of the cross section caused by the radial components of the axial deformations in the bent cylinder leads to a large reduction of the effective section modulus of the cylinder, and instability occurs as a single transverse wave on the compression side of the shell. This is the type of behavior investigated by Brazier (ref. 27).

The behavior of cylinders in the upper-transition and long ranges is evident from the plot of C as a function of r/t shown in figure 16. The pertinent curves of figure 7, which appear in this figure, were obtained by utilizing the imperfection theory of Donnell (discussed in the sections entitled "Circular Cylinders Under Axial Compression" and "Spherical Plates Under External Pressure") in combination with test data obtained by several investigators on axially compressed circular cylinders.

The relation between C and r/t is shown in figure 7 for a range of U values. The upper limit of the axial-compression data corresponds to $U = 0.00015$, which is representative of Lundquist's data, whereas the lower limit for $U = 0.00035$ is representative of Donnell's data. The difference in U for the specimens of Lundquist and Donnell may be the result of the different material thicknesses used. The cylinders of Lundquist were shells on the order of 0.025 inch thick, which are typical of aircraft structures, whereas Donnell utilized shim stock on the order of 0.004 inch thick.

For comparison with the bending data of these investigators, the pertinent values of U from the axial curve were multiplied by Flügge's theoretical value of 1.3 (ref. 28) to obtain a curve with which the bending test data could be compared. This increase is attributed to the strain gradient associated with the linear cross-sectional strain distribution and is termed herein the gradient factor γ. In general, there is relatively good agreement with these curves for aluminum and for steel. However, the large scatter in the brass data would appear to render it of dubious value for comparison with the empirical unified theory being used here for comparison.

A comparison of axial-compression and bending data obtained by Lundquist on Duralumin cylinders (refs. 14 and 29) appears in figure 17. Corresponding data obtained by Donnell appear in table 2. Both Lundquist and Donnell reported an average value of 1.4 for the gradient factor on the basis of these data. Since stress and strain are linearly related in the elastic range the gradient factor pertains to both. However, there is considerable scatter in the data, as may be seen from table 2 and figure 17.

The tests of Donnell were run on matched cylinders, some of which were tested in axial compression and some, in pure bending. Because of the close dimensional agreement between corresponding cylinders of these two types of tests, γ was calculated for each cylinder as given in table 2.

The data of Lundquist, however, do not permit this cylinder-for-cylinder comparison, and consequently it was necessary to compare the buckling stresses for the two types of loading by a method such as that shown in figure 17, in which curves have been drawn through the mass of test data for both types of loading. The ratio of the σ/E intercepts at any value of r/t leads to the gradient factor γ since the slopes of the curves are virtually the same. Thus, at $r/t = 1{,}000$, $\gamma = 0.000295/0.000205 = 1.44$ from figure 17.

Numerical Value of Buckling Stress for Circular Cylinders

For long cylinders, the buckling stress may be determined from

$$\sigma_{cr} = C_b E t/r \tag{34}$$

On the basis of test data presented in figure 16, it is recommended that $C_b = 1.3C$, where C is the coefficient determined for axially compressed circular cylinders from the data in the section "Circular Cylinders Under Axial Compression." Considering the scatter in the test data, the gradient factor of 1.3 represents a conservative average value to be used with the curve of C as a function of r/t from figure 7 for an average value of $U = 0.00025$. For short and transition-range cylinders no data are available to permit recommendation of a gradient factor.

Behavior of Elliptic Cylinders in Bending

Since the curvature varies with location, the buckling behavior of a long elliptic cylinder involves the location of the point of critical curvature as well as the use of a suitable gradient factor. Tests indicate that the buckles are diamond shaped and similar to those observed on circular cylinders.

Since it has been assumed that the gradient factor is a result of the linear variation of strain across the cylinder section, then a similar increase is to be expected for long elliptic cylinders at the point where the critical curvature is located. This is substantiated by test data of Lundquist and Burke (ref. 30) and Heck (ref. 31) on aluminum-alloy elliptic cylinders which cluster in the region of the circular-cylinder data, as shown in figure 18.

In order to reduce the data to a form which would permit comparison with the axial-compression-stress data, it is first necessary to determine the point of critical curvature $(y/a)_{cr}$ which corresponds to the buckle location on the cross section. By use of the procedure described below, the critical curvature is readily obtained from figure 19. For example, for ellipses tested by Lundquist and Burke with $a = 7.5$ inches, the critical radius of curvature $\bar{r}$ is 6.08 inches for $b/a = 0.8$ and 8.13 inches for $b/a = 0.6$. The test data for these cylinders are shown in terms of C as a function of $\bar{r}/t$ in figure 18 and as k_b as a function of Z_L in figure 20. It should be noted that, in the equation for Z_L,

$$Z_L = \frac{L^2}{\bar{r}t}(1 - \nu_e^2)^{1/2} \tag{35}$$

the radius of curvature at $(y/a)_{cr}$ is used. The local-buckling stress at $(y/a)_{cr}$ is found from equation (33).

Although no axial-compression data exist with which to compare these bending results directly, it may be assumed that the quality of fabrication of the bending specimens was similar to that of the specimens previously tested by Lundquist in compression. Consequently, a value of $U = 0.00015$ was used to correlate the data. As may be seen in figure 18, the gradient factor γ has approximately the same value of 1.3 for the elliptic cylinders tested as for the circular cylinders tested in bending.

The relation between k_b and Z_L is depicted in figure 20, which shows no appreciable effect of $\bar{r}/t$ for a range from 250 to 750. For all practical purposes, all the data appear to cluster about one curve. This is also substantiated by figure 18, which reveals a rather flat distribution of the data over a range of values of $\bar{r}/t$. The curve corresponding to $k_b = 1.3k_c$ has been plotted in figure 20 for $r/t = 500$, where it is seen to fit the data well.

Computation of Buckling Stress for Elliptic Cylinders

From the standpoint of the analysis of a structure, it is generally desirable to compare applied stress with allowable stress. On an elliptic cylinder in bending, therefore, it is necessary to locate the position on the cross section at which buckling occurs (see fig. 21) and to compute the section modulus for this location. The quotient of applied moment and this section modulus yields the applied stress, and the local radius

of curvature permits computation of the allowable stress for this position. In summary, then, the following steps are suggested:

(1) Compute the section modulus of the circumscribed circle $S_a = \pi a^2 t$ (see fig. 21).

(2) Find the extreme-fiber section modulus of the elliptic cylinder using the relation $S_e = (S_e/S_a)S_a$ together with figure 22 in which S_e/S_a appears as a function of b/a.

(3) From figure 19 find $(y/a)_{cr}$ and $\bar{r}/a$ as functions of b/a.

(4) Compute the applied stress at the location of the critical curvature from $\sigma_{y_{cr}} = M(y/a)_{cr}/S_e$.

(5) Compute the allowable stress at this location (for long cylinders only) using $\sigma_{cr} = C_b E t/\bar{r}$, in which C_b is found from the curve of figure 18 for the pertinent value of $\bar{r}/t$. The gradient factor of 1.3 is included in this curve.

The location and magnitude of the critical curvature $1/\bar{r}$, where $\bar{r}$ is the critical radius of curvature, can be determined by plotting the nondimensional curvature of the ellipse

$$a/r = (b/a)\left\{1 - \left[1 - (b^2/a^2)\right](y/a)\right\}^{-3/2} \tag{36}$$

as a function of y/a for selected values of b/a. Since the stress across the section varies linearly from zero at the neutral axis, and since the axis of a/r may also be considered to be an arbitrary-magnitude stress scale (fig. 23), a line from the origin tangent to the a/r curve determines the location of $(y/a)_{cr}$ and $\bar{r}$, or

$$\frac{(a/r)}{(y/a)} = \frac{d(a/r)}{d(y/a)} \tag{37}$$

Figure 19 displays $(y/a)_{cr}$ and $\bar{r}/a$ as functions of b/a. Actually, it has been analytically determined that:

$$(y/a)_{cr} = 0.5\left[1 - (b^2/a^2)\right]^{-1/2} \tag{38}$$

$$(\bar{r}/a) = 0.649a/b \tag{39}$$

Note that when $b/a > 0.866$, buckling must occur at the extreme of the major axis, and $\bar{r} = a$.

Behavior of Circular-Arc Sections

A cylinder consisting of two circular arcs symmetric about their common chord tends to flatten during bending in the same manner as a very long circular cylinder which becomes unstable in the Brazier mode. The behavior of long circular-arc-section cylinders was analyzed theoretically by Fralich, Mayers, and Reissner (ref. 32), who investigated the nonlinear relation between moment and stress and found that the instability stress may be computed by the expression

$$\sigma_{cr} = 0.285Et/r \tag{40}$$

in which r is the radius of curvature of each arc in the doublet.

Anderson, Pride, and Johnson (ref. 33) performed tests on three circular-arc-section cylinders of 7075-T6 aluminum alloy with the results shown in table 3. The cylinder section geometry is shown in figure 14. Because of its shape, a circular-arc cylinder undergoes chordwise deformation of the section which leads to a neutral axis shift. This secondary effect was neglected in the derivation of equation (40).

It might be expected that for certain cylinder proportions local buckling would precede Brazier instability. For example, this could be anticipated in circular-arc cylinders corresponding to the upper transition range of circular-cross-section cylinders. Also, at a certain value of r/t the local-buckling stress could be found from a curve of C as a function of r/t, such as that for axially compressed circular cylinders (fig. 7), providing an appropriate gradient factor could be found for the circular-arc section in bending in terms of the axial-compression case. This is complicated by the fact that each arc of the profile actually is a curved plate with boundary conditions along the contiguous edges of the section arcs.

The gradient factors for the three test cylinders were obtained by taking the ratio of the test C to the theoretical C. The test C is equal to the ratio of measured buckling stress to the theoretical value from equation (40), multiplied by 0.285 (the coefficient of eq. (40)). This C has been designated C_1 in table 4. The coefficient from figure 7 for $U = 0.00015$, which applies to the aluminum-alloy data of

Lundquist on circular cylinders, is designated C_2 in table 4, in which γ is shown as the ratio of these two C values. Because of the sparse data, no recommendation can be made for a value of γ for circular-arc sections.

Inelastic Behavior of Long Circular Cylinders in Bending

It was shown in the preceding sections that a long circular cylinder which buckles elastically under bending sustains a stress approximately 30 percent greater than would the same cylinder loaded in axial compression. This has been attributed to the gradient effect. When the extreme-fiber stresses are in the inelastic range, the redistribution of the cross-sectional stresses leads to a significant reduction in the stress gradient, which would be expected to reduce the gradient factor. For large inelastic stresses on a cylinder consisting of a material with a flat strain-hardening curve, for example, the stress would be virtually constant around most of the compression arc.

As a countermeasure to the diminished stress-gradient effect, the nonlinearity of stress distribution permits the cylinder to sustain a plastic bending moment greater than the fictitious elastic moment calculated according to $\sigma_{cr}S_c$. This is the well-known modulus of rupture effect. A further plasticity effect is the decrease in the local rigidity of the cylinder wall, which is represented by the plasticity-reduction factor η.

For a beam with the extreme-fiber stress in the inelastic range, it has become common practice to define a fictitious elastic stress σ_r as the bending modulus of rupture:

$$\sigma_r = M/S_c \tag{41}$$

Since the actual stress distribution is nonlinear and depends upon the shape of the cross section, it is customary to use a "shape factor" to determine the actual plastic stress at the extreme fiber σ_b. The shape factor is defined as

$$\rho = \sigma_r/\sigma_b \tag{42}$$

Thus, the actual stress σ_b in terms of the moment and section modulus is

$$\sigma_b = M/\rho S_c \tag{43}$$

For both the reduction of experimental data and design purposes, it is convenient to use the ratio of σ_r, computed from equation (41) for a cylinder under bending, to the buckling stress of the corresponding cylinder under axial compression. Thus,

$$\frac{M/S_c}{\sigma_{c_{cr}}} = \rho \frac{\sigma_{b_{cr}}}{\sigma_{c_{cr}}} = \rho\gamma_\sigma \tag{44}$$

where:

$$\sigma_{b_{cr}} = \gamma_\epsilon C\eta_b E(t/r)$$

$$\sigma_{c_{cr}} = C\eta_c E(t/r)$$

In the elastic range it was not necessary to distinguish between the strain gradient factor γ_ϵ and the stress gradient factor γ_σ. They were the same and equal to 1.3. As a simplification of the problem for the inelastic case, it is assumed that

$$\gamma_\epsilon = 1.3 = \epsilon_{b_{cr}}/\epsilon_{c_{cr}} = \left(\sigma_{b_{cr}}/\eta_b\right)\Big/\left(\sigma_{c_{cr}}/\eta_c\right) \tag{45}$$

Thus, from equation (45), the value of γ_σ is obtained as the ratio of $\sigma_{b_{cr}}$ to $\sigma_{c_{cr}}$ from a plot of σ against σ/η as shown in figure 24. The stress $\sigma_{c_{cr}}$ corresponds to the selected value of $\sigma_{c_{cr}}/\eta_c (= CEt/r)$ and $\sigma_{b_{cr}}$ corresponds to $1.3\sigma_{c_{cr}}/\eta_c$.

In order to demonstrate the influence of the two factors γ_σ and ρ of equation (44) for a typical material, the stress-strain curve for 6061-T6 aluminum alloy shown in figure 24 was used for purposes of calculation, from which the plot of σ_{cr}/η was derived as a function of σ. The plasticity-reduction factor η is that for an axially compressed circular cylinder as given in the section "Circular Cylinders Under Axial Compression."

The factors γ_σ and ρ are depicted in figure 25(a) as functions of $\sigma_{c_{cr}}/\sigma_{cy}$. It can be seen that γ_σ decreases from 1.3 to unity, while ρ rises from unity to the fully plastic value of $4/\pi$. The product of these two factors falls slightly from 1.3 and then rises to $4/\pi$. The most rapid changes are confined to the region of $\sigma_{c_{cr}}/\sigma_{cy}$ near 1.

The trends of figure 25(a) are substantiated by the experimental data of figure 25(b) which were obtained from matched cylinders, one group of which was tested in compression while the other was tested in bending. The data for 2017-T4 aluminum-alloy cylinders were obtained by Osgood (ref. 21) and the 7075-T6 aluminum-alloy cylinders were tested by Moore and Clark (ref. 23). Osgood's photographs of the failed specimens indicate the presence of Brazier instability at large buckling stress which tends to account for the decrease of $\gamma_\sigma\rho$ for the 2017-T4 data beyond the yield stress.

The different shapes of the curves for the two materials reflect different inelastic properties. The sudden change for 7075-T6 alloy is consistent with the sharp knee of the stress-strain curve for that material, whereas the more gradual variation for 2017-T4 alloy would follow from the rounded knee of its stress-strain curve.

CIRCULAR CYLINDERS UNDER TORSION

Historical Background

The early torsional-instability investigations were concerned with long elements. Greenhill determined the buckling stress of a long twisted rod or wire (ref. 34) and Schwerin calculated the local buckling stress of a long, thin-wall tube with two helical waves (ref. 35). Donnell used the eighth-order equilibrium differential equation, equation (10), and extended the analysis of the torsion-buckling problem to moderate- and short-length thin-wall cylinders (ref. 6). Fair agreement with experimental data of Donnell (ref. 6) and Lundquist (ref. 36) was obtained.

Donnell's results were based upon certain simplifications employed in the numerical computations. Leggett analyzed the problem without such simplifications and obtained improved agreement with test data (ref. 37). Batdorf, Stein, and Schildcrout (ref. 38) utilized a modified form of the single equilibrium equation of Donnell and by use of Galerkin's method obtained results in good agreement with those of Leggett.

Gerard included the effects of plasticity in the three simplified equilibrium equations from which the Donnell equation was derived and showed that the secant modulus is the applicable plasticity-reduction

factor for this case (ref. 7). Close correlation was obtained with the test data of Stang, Ramberg, and Back (ref. 39), of Moore and Paul (ref. 40), of Moore and Wescoat (ref. 41), and of Moore and Clark (ref. 23).

The effects of internal pressure were investigated theoretically by Hopkins and Brown (ref. 42), who obtained fair correlation with the test data of Crate, Batdorf, and Baab (ref. 43).

Experimental Data

The test data for elastic buckling of thin-wall cylinders under torsion appear in figure 26 in the form of the torsional-buckling-stress coefficient plotted as a function of Z_L. The theoretical curve of Batdorf, Stein, and Schildcrout is shown and it appears to yield reasonably good agreement in this logarithmic plot. However, when a section of the curve is plotted linearly, as in figure 27, the differences between the theory and the data are apparent. It may be seen that the lower data points are as much as 40 percent below the theoretical value of buckling stress for a particular value of Z_L. On the average the test data lie 16 percent below the theoretical curve.

In addition to the low values of the data, appreciable scatter is evident. This may be partly due to initial imperfections in the cylinders which were rolled from flat strips with a longitudinal connection along the contiguous edges. Also, some of the scatter may be the result of the method by which buckling was determined. The objective electric-strain-gage indication of buckling, in use today, was unknown when Donnell and Lundquist ran their tests. It was necessary to discern buckling visually. Furthermore, Donnell and Lundquist reported collapsing stresses and not buckling. These two situations leave room for greater departure between theory and actual buckling stresses than the data reveal.

Buckling Behavior of Cylinders Under Torsion

For a thin-wall cylinder loaded in torsion in the elastic range, buckling is not accompanied by immediate collapse as is the case with axially compressed cylinders. This is illustrated for typical test data by the curve shown in figure 28, from which it may be seen that after buckling a practical twisted cylinder will behave somewhat like a column. The load gradually increases with small lateral deflection of the cylinder wall. At a load near buckling the curve gradually flattens, and large lateral deflection follows with little variation in load until failure occurs. At failure, the torque drops sharply with continued lateral deflection of the wall. The mechanism by which a twisted tube may attain

a failure load in excess of the buckling load has been ascribed in the section "Physical Behavior of Curved Elements" to the tensile membrane stresses generated along the buckle ridges when the deflection becomes large.

Both Donnell and Lundquist observed that small initial dimples in the surfaces of the test cylinders did not seem to affect the buckle formation. Also, from the experimental results the initial imperfections do not appear to affect the buckling strengths to any appreciable extent. Contrary to their role in the compressive-buckling behavior of circular cylindrical shells, small initial imperfections seem to have small influence upon the buckling behavior of cylinders loaded in torsion.

It is to be noted that the Greenhill type of instability may have occurred in the tubes tested by Stang, Ramberg, and Back, which buckled well within the plastic range (ref. 39). Several failed by helical deformation of the tube axis without distortion of the cross section, which was the nature of the instability predicted by Greenhill for long elements that would not buckle locally (ref. 34).

Numerical Values of Torsional Buckling Stress

The theoretical curve of buckling-stress coefficient k_t as a function of Z_L appears in figure 26 together with the corresponding test data. As mentioned previously, these data report failure and not buckling. Consequently, the theoretical curve is somewhat optimistic. However, the reported data do not indicate the buckling stresses of the cylinders and, therefore, it would be advisable to use a more conservative value than is furnished by the theoretical curve.

A clue to the selection of such a curve is provided by the model of postbuckling behavior for the twisted cylinder as described above. It is indicated that the failure stress of a perfect cylinder should not be much greater than its buckling stress. Since the average departure of the test data is about 16 percent, the buckling stress of a cylinder under torsion may be taken as 84 percent of the theoretical value on the average.

For very short cylinders the buckling coefficient k_t corresponds to that for a long flat plate under shear k_s with the buckling stress expressed in the form:

$$\tau_{cr} = \frac{k_t \pi^2 E}{12(1 - \nu_e^2)} \left(\frac{t}{L}\right)^2 \qquad (46)$$

For clamped edges the torsional-buckling coefficient is 8.98 and for simply supported edges it is 5.35. For intermediate-length cylinders the curves approach straight lines which correspond to

$$\tau_{cr} = 0.93(\pi^2/12)(1 - \nu_e^2)^{-5/8}E(t/r)^{5/4}(r/L)^{1/2} \tag{47}$$

for clamped edges and

$$\tau_{cr} = 0.85(\pi^2/12)(1 - \nu_e^2)^{-5/8}E(t/r)^{5/4}(r/L)^{1/2} \tag{48}$$

for simply supported edges. These expressions apply theoretically for $10(t/r)^{1/2} < L/r < 3(r/t)^{1/2}$.

In these cases the number of circumferential buckles was greater than two. When the cylinder L/r exceeds $3(r/t)^{1/2}$ there are only two circumferential buckles, and the buckling stress for long cylinders as derived by Donnell is

$$\tau_{cr} = 0.272(1 - \nu_e^2)^{-3/4}E(t/r)^{3/2} \tag{49}$$

Plasticity-Reduction Factors

A plasticity-reduction factor must be determined for each of the three cylinder length ranges. For very short cylinders, flat-plate action is approached. Gerard has demonstrated empirically that the shear secant modulus yields agreement with test data (see fig. 29) for long flat plates loaded in pure shear (ref. 44). The equation for the buckling stress of the cylinder in this range, as shown in reference 1, is then

$$\tau_{cr} = \eta \frac{k_s\pi^2E}{12(1 - \nu_e^2)}\left(\frac{t}{b}\right)^2. \tag{50}$$

where $\eta = (E_s/E)(1 - \nu_e^2)/(1 - \nu^2)$ and corresponds to a value of $\tau = \sigma/2$.

For very long cylinders, to which equation (49) is applicable for elastic buckling, the secant modulus is again the plasticity-reduction modulus, as was shown by Gerard theoretically (ref. 7). This agrees with

test data, as may be seen from figure 30. Thus, the inelastic counterpart of equation (49) is

$$\tau_{cr.} = 0.272\eta(1 - \nu_e^2)^{-3/4}\bar{E}(t/r)^{3/2} \tag{51}$$

where $\eta = (E_s/E)\left[(1 - \nu_e^2)/(1 - \nu^2)\right]^{3/4}$ and corresponds to a value of $\tau = \sigma/2$.

No inelastic theory has appeared in the literature for intermediate-length cylinders. However, the applicability of the secant modulus in the limiting cases would seem to justify its use in this range. This is partially bolstered by test data, in which, unfortunately, there is large scatter (fig. 31). Still, the trend is seen to agree with the secant-modulus plasticity-reduction factor.

Inelastic-buckling stresses for twisted cylinders may be found from the nondimensional curves of figure 32 by using

$$\epsilon_{cr} = \tau_{cr}/\eta E \tag{52}$$

Effects of Internal Pressure

By use of Donnell's equation, Hopkins and Brown analytically calculated the effect of internal pressure on the buckling stress of twisted cylinders (ref. 42). Fair correlation was obtained with the experimental results of Crate, Batdorf, and Baab, who utilized an empirical interaction equation to fit the test data (ref. 43).

On the basis of tests performed on a single cylinder with different stiffener ring spacings, Crate, Batdorf, and Baab derived the interaction relation

$$R_t^2 + R_p = 1 \tag{53}$$

in which the pressure ratio R_p is equal to the quotient of the applied internal pressure and the external hydrostatic pressure that would buckle the cylinder by itself. The torsional- and hydrostatic-buckling stresses can be found from the curves discussed in this section and in the section "Circular Cylinders Under External Pressure."

The test results of Crate, Batdorf, and Baab are shown in figure 33 from which it can be observed that good agreement of test data with the interaction curve is obtained.

Elliptic and D-Section Cylinders

A circular cylinder loaded in torsion buckles over its entire surface. If initial imperfections are small, buckling will occur suddenly and will coincide with failure. If imperfections are appreciable, the buckling stress is not precisely defined, as it is for a perfect cylinder; however, failure will occur at a stress substantially the same as for the perfect cylinder.

In general, the behavior of a noncircular cylinder follows that of a circular cylinder with initial imperfections. When torque is applied to a cylinder with an elliptic cross section, buckling occurs first at the ends of the minor axis and progresses toward the ends of the major axis. When the buckle reaches this point the cylinder collapses. The reason for this behavior may be evident if the radius variation from the minor axis to the major axis is considered. Since the radius at the major axis is the smallest for the cross section, this region stabilizes the cylinder against collapse until the buckle forces failure.

D-section cylinders behave in the same manner as complete cylinders. In fact, all cylinders with the same Z_L fail at the same k_t, as may be seen in figure 34. In this figure buckling coefficients are plotted as a function of Z_L for elliptic cylinders tested by Lundquist and Burke (ref. 30) and for circular and elliptic D-tubes tested by Sherwood (ref. 45) and by Kavanaugh and Drinkwater (ref. 46). The buckling-stress expression is the same as that given for circular cylinders in equation (46) and for

$$Z_L = \frac{L^2}{at}(1 - \nu_e^2)^{1/2}$$

For Z_L the semimajor axis of the ellipse or D-tube section is taken equal to r. This is depicted in the sketches accompanying the data of figure 34, which also contains the theoretical circular-cylinder curve of Batdorf, Stein, and Schildcrout (ref. 38). As is apparent from this figure, the agreement is good. Some of the test data for the elliptic cylinder rise above the theoretical curve. However, the main mass lies almost entirely within the circular-cylinder scatter band.

CIRCULAR CYLINDERS UNDER EXTERNAL PRESSURE

Historical Background

A rather complete bibliography up to 1939 on the buckling of circular cylinders under pressure is contained in a paper by Sturm (ref. 47). The present section, for the most part, is confined to the work of Windenberg and Trilling (ref. 48), of Sturm, and the more recent work of Batdorf (ref. 3).

Windenberg and Trilling performed tests from which empirical relations were obtained between certain cylinder parameters and buckling stresses. Sturm investigated radial and hydrostatic buckling both theoretically and experimentally, with the test data confined to the long-cylinder range. He solved the set of differential equations for both simply supported and fixed ends. Batdorf employed Donnell's single equation to obtain solutions to the cases of simply supported cylinders under radial and hydrostatic pressure. The simplicity of using Donnell's equation was demonstrated in the section "Stability Theory of Curved Elements."

Kempner, Pandalai, and Patel investigated the postbuckling elastic behavior of hydrostatically loaded cylinders and demonstrated theoretically that significant pressure increases could be sustained in short cylinders after buckling (ref. 49). This work tends to substantiate the explanations given in the section "Physical Behavior of Curved Elements" concerning those cases in which large-deflection effects are likely to be of importance.

Test Data

The test data for failure of circular cylinders under pressure loads appear in figure 35(a) for radial pressure alone and in figure 35(b) for hydrostatic pressure. On the whole, the agreement with Batdorf's theoretical results is good, with relatively little scatter. This agreement suggests that small initial imperfections are unimportant in this case. In fact, Sturm's test data indicate that initial eccentricities in the test specimens varied from negligibly small to some considerably greater than the wall thickness. Furthermore, the results reported by Windenberg and Trilling (ref. 48) as well as by Sturm (ref. 47) were failing stress, and not buckling stress, which tends to smooth out the effects of small imperfections.

The test data of Windenberg and Trilling for the hydrostatic-loading case appear to lie along a straight line at a slight slope to the theoretical line of Batdorf. The agreement with theory is good for values of Z_L beyond 100. Below this value of Z_L, however, the test data are

below the theoretical values. A close examination of these data indicated that plasticity effects may have lowered the failing stress compared with the theoretical elastic-buckling stress. This suspicion is based on the fact that the data are at a fairly large fraction of the tensile yield strengths reported. Compression yield strengths for straightened sheet materials are generally considerably below the tension yield values, which would tend further to increase the influence of plasticity effects.

Behavior of Cylinders

A long circular cylinder under either radial or hydrostatic loading will buckle into two circumferential harmonic waves in the same manner as a ring. As the cylinder length decreases, the number of circumferential waves increases with a consequent increase in buckling stress. Sturm has shown that when the buckling pressure is plotted as a function of L/r for particular values of r/t, peaks will occur in the curves similar to those obtained for flat plates when k is plotted as a function of a/b. Each of these peaks represents the transition from n circumferential buckles to $n + 1$ buckles as the energy for $n + 1$ buckles becomes less than the energy for n buckles.

For very short cylinders under radial pressure, Batdorf has demonstrated that the behavior corresponds to that of a long flat plate under longitudinal compression, with the boundary conditions along its longitudinal edges corresponding to those along the cylinder edges. The behavior of hydrostatically loaded short cylinders theoretically approaches that of an infinitely long flat plate with biaxial compression loading in which the transverse component is half of the longitudinal. In both these cases the buckling stress and wave number are determinable from the curves of reference 1, with a/b equal to $2\pi r/L$.

The low data for $Z_L < 100$ obtained by Windenberg and Trilling pertain to cylinders reported to be fairly free from initial imperfections. Some of the decrease may be chargeable to the effects of plasticity, since the stresses approached the yield for some of these cylinders.

There may also be a conflict of testing procedure and theoretical analysis. Theory assumes that the deformation of the cylinder under the external loads is not restrained. However, radial rigidity of the end plates of a test cylinder under hydrostatic pressure would result in a relative inward displacement of the cylinder wall before buckling begins. If the cylinder were long, this initial eccentricity might not affect the buckling stress. However, it may exert appreciable influence on the buckling stress of a short cylinder under hydrostatic pressure.

Buckling-Stress Equations

Radial pressure.- Under inward-acting radial pressure, the circumferential-compression stress generated in the cylinder wall is

$$\sigma_y = \frac{pr}{t} \qquad (54)$$

The buckling stress of the cylinder under this loading is

$$\sigma_{cr} = \frac{k_y \pi^2 E}{12(1 - \nu_e^2)}\left(\frac{t}{L}\right)^2 \qquad (55)$$

When more than two complete waves are formed around the circumference of the cylinder, Donnell's equation may be used to compute the buckling stress. This was done by Batdorf for cylinders with simply supported edges as shown in the section "Circular Cylinders Under Axial Compression." Values of k_y are shown in figure 35(a).

When the length approaches zero, the cylinder degenerates into a long, longitudinally compressed, flat plate. In reference 1, the buckling coefficient was shown to have a value of 4 for simply supported edges and 6.98 for clamped edges.

When the cylinder is of sufficient length, buckling will occur in two circumferential waves, and Donnell's equation, which is based on the assumption that $n^2 \gg 1$, cannot be used. A solution for a long cylinder has been given by Timoshenko in the form

$$\sigma_{cr} = \frac{E}{4(1 - \nu_e^2)}\left(\frac{t}{r}\right)^2 \qquad (56)$$

for $(L/r)^2 > 5(r/t)$. Figure 35(a) contains the theoretical curves for all three cylinder length ranges.

Hydrostatic pressure.- Under hydrostatic pressure, which is a particular case of the general combination of radial pressure and axial loading on a cylinder, the following biaxial-stress field is generated in the cylinder wall:

$$\left.\begin{aligned}\sigma_y &= \frac{pr}{t} \\ \sigma_x &= \frac{pr}{2t}\end{aligned}\right\} \tag{57}$$

For simply supported edges, the solution obtained by Batdorf by use of Donnell's equation is given in the section "Circular Cylinders Under Axial Compression."

When the cylinder length becomes small the circumferential-buckling coefficient approaches 2. This result follows directly from the flat-plate interaction curves corresponding to the biaxial-stress field of equation (57).

For long cylinders, the behavior under hydrostatic pressure is the same as that for radial pressure alone (eq. (56)) according to linear theory. The buckling-coefficient curves for this case appear in figure 35(b) together with the theoretical curves for the other two cylinder length ranges.

Effects of Plasticity

When the circumferential stress in the cylinder wall under radial pressure exceeds the proportional limit, equation (55) may be written in the form

$$\sigma_{cr} = \eta \frac{k_y \pi^2 E}{12(1 - \nu_e^2)} \left(\frac{t}{L}\right)^2 \tag{58}$$

The plasticity-reduction factor for long cylinders was found by Bijlaard (ref. 24) to be the same as that for a wide plate column, which was shown in reference 1 to be

$$\eta = \frac{E_s}{E} \frac{(1 - \nu_e^2)}{(1 - \nu 2)} \left(\frac{1}{4} + \frac{3}{4} \frac{E_t}{E_s}\right) \tag{59}$$

utilizing a value of 0.5 for the plastic Poisson's ratio after the manner of Stowell. This result applies to long cylinders only $((L/r)^2 > 5(r/t))$ and corresponds to the curves of figure 35(b) for which specific values of r/t are indicated.

CIRCULAR CYLINDERS UNDER COMBINED LOADS

Historical Background

The first investigations into the buckling of circular cylinders under combined loads were experimental. Bridget, Jerome, and Vosseller conducted tests on steel and brass cylinders in torsion combined with axial tension or compression and derived empirical interaction curves from the results (ref. 50). Wagner and Ballerstedt constructed an interaction equation from data obtained from tests on brass cylinders under torsion and tension (ref. 51).

Theoretical analyses were made by Leggett (ref. 52) and by Kromm (ref. 53) on the combination of torsion and axial compression, using the basic linear shell equilibrium equations. Subsequently, Bruhn conducted a large number of tests on celluloid cylinders under various combinations of axial compression, axial tension, bending, and torsion (ref. 54). He compared his results with empirical interaction relations.

More recently Batdorf, Stein, and Schildcrout investigated buckling under axial compression and torsion using Donnell's equation (ref. 55). They derived theoretical interaction relations which they modified for practical application by substituting empirical buckling stresses for the theoretical values in the denominators of the stress ratios.

Interaction Equations

The use of interaction equations in terms of stress ratios for solution of combined-load buckling problems on flat plates was described in reference 1. Interaction equations for various combinations of loadings on circular cylinders appear in table 5 of this report. In the following paragraphs these equations are discussed in detail.

Axial Compression and Bending

Since the nature of the buckle pattern is the same for axial compression and bending of a circular cylinder, a linear interaction equation might be expected for this case. Bruhn has shown this to be a good approximation to the data in figure 36(a).

Axial Load and Torsion

Theoretical analyses of combined-load buckling of cylinders have been limited to application of linear theory to the combination of axial load and torsion. This was done by Kromm, Leggett, and Batdorf, Stein, and Schildcrout, whose work differs mainly in mathematical details. They all obtained essentially the same results.

From linear analysis, Batdorf, Stein, and Schildcrout (ref. 55) obtained an interaction equation for axial compression and torsion,

$$R_c + R_t^2 = 1 \tag{60}$$

which is applicable for small values of Z_L (see table 5). For large values of Z_L, they suggested retaining the form of equation (60) with the provision that empirical results for the shear- and axial-compression-buckling stresses be used in the stress-ratio denominators instead of the theoretical values in order to obtain correlation with the data for numerical stresses in the limiting cases of $R_c = 0$ or $R_t = 0$. The ranges of applicability of this equation are shown in table 5, and the agreement with Bruhn's test data is shown in figure 36(b). Similar agreement was obtained with the data of Bridget, Jerome, and Vosseller (ref. 50).

For axial tension and torsion, Batdorf, Stein, and Schildcrout recommended

$$0.8R_c + R_t = 0.9\left[-1 < R_c < 0,\ 30 < Z_L < 7.7(r/t)^2\right] \tag{61}$$

Bruhn obtained good agreement with test data using $0.4R_c + R_t = 1$ for the same range of R_c and Z_L.

Bending and Torsion

The experimental results of Bruhn are shown in figure 36(c) together with three interaction equations. The parabolic equation is seen to be conservative, while the equation for the circle gives too large a value at large values of R_t. The best overall agreement is obtained with the relation

$$R_b^{1.5} + R_t^2 = 1 \tag{62}$$

Axial Compression, Bending, and Torsion

Bruhn performed tests on cylinders with $230 < r/t < 800$ under the combination of axial compression, bending, and torsion, and obtained

results that show considerable variation in predicted value of one stress ratio for selected values of the other two (ref. 54). A typical set of these data is shown in figure 37 from which these variations are apparent. However, the two-dimensional interaction curves derivable from these charts agree reasonably well with those of figure 36. Additional tests conducted on cylinders covering a range of axial tension as well as compression agree fairly well with the expression

$$R_c + R_b + R_t^2 = 1 \tag{63}$$

It may be concluded, therefore, that interaction relationships for this combination are uncertain at present.

Transverse Shear and Bending

Lundquist conducted tests on the behavior of circular cylinders under combined transverse shear and bending (ref. 56), and Lundquist and Burke continued this program to include elliptic cylinders (ref. 30). By varying the lengths of the cantilevered cylinders, it was possible to determine the shear-buckling stress under combined bending and shear. By extrapolation of these results to a zero bending stress, the equivalent pure transverse shear-buckling stress was obtained.

These stresses were compared with the torsional-buckling stresses for these same cylinders as determined from the theoretical curve of figure 26, which revealed a value of about 1.6 for the ratio of the transverse to torsional shear-buckling stresses for both circular and elliptic cylinders. This value, however, represents an average for the data. The minimum value of 1.25 was used by Lundquist and Burke in the derivation of interaction relationships for combined transverse shear and bending. The buckling stress in pure bending was available from previous investigations described in the section "Cylinders in Bending."

As a result of this analysis, it is possible to express the stress ratios in the form

$$R_b + R_s^2 = 1 \tag{64}$$

In computing R_b use figure 16 to find the buckling stress under bending alone. For R_s multiply the theoretical torsional-buckling stress obtained from figure 26 by 1.25 to account for the transverse-shear effects. This value of 1.25 is conservative when compared with the average of the test data.

CURVED PLATES UNDER AXIAL COMPRESSION

It is natural to expect that the behavior of curved plates under compression would be similar in many respects to that of a circular cylinder under compression since a curved plate is essentially a section of a cylinder. Long plates of sufficient curvature and width do, in fact, exhibit the same characteristics as long cylinders. Both buckle at stresses considerably below the predictions of linear theory and it is apparently necessary to utilize large-deflection theories to obtain improved agreement with test data. Also in both cases diamond buckle patterns are observed.

In this section, an attempt has been made to extend the unified approach, which was applied to cylinders under axial-compression and bending loadings, in order to correlate test data with theory for axially compressed curved plates. Since previous analytic investigations on axial-compressive buckling of curved plates were primarily limited to use of linear theory, close agreement with test data was found to occur only near the flat-plate limit, as might be expected by analogy to the cylinder results. Consequently, it was necessary to extend by empirical methods the unified approach of the sections "Cylinders in Bending" and "Circular Cylinders Under Axial Compression."

Historical Background

Redshaw applied the classical energy approach to the determination of the buckling stress of axially compressed curved plates and obtained an explicit equation for the buckling stress which reduces to the flat-plate-buckling stress as one limit and to the classical cylinder-buckling stress as the other limit (ref. 57). Sechler and Dunn suggested modifying Redshaw's equation by using experimental values for the cylinder-buckling stress instead of the classical theoretical value (ref. 58). Both of these methods can be reduced to the form in which the curved-plate-buckling coefficient is plotted as a function of the curvature parameter.

Stowell proposed a form for Redshaw's equation which utilizes the classical cylinder-buckling stress and the flat-plate stress as limits and employed a transition curve of the form utilized in the section "Circular Cylinders Under Axial Compression" for cylinders (ref. 59).

Test data on curved plates were obtained by Cox and Clenshaw (ref. 60), Crate and Levin (ref. 61), Jackson and Hall (ref. 62), Welter (refs. 63 and 64), and Schuette (ref. 65). Generally, no attempt was made to correlate these data with the nonlinear theories of axial-compressive buckling until the comprehensive treatment by Cox and Pribram (ref. 66), who utilized the energy-buckling criterion of Tsien to explain

the behavior of axially compressed curved plates. As shown in the section "Stability Theory for Curved Elements," Batdorf utilized Donnell's equation to derive the buckling coefficient for an axially compressed curved plate, and Batdorf, Schildcrout, and Stein (ref. 67) attempted a synthesis of the test data of Crate and Levin and of Cox and Clenshaw. Except for some test data by Schuette in the inelastic range, all the preceding work was confined to elastic behavior.

Summary of Test-Specimen Details

The dimensions of the plates tested during the four investigations described herein are summarized in table 6. Schuette tested magnesium-alloy plates (ref. 65), whereas the remainder of the tests were performed on aluminum alloys. Two series of tests were run by Jackson and Hall (ref. 62) because in the first series the behavior of the supporting combs on the plate unloaded edges led to erratic results. The present report contains data for the second series only, in which this defect apparently was remedied.

Buckling Behavior of Axially Compressed Curved Plates

A curved plate loaded in axial-compression buckles in the same manner as a cylinder when the plate curvature is large, and when the plate curvature is small it buckles essentially as a flat plate. Between these two limits there is a transition from one type of behavior to the other.

When load is applied to the plate it attains a critical load, after which the load suddenly drops (at constant end shortening in a rigid testing machine). Upon further axial deformation the load continues to rise again and reaches a failure load which is greater than the buckling load if the latter occurs elastically. When the plate buckles plastically, buckling and failure are coincident. For a treatment of failure of compressed curved plates, refer to Part IV of this Handbook (ref. 68).

Tests by Cox and Clenshaw (ref. 60) and by Jackson and Hall (ref. 62) revealed that upon successive tests of a particular plate the upper buckling load is usually reduced, whereas the lower buckling load and failure level remained essentially constant.

The numerical values of buckling stress depend not only upon the geometry of the plate but also upon the boundary conditions. In contrast with cylinders with two edges along which boundary conditions exist, there are four edges for curved plates, which not only increase the difficulty of predicting the plate-buckling behavior, but also require additional parameters to describe the behavior.

Test data for each of four investigations are shown in figure 38(a) in terms of k_c and Z_b, where

$$\left.\begin{aligned} k_c &= \frac{12(1 - \nu_e^2)\sigma_{cr}}{\pi^2 E}\left(\frac{b}{t}\right)^2 \\ Z_b &= (b^2/rt)(1 - \nu_e^2)^{1/2} \end{aligned}\right\} \tag{65}$$

At small Z_b values, the buckling coefficient approaches that of a flat plate. The boundary conditions of the plates tested were between simple support and clamped. Thus an average of the buckling coefficients of these two limiting cases, $k_{pl} = 5.7$, was used for correlation purposes.

At large values of Z_b, it can be observed that the buckling coefficient is linearly related to Z_b. Thus, the buckling stress in this region of large values of Z_b reduces to the form of equation (30). In order to indicate this behavior more clearly, the data of figure 38(a) have been replotted in figure 38(b) according to r/t groupings. The solid lines of unit slope represent behavior according to equation (30) in which the values of C were obtained from figure 7 for circular cylinders. It can be observed that in the large Z_b region the curved plate approaches the cylinder in behavior.

In the intermediate region, a transition curve was fitted to the two limiting cases discussed above. This transition curve is of the same type used for cylinders in the section "Circular Cylinders Under Axial Compression." It can be observed that the experimental data lie above this curve. The cylinder data in the transition region displayed a similar type of behavior which was attributed to length effects.

The range of geometric variables possible on a curved plate are depicted in figure 4, which shows the many combinations of width and length possible for such an element. In each case, a somewhat different type of buckling behavior may be expected depending upon the curvature of the plate. The two limiting cases of a short, wide plate with small curvature and a long plate of large curvature effectively have two edges along which boundary conditions may influence the buckling behavior of the plate. Such plates behave essentially as circular cylinders. All other cases depicted in figure 4 involve boundary conditions along four edges. Most practical plates are of this type.

In the transition region the buckling coefficient should reflect the influences of the geometric parameters of the curved plate as well as the boundary conditions. For this region, the buckling coefficient can be written in the following functional form:

$$k_c = f(Z_b, r/t, L/r, r/b) \tag{66}$$

For the cylinder, the first three parameters appeared. For the curved plate, an additional parameter r/b reflects the additional set of boundaries.

Attempts were made to synthesize the available test data according to the different parameters of equation (66). Since it is likely that a long wide plate of appreciable curvature would buckle in the diamond pattern observed in axially compressed circular cylinders, it appeared reasonable to expect b and L to influence k_c as they approached the size of a diamond buckle. For example, if the plate length were to be decreased while maintaining the rest of the plate geometry constant, the circumferential plate edges would begin to confine the buckle pattern until eventually only one buckle would remain lengthwise while several might still exist circumferentially. Any further reduction in plate length might be expected to cause a transition from one diamond buckle to a single sine curve representative of plate behavior. Thus, at the transition geometry a peak would be expected in the plot of k_c against Z_b.

The presence of peaks in the data may be demonstrated in a general fashion by plotting all the test data in terms of k_c as a function of Z_b together with the compressed-cylinder semiempirical curves of figure 6 as shown in figure 38(b) for $r/t = 300$, 500, and 1,000. Then the magnification factor $\mu = k_{c_{exp}}/k_{c_{emp}}$ is plotted for all the data as a function of Z_b as shown in figure 39. This plot reveals that peaks exist at approximately the same values of Z as were found for axially compressed circular cylinders. However, it is evident that the peaks are not so positively defined as they are for compressed cylinders. The scatter in the data is large, yielding magnification factors ranging from 1 to 3 or more at the same values of Z_b for plates with the same values of r/t.

Further evidence of the existence of a magnification factor in the transition region is shown in figure 40 which contains envelopes of the data obtained by Crate and Levin (ref. 61), Cox and Clenshaw (ref. 60), Jackson and Hall (ref. 62), and Schuette (ref. 65). Peaks are observed

at Z_b values of approximately 5, 50, and 500. The first peak was not observed in the cylinder data of figure 9 although the second and third roughly correspond.

Attempts to define quantitatively the behavior of curved plates in the transition region were unsuccessful. For example, each point in figure 39 was marked with the pertinent L/r and r/b values. Attempts to draw contour lines through the data for constant values of L/r, r/b, or L/b did not reveal any consistent trend.

In general, therefore, it may be concluded that there is considerable evidence for the existence of a magnification factor. However, the inability to obtain consistent trends for the various geometric parameters used precludes any recommendations for design and analysis purposes.

Initial Eccentricity

Jackson and Hall measured the initial surface irregularities of 18 of the plates which they tested (ref. 62). Ordinarily this information might be used to determine U for long specimens. However, the values of Z_b for these plates were in the lower transition range close to the flat-plate limit and consequently would be of little value in analyzing curved plates of large values of Z_b on which the relation of C against r/t is based.

Cox and Pribram utilized these data to construct curves of buckling coefficient as a function of Z_b for different values of a_o, basing the construction of the curves on the semiempirical approach which they used to derive a general theory for the behavior of axially compressed curved plates (ref. 66). However, the use of these curves requires a prior knowledge of the magnitude of a_o, which seldom is available to designers.

Inelastic-Buckling Behavior

As was demonstrated in the preceding sections, a curved plate with a large value of Z_b buckles in a diamond pattern at a stress equal to that of the corresponding cylinder. This would appear to imply similar correspondence in the inelastic behavior. It was shown for cylinders in the section "Circular Cylinders Under Axial Compression" that the axial-compression plasticity-reduction factor, when applied to the elastic-buckling-stress expression, yields the inelastic-buckling stress for a long axially compressed circular cylinder

$$\sigma_{cr} = \eta C E t/r \tag{67}$$

where

$$\eta = \frac{\sigma_{cr}}{CEt/r} = \frac{E_s}{E}\left[\frac{(1 - \nu_e^2)}{(1 - \nu 2)}\frac{E_t}{E_s}\right]^{1/2} \tag{68}$$

In this section the inelastic test data of Schuette on magnesium-alloy curved plates (ref. 65) are compared with equation (68) to determine whether correlation exists.

It was assumed that the value of U for all the test data of Schuette was constant. The relation between C and r/t was then determined in the inelastic range by fitting a curve through the elastic data, as shown in figure 41, utilizing the theory of Donnell and Wan (ref. 20) to extend this curve to low values of r/t. It can be observed that for this case U is 0.000092. To aid in locating this curve, it was noted that for r/t = 300 a value of C = 0.36 fits the test data of Schuette shown in figure 38(a).

In figure 42, test data and theory are compared for the three magnesium alloys Ma, Mh, and J-1h. The plasticity-reduction factor is plotted as a function of stress. The theoretical value of η was obtained from stress-strain curves presented by Eastman, McDonald, and Moore (ref. 69). The experimental value was found by computing the ratio of experimental buckling stress to CEt/r, as shown in equation (68). As may be seen from figure 42, the agreement is good. The secant-modulus plasticity-reduction factor is also shown in these figures for comparison. Schuette originally recommended that it be used in the inelastic-buckling-stress equation

$$\sigma_{cr} = 0.42E_s t/r \tag{69}$$

in which the average value of C = 0.42 was used for all the test data. However, better agreement is obtained with the factor for axially compressed circular cylinders, particularly for the alloy Mh, for which the scatter is small, by using the curve of figure 41.

Effect of Normal Pressure

Application of pressure to the concave face of a curved plate raises the axial-compressive stress that the plate can sustain before buckling. Rafel and Sandlin (ref. 70) and Rafel (ref. 71) performed

tests on curved plates under this load combination, the results of which may be correlated with the interaction equation

$$R_c^2 + R_p = 1 \tag{70}$$

where R_p is the ratio of the applied internal pressure to the external pressure which would buckle the cylinder of which the plate is a section (see fig. 43).

SPHERICAL PLATES UNDER EXTERNAL PRESSURE

The buckling behavior of externally pressurized spherical plates is similar to that of axially compressed circular cylinders and curved plates in two ways. First, linear theory predicts the same buckling stress for externally pressurized spheres, long compressed cylinders, and long curved plates. Second, test data are considerably below the results of linear theory and large-deflection theories have been used to obtain improved agreement. Consequently, it appears reasonable to correlate test data on spherical plates in the same manner as used previously for cylinders and curved plates.

For long cylinders, the theory of Donnell and Wan (ref. 20) led to the determination of the buckling stress as a function of r/t. It was thus possible to construct a relationship for C (in the modified classical buckling-stress equation) as a function of r/t for axially compressed circular cylinders which involved selecting a numerical value for the unevenness factor U. For a value of $U = 0.00025$, the theoretical curve of C merged with that derived empirically by Batdorf. This matching of theory with test results was necessary because of the lack of measurements of initial imperfections of the cylinder and curved-plate test specimens.

For spherical plates, on the other hand, experimental data are available on the magnitude of the geometrical imperfections although a theory for the influence of such imperfections is lacking. By using the parameters of the Donnell-Wan theory, however, it was possible to establish from experimental data a reasonable estimate of the effect of geometrical initial imperfections.

Historical Background

Timoshenko (ref. 4) reported linear analyses of the buckling of spherical shells under external pressure by Zoelly (ref. 72), Schwerin (ref. 73), and Van der Neut (ref. 74), who obtained the same expression

for this case as for a long axially compressed circular cylinder. As in the case of the axially compressed circular cylinder, a nonlinear theoretical investigation by Tsien (ref. 12) revealed the presence of equilibrium buckle configurations at large deflections for a spherical shell under external pressure. The theory permitted the calculations of both the upper buckling load (which occurs during the loading of the shell) and the lower equilibrium load utilizing the energy criterion previously employed on axially compressed cylinders. These theoretical values are in agreement with the trend of the data obtained from tests on clamped spherical plates under external pressure.

Additional tests were recently conducted by Kaplan and Fung to determine whether the classical criterion or the energy criterion is applicable to the buckling of externally pressurized spherical plates (ref. 75). They concluded that the classical criterion is applicable to very shallow plates, while the deeper plates tend to buckle according to the energy criterion.

Initial Imperfections

In 1934 Donnell postulated the initial imperfections of a circular cylindrical shell as the reason for values of the experimentally observed axial-compressive-buckling stresses being low compared with the classical theoretical value of $0.6Et/r$ for long cylinders (ref. 8). Subsequently, Donnell and Wan extended this concept, utilizing the large-deflection approach developed by Donnell together with a relation between initial imperfection and the buckle geometry of the cylinder (ref. 20). This involves a parameter which Donnell and Wan term the "unevenness factor" of the cylinder.

More recently Loo extended this approach to include torsional buckling (ref. 76) by redefining initial imperfection in a form slightly different from that utilized by Donnell and Wan:

$$a_o = U_o\left[\frac{L_1 L_2}{L_1 + L_2}\left(\frac{1}{t}\right)\right]^g \tag{71}$$

In this expression a_o is the initial imperfection and L_1 and L_2 are the wave lengths of the buckle measured axially and circumferentially on the cylinder. The value of a_o is selected to include not only geometric imperfection, but, also theoretically, residual stresses, material anisotropy, and loading eccentricities. Numerically, it is the ratio of the amplitude of the equivalent imperfection sine wave to the thickness of the wall of the cylinder.

By properly selecting L_1 and L_2, equation (71) can be applied to the case of externally pressurized spherical plates and cylinders as well to the other cases examined by Loo. This suggests the possibility of generalizing equation (71) to permit an overall evaluation of initial imperfection. This is done by first recognizing that L_1 and L_2 usually are proportional to one another in any particular case and that either of these two dimensions can be expressed as some proportion of a geometric parameter of the structure under consideration, such as the radius of the cylinder surface or the diameter of the spherical-plate aperture. Symbolically defining this dimension as X, and including the proportionality constants in a single symbol K, equation (71) becomes

$$a_o = U_o(KX/t)^g \tag{72}$$

The amount of initial imperfection is fixed for a particular structure manufactured in a specific manner, and the magnitudes of X and k are reasonably well known for a specified type of loading. The unknown quantity in this expression is then U_o. Donnell found it necessary to determine U_o in order to fit the theory to the test data. In this report it is determined experimentally.

The expression for U_o is obtained by writing equation (72) in the form

$$U_o = a_o(KX/t)^{-g} \tag{73}$$

It is apparent from this relation that large buckle wave lengths lead to small values of U_o and small lengths lead to large values. Actually, the quantity $(KX/t)^{-g}$ is a measure of the sensitivity of U_o to the wave-length pattern and, consequently, to the type of loading. If this is termed the "sensitivity factor" S, then

$$S = (t/KX)^g \tag{74}$$

and equation (73) becomes

$$U_o = a_oS \tag{75}$$

This general expression relates unevenness to initial imperfection and sensitivity to this imperfection in terms of the buckle wave lengths.

Returning to equation (71), it is seen that in general

$$S = \left[\frac{(L_1 + L_2)t}{L_1 L_2}\right]^g \tag{76}$$

Donnell and Wan (ref. 20) and Loo (ref. 76) found satisfactory agreement of the general theory with test data when g is chosen equal to 2. For spherical plates, it appears likely that $L_1 = L_2$ due to axisymmetry. Thus for this case

$$S = (2t/L_1)^2 \tag{77}$$

If the diameter of the spherical plate d is selected as X, and if there are n buckle half waves across the cap, then $L_1 = d/n$; equation (77) becomes

$$S = (2nt/d)^2 \tag{78}$$

and U_o follows from equation (75) in the form

$$U_o = a_o(2nt/d)^2 \tag{79}$$

Analysis of Initial-Imperfection Data

Donnell and Wan presented a theoretically derived relation between σ_{cr}/σ_{cl} and $U_o r/t$ for axially compressed circular cylinders, from which the relation between C and r/t is readily obtained for a specific value of U_o (ref. 20). The data on spherical plates would be most effectively evaluated, therefore, by deriving the curve of C as a function of r/t empirically. The manner of accomplishing this follows.

Kaplan and Fung measured the initial profile of each spherical-plate specimen and recorded the deviation from a sphere through the pole of the plate (ref. 75). This permits computing a value of a_o for each plate which is equal to the maximum initial departure taken as a fraction of the spherical-plate thickness. Thus one quantity in equation (75) can be found. It now remains to determine the numerical value of the sensitivity factor.

This factor S for the spherical plates is expressed in equation (78). In this relation the only unknown quantity is the value of n, the number of buckle half waves across the base diameter of the plate. This is determinable from Kaplan and Fung's data, in which the buckle shapes are presented for several cases. The width of the buckle was obtained by projecting the buckle shape down to the datum line used to measure the plate profile. The number of buckles is related to Z_d as shown in figure 44 for the points taken from Kaplan and Fung. For values of Z_d less than 42 there is one buckle at the pole of the plate. For $42 < Z_d < 85$ there are two buckles equally spaced about the pole, and for $Z_d > 85$ there are three buckles, the center one of which occurs at the plate pole. Thus the few points displayed in figure 44, together with this information, do not permit precise determination of n for each specimen. However, since the principal purpose of this section is to compare the empirical trend with Donnell's theory, this purpose is served satisfactorily by drawing a straight trend line through the data in figure 44.

When this is done, n can be found for each specimen, after which S can be found from equation (78). Then U_o follows for each specimen, and $U_o r/t$ can be calculated. This is then plotted as a function of σ_{cr}/σ_{cl} as shown in figure 45, utilizing the relations

$$\sigma_{cr} = p_{cr} r/2t \tag{80}$$

$$\sigma_{cl} = 0.6Et/r \tag{81}$$

which yield

$$\sigma_{cr}/\sigma_{cl} = p_{cr}(r/t)^2/(1.2E) \tag{82}$$

The empirical plot of C as a function of r/t can now be made when the average value of U_o is determined for the caps. This is found to be 2×10^{-4} from table 7, which is so close to the value of 2.5×10^{-4} found in the section "Circular Cylinders Under Axial Compression" for axially compressed circular cylinders that this latter value will be used for purposes of consistency. Little difference will exist between the two curves. Figure 46 contains the plot of C as a function of r/t together with the test points obtained by using $C = \sigma_{cr} r/Et$. The agreement appears to be reasonable.

On the basis of the agreement of the empirical curve with the average of the test data, it may be inferred that the geometric portion of the total initial imperfection controls the average behavior of the spherical plates while the other factors such as residual stress may contribute to the scatter observed in the test data.

It may also be inferred that the concept of initial imperfections and the parameters selected by Donnell and Wan (ref. 20) in general provide a reasonable basis for evaluating the buckling behavior of curved plates and shells, although the theory required and the interpretation of the sensitivity parameter S may be different in each case. Further research is indicated to determine theoretically the empirically derived relation shown in figure 45. In this connection, Klein showed correlation between σ_{cr}/σ_{cl} (as a function of r/t) and an imperfection parameter that is essentially a different form of a_o (ref. 77).

Compressive-Buckling Coefficients

From figure 46, it is now possible to construct empirical curves of k_p as a function of Z_d in the manner of figure 5 and to compare them with the test data for externally pressurized spherical plates. This has been done in figure 47, in which the two curves for r/t equal to 200 and 2,000 have been drawn, since all the data lie within this range. The value of k for the circular flat plate is 6.0. Because of the flatness of the curve of C at large values of r/t, the spacing between the two lines is small compared with that shown in figure 6 for axially compressed circular cylinders. It may be seen that the agreement of the test data with the empirical curves is good. A peak appears to occur at $Z_d = 50$; however, the data are too few to substantiate it conclusively.

The results reported by Tsien pertain to values of r/t greater than 1,000, with the experimental buckling coefficients a large percentage of the classical value (ref. 12).

Numerical Values of Buckling Stress

For computation of elastic-buckling stresses of externally pressurized spherical plates, the equation

$$\sigma_{cr} = \frac{k_p \pi^2 E}{12(1 - \nu_e^2)} \left(\frac{t}{d}\right)^2 \qquad (83)$$

may be used for all values of Z_d. When Z_d is large and the plate approaches pure sphere behavior, it is permissible to use equation (30) to find the buckling stress. The curves to be used in conjunction with these equations may be found in figures 46 and 47.

Effects of Plasticity

The plasticity-reduction factor for a sphere under external pressure was theoretically derived by Bijlaard (ref. 24). When Poisson's ratio in the inelastic range is chosen equal to the fully plastic value of 0.5, the factor is equal to that found by Gerard for axially compressed long circular cylinders (ref. 7),

$$\eta = \frac{E_s}{E}\left[\frac{(1 - \nu_e^2)}{(1 - \nu 2)}\frac{E_t}{E_s}\right]^{1/2} \tag{84}$$

This factor is applicable only to spherical plates of large Z_d values for which the behavior is primarily that of a sphere with little flat-plate influence. Consequently, the buckling-stress equation to be used is that given by equation (67).

CURVED PLATES UNDER SHEAR

The usual convention adopted for plates loaded in shear requires that the b dimension be the shorter side. When this is applied to curved plates some ambiguity arises, since such plates may be curved either along the short edge or along the long edge. For clarity, therefore, a long curved plate is defined as one in which the long side is parallel to a generator of the cylinder of which the plate is a segment, and a wide plate is defined as one in which the long side is perpendicular to the cylinder generators. Since the generators of a right circular cylinder are parallel to the axis of the cylinder, these edges have been referred to as the axial and circumferential edges, respectively.

Historical Background

Leggett analyzed the problem of shear buckling of long strips of small curvature with both simply supported and clamped axial edges (ref. 37). It was assumed that motion in both the axial and circumferential directions was prevented along the edges of the strips. Kromm

analyzed the same problem for simply supported edges without restraining the motion normal to the axial edges of the plate and arrived at lower buckling stresses. These results agree with the subsequent work of Batdorf, Schildcrout, and Stein which was based on the use of Donnell's equation (refs. 67 and 78). They investigated the buckling of a long curved plate under shear with both simple support and clamping along the axial boundaries for a complete curvature range. They also investigated wide curved plates (ref. 79).

Good correlation has been obtained of theory with the experimental data of Rafel (ref. 80), Rafel and Sandlin (ref. 70), Moore and Wescoat (ref. 41), Kuhn and Levin (ref. 81), and Chiarito (ref. 82). Further, the effects of internal pressure were investigated theoretically by Brown and Hopkins (ref. 83), who obtained fair correlation with the test data of Rafel and Sandlin.

Test Data

The experimental results appear together with the theoretical curves of Batdorf, Stein, and Schildcrout (refs. 67, 78, and 79) in figure 48. Somewhat better correlation is apparent for curved plates with small initial eccentricities than for those with larger eccentricities. A rather detailed discussion of the test data is included in the report of Batdorf, Schildcrout, and Stein.

The results shown in figure 48(a) were obtained from plates which snap-buckled or in which the buckling stress was measured in a manner that tended to minimize the effects of initial eccentricity such as by the selection of the top of the knee of a torque-twist plot. The data of figure 48(b) were obtained primarily from determinations of buckling torque by means considerably more sensitive than were used for the data of figure 48(a). For example, Kuhn and Levin used optical strain gages to plot sheet strain as a function of load and selected the point of departure from a straight line as the torque at which buckling was presumed to occur. In this latter group one snap buckle occurred.

In general, the data agree fairly well with the theory. The results of Kuhn and Levin for strips of large width lie as close to the cylinder curve as some of the data reported in the section entitled "Cylinders Under Torsion." This tends to substantiate further the use of the linear theory for torsional buckling of cylinders. It should be noted in figure 48(a) that the buckling coefficients for $Z_b = 0$ are equal to those reported in reference 1 for flat plates loaded in shear.

Behavior of Curved Plates Buckling Under Shear

An infinitely long rectangular plate with transverse curvature will buckle under shear loading at a stress greater than the flat plate of the same developed width as a result of the restraint of radial deflection due to the curvature. Curves of buckling coefficient appear in figures 49(a) and 49(b) as a function of Z_b for the infinitely long curved plate with both clamped and simply supported edges with no restraint to motion normal to the axial edges. The values of the buckling coefficients for these two cases have a constant ratio for all values of Z_b. This suggests that for intermediate values of edge rotational restraint, the buckling coefficient could be determined with the aid of figure 23(a) of reference 1, in which k_s is plotted as a function of edge rotational restraint for an infinitely long flat panel.

As the plate length becomes relatively short the buckling stress is influenced not only by the axial boundary conditions but by the circumferential conditions as well. When the length becomes small compared with the plate width, the curved plate behaves like a short cylinder, or like a flat plate, which is the limiting case of a short cylinder. In this case, the axial boundary conditions no longer influence the buckling stress of the curved plate and the circumferential boundary conditions govern.

In this transition from infinite to zero length, two a/b ranges are defined depending upon whether the plate is long or wide. The square plate $(a/b = 1)$ marks the division between these ranges. In the wide-plate range the limiting buckling behavior is that of the cylinder, while in the long-plate range the infinitely long plate is at the other limit. The relation between buckling coefficient and Z_b may be seen in figures 49(a) to 49(d). It should be recalled that, because of its definition, a/b is always greater than 1, and the meanings of k_s and Z_b change at $a/b = 1$. It is evident from the curves that wide plates tend toward cylinder behavior more rapidly, as a/b increases, than do the long plates toward the behavior of the infinitely long plate.

Numerical Values of Buckling Stress

On the basis of the good agreement between data and theory for curved plates loaded in pure shear, the curves presented in figure 49 may be used in conjunction with the buckling-stress equation

$$\tau_{cr} = \frac{k_s \pi^2 E}{12(1 - \nu_e^2)} \left(\frac{t}{b}\right)^2 \tag{85}$$

For small values of Z_b, equation (85) becomes the flat-plate equation and k_s may be found from the charts presented in Part I of the Handbook (ref. 1).

The buckling stress for a long curved plate loaded in shear has been found by Batdorf, Stein, and Schildcrout (ref. 79) to be of the form

$$\tau_{cr} = \frac{k_s \pi^2 E}{12(1 - \nu_e^2)} \left(\frac{t}{b}\right)^2 (Z_b)^{1/2} \tag{86}$$

where $Z_b > 30$. The ratio of the curved-plate-buckling stress to the corresponding flat-plate-buckling stress has been found to be $0.37(Z_b)^{1/2}$ for $Z_b > 30$, for both simply supported and clamped edges. Utilizing this ratio for plates with any elastic rotational restraint, the buckling stress of a curved plate loaded in shear with $Z_b > 30$ can be found from

$$\tau_{cr} = 0.37 \tau_{cr_{\text{flat plate}}} (Z_b)^{1/2} \tag{87}$$

The critical shear stress of the long flat plate may be determined from reference 1.

Plasticity-Reduction Factors

The shear secant modulus was shown to be the appropriate plasticity-reduction factor for long, flat, rectangular plates in shear (ref. 1) and for long circular cylinders in torsion (see section "Cylinders Under Torsion"). It is reasonable to suggest, therefore, that the shear secant modulus may be applicable to long plates with slight curvature and to wide curved plates which tend to behave as long cylinders and long flat plates, respectively.

Effects of Internal Pressure

Brown and Hopkins (ref. 83) solved the classical equilibrium equations to determine the effect of radially outward pressure upon the shear-buckling stress of curved panels and obtained fair agreement with test data of Rafel and Sandlin (ref. 70).

The data also correlate well with the parabolic interaction curve used for the effect of internal pressure upon cylinders in torsion and upon curved plates in axial compression. For curved plates in shear,

$$R_s^2 + R_p = 1 \tag{88}$$

Agreement of the test data with this relation is shown in figure 50, which is of the form used by Crate, Batdorf, and Baab to correlate the data for cylinders buckling in torsion under internally applied pressure (ref. 45).

CURVED PLATES UNDER COMBINED SHEAR AND LONGITUDINAL COMPRESSION

By use of a set of equilibrium equations, Kromm investigated the critical loading for a long curved plate with simply supported edges subjected to the simultaneous application of shear and longitudinal compression (ref. 53). With the aid of Donnell's equation, Batdorf, Schildcrout, and Stein extended this analysis to long curved plates with clamped edges (refs. 67 and 84).

As indicated in the preceding section, a long curved plate under shear buckles at a stress in close agreement with the theoretical value derived from linear theory. However, as shown in the section "Curved Plates Under Axial Compression," the action of axially compressed long curved plates departs appreciably from the predictions of linear theory. Consequently, a linear analysis of buckling under the combination of these loads would be unconservative. Batdorf, Schildcrout, and Stein recognized this and, therefore, recommended the use of empirical data to determine the buckling stress of the curved panel under axial compression.

Batdorf, Schildcrout, and Stein derived a theoretical interaction equation by use of linear theory in the form

$$R_s^2 + R_x = 1 \tag{89}$$

in which the axial stress may be either tension or compression. Since compression stress would have the positive sign in this convention, it would be necessary to use the negative sign for tension.

The stress ratios are defined as the ratio of the stress in the long panel at buckling under combined loading to the buckling stress

under simple loading. In order to account for the discrepancy between theory and experiment for axial-compressive loading, Batdorf, Schildcrout, and Stein suggested using the empirical instead of the theoretical value of buckling stress which may be found in the section "Curved Plates Under Axial Compression." When this change is made, equation (85) may be used to compute critical combinations of loading for this case. Comparisons of test data with the parabolic interaction curves for simply supported curved plates under combined shear and axial compression are given in figure 51.

Research Division, College of Engineering,
New York University,
New York, N. Y., July 20, 1955.

APPENDIX A

APPLICATION SECTION

Procedures for numerical computation of buckling stress of curved plates and shells are summarized in this appendix. For information on details of stress-strain curves, Poisson's ratio, and the effects of cladding, reference 1 should be consulted.

In the summaries below, references are made to the ranges of behavior of the components discussed. The geometric parameters are displayed in figure 4, while sketches appear in figure 5 depicting the influence of geometry upon the buckle pattern for an axially compressed cylinder.

Compressive Buckling

Circular cylinders.- In the short-cylinder range $\left(L^2/rt < 1\right)$, the flat-plate equation may be used:

$$\sigma_{cr} = \eta \frac{k_c \pi^2 E}{12\left(1 - \nu_e^2\right)}\left(\frac{t}{L}\right)^2 \tag{A1}$$

For values of η and k_c, the charts in reference 1 for axially compressed flat plates may be used.

In the transition-length range $\left(1 < L^2/rt < 100\right)$ equation (A1) may be used for elastic stresses, employing figure 6 to determine k_c. If desired, use may be made of the magnification-factor chart of figure 9 to account for end effects.

In the long-cylinder range $\left(L^2/rt > 100\right)$, the modified classical buckling-stress equation (67)

$$\sigma_{cr} = \eta C E t/r \tag{67}$$

may be used, where C can be obtained from figure 7.

The plasticity-reduction factor for this case is equation (75)

$$\eta = \frac{E_s}{E}\left[\frac{E_t}{E_s}\frac{\left(1 - \nu_e^2\right)}{\left(1 - \nu^2\right)}\right]^{1/2} \tag{75}$$

which is given in nondimensional form in figure 11. In this chart

$$\epsilon_{cr} = Ct/r \tag{32}$$

Elliptic cylinders.- Timoshenko recommends using circular-cylinder-buckling data to compute the buckling stress of an elliptic cylinder. The pertinent radius of curvature occurs at the ends of the minor axis and is equal to a^2/b.

Curved plates.- Curved plates of large radius $\left(b^2/rt < 1\right)$ may be analyzed as flat plates using equation (A2) together with values of k_c and η from reference 1 for axially compressed flat plates:

$$\sigma_{cr} = \frac{k_c \pi^2 E}{12\left(1 - \nu_e^2\right)}\left(\frac{t}{b}\right)^2 \tag{A2}$$

For elastic stresses in the transition-length and transition-width ranges, figure 38(b) may be used to find k_c in conjunction with equation (A2). For curved plates of large radius $\left(b^2/rt > 100\right)$ equations (67) and (75) are valid, and the nondimensional buckling chart of figure 11 may be used.

For the effects of internal pressure the interaction equation

$$R_c^2 + R_p = 1 \tag{A3}$$

may be used, in which R_p is the quotient of the applied internal pressure and the critical external pressure that would buckle the cylinder.

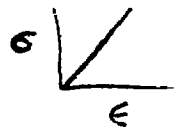

$E = \frac{\sigma}{\epsilon}$

Bending Buckling of Long Cylinders

Circular cylinders.- For long circular cylinders that buckle elastically

$$\sigma_{cr} = C_b E t/r = C_b \frac{\sigma}{\epsilon} \frac{t}{r} \qquad (34)$$

$\epsilon = \frac{\sigma}{E}$

where C_b, which contains a gradient factor of 1.3, may be found from figure 18.

To compute inelastic-buckling stresses of circular cylinders in bending, figure 25 may be used.

Elliptic cylinders.- For long elliptic cylinders that buckle elastically proceed as outlined in the section "Cylinders in Bending," employing figures 18, 19, 21, and 22.

Torsional Buckling of Cylinders

Circular cylinders.- For short cylinders $\left(L/r < 10(t/r)^{1/2}\right)$ the flat-plate equation

$$\tau_{cr} = \eta \frac{k_s \pi^2 E}{12\left(1 - \nu_e^2\right)}\left(\frac{t}{L}\right)^2 \qquad (A4)$$

may be used employing values of η and k_s from reference 1 for flat plates in shear.

For transition-length cylinders $\left(10(t/r)^{1/2} < L/r < 3(r/t)^{1/2}\right)$ either the general buckling-stress equation

$$\tau_{cr} = \eta \frac{k_t \pi^2 E}{12\left(1 - \nu_e^2\right)}\left(\frac{t}{L}\right)^2 \qquad (A5)$$

may be used employing figure 26 to determine k_t or one of the following equations may be employed: For clamped edges:

$$\tau_{cr} = \eta \frac{0.93 \pi^2 E}{12\left(1 - \nu_e^2\right)^{5/8}}\left(\frac{t}{r}\right)^{5/4}\left(\frac{r}{L}\right)^{1/2} \qquad (A6)$$

For simply supported edges:

$$\tau_{cr} = \eta \frac{0.85\pi^2 E}{12\left(1 - \nu_e^2\right)^{5/8}}\left(\frac{t}{r}\right)^{5/4}\left(\frac{r}{L}\right)^{1/2} \tag{A7}$$

For long cylinders $\left(L/r > 3(r/t)^{1/2}\right)$:

$$\tau_{cr} = \eta \frac{0.272E}{\left(1 - \nu_e^2\right)^{3/4}}\left(\frac{t}{r}\right)^{3/2} \tag{49}$$

utilizing η from equation (A8) or the nondimensional buckling chart of figure 32.

The stresses obtained from equations (A4) to (A7) are approximately 16 percent higher than the average of the test data. For conservatism this correction factor may be used.

The plasticity-reduction factor is

$$\eta = \frac{E_s}{E}\left(\frac{1 - \nu_e^2}{1 - \nu^2}\right)^{3/4} \tag{A8}$$

The nondimensional buckling chart of figure 32 may be used with

$$\epsilon_{cr} = \tau_{cr}/\eta E \tag{52}$$

The effect of internal pressure may be included by using the interaction equation

$$R_t^2 + R_p = 1 \tag{53}$$

Elliptic cylinders and D-tubes.- The data for circular cylinders in torsion may be used providing that the semimajor axis of the elliptic section is chosen equal to r. Then

$$Z_L = L^2\left(1 - \nu_e^2\right)^{1/2}/at \tag{A9}$$

Shear Buckling of Curved Plates

For plates of large radius flat-plate buckling-stress equation (A4) is applicable. For values of k_s and η Part I of the Handbook (ref. 1) may be used.

For transition-length plates

$$\tau_{cr} = \frac{k_s \pi^2 E}{12\left(1 - \nu_e^2\right)}\left(\frac{t}{b}\right)^2 \tag{85}$$

for which k_s may be found in figure 49.

For $b^2/rt > 30$

$$\tau_{cr} = 0.37\left(Z_b\right)^{1/2} \tau_{cr_{flat\ plate}} \tag{87}$$

For the effects of internal pressure, the interaction equation

$$R_s^2 + R_p = 1 \tag{88}$$

may be used.

Buckling Under External Pressure

Circular cylinders.- For short and transition-length cylinders $\left(L^2/rt < 100\right)$ which buckle elastically under radial pressure

$$\sigma_{cr} = \frac{k_y \pi^2 E}{12\left(1 - \nu_e^2\right)}\left(\frac{t}{L}\right)^2 \tag{55}$$

where figure 35(a) may be used to find k_y.

Under hydrostatic pressure

$$\sigma_{cr} = \eta \frac{k_p \pi^2 E}{12\left(1 - \nu_e^2\right)}\left(\frac{t}{L}\right)^2 \tag{A10}$$

where figure 35(b) is used to find k_p.

For long cylinders $\left(100 \frac{t}{r} < (L/r)^2 < 5r/t\right)$ the buckling stress may be found from either equation (55) or equation (A10) and is essentially the same for both cases. It may also be computed using

$$\sigma_{cr} = 0.93E(t/r)^{3/2}(r/L) \tag{A11}$$

For very long cylinders $\left((L/r)^2 > 5(r/t)\right)$ under either radial or hydrostatic pressure

$$\sigma_{cr} = \eta \frac{0.25E}{\left(1 - \nu_e^2\right)}\left(\frac{t}{R}\right)^2 \tag{A12}$$

in which

$$\eta = \frac{E_s}{E} \frac{\left(1 - \nu_e^2\right)}{\left(1 - \nu^2\right)}\left(\frac{1}{4} + \frac{3}{4} \frac{E_t}{E_s}\right) \tag{59}$$

Spherical plates.- In all diameter ranges, for elastic buckling,

$$\sigma_{cr} = \frac{k_p \pi^2 E}{12\left(1 - \nu_e^2\right)}\left(\frac{t}{d}\right)^2 \tag{83}$$

where k_p may be found in figure 47.

For plates with $d^2/rt > 100$, the modified classical buckling-stress equation

$$\sigma_{cr} = \eta C E t/r \tag{67}$$

may be used in conjunction with figure 46 and η from equation (75).

Buckling Under Combined Loads

Circular cylinders.- See table 5 and figures 36 and 37 for interaction equations and stress-ratio relationships.

Curved plates.- For curved plates under combined axial compression and shear, with $10 < Z_b < 100$ and $1 < a/b < 3$,

$$R_s^2 + R_x = 1 \tag{89}$$

REFERENCES

1. Gerard, George and Becker, Herbert: Handbook of Structural Stability. Part I - Buckling of Flat Plates. NACA TN 3781, 1957.

2. Becker, Herbert: Handbook of Structural Stability. Part II - Buckling of Composite Elements. NACA TN 3782, 1957.

3. Batdorf, S. B.: A Simplified Method of Elastic-Stability Analysis for Thin Cylindrical Shells. I - Donnell's Equation. NACA TN 1341, 1947.

4. Timoshenko, S.: Theory of Elastic Stability. First ed., McGraw-Hill Book Co., Inc., 1936.

5. Flügge, Wilhelm: Statik und Dynamik der Schalen. Julius Springer (Berlin). 1934.

6. Donnell, L. H.: Stability of Thin-Walled Tubes Under Torsion. NACA Rep. 479, 1933.

7. Gerard, George: Compressive and Torsional Buckling of Thin-Wall Cylinders in Yield Region. NACA TN 3726, 1956.

8. Donnell, L. H.: A New Theory for the Buckling of Thin Cylinders Under Axial Compression and Bending. Trans. A.S.M.E., vol. 56, no. 11, Nov. 1934, pp. 795-806.

9. Von Kármán, T.: Encyklopädie der Mathematische Wissenschaften. Vol. IV, 1910, p. 349.

10. Von Kármán, Theodore, and Tsien, Hsue-Shen: The Buckling of Thin Cylindrical Shells Under Axial Compression. Jour. Aero. Sci., vol. 8, no. 8, June 1941, pp. 303-312.

11. Batdorf, S. B.: A Simplified Method of Elastic-Stability Analysis for Thin Cylindrical Shells. II - Modified Equilibrium Equation. NACA TN 1342, 1947.

12. Tsien, Hsue-Shen: A Theory for the Buckling of Thin Shells. Jour. Aero. Sci., vol. 9, no. 10, Aug. 1942, pp. 373-384.

13. Robertson, Andrew: The Strength of Tubular Struts. R. & M. 1185, British A.R.C., 1927.

14. Lundquist, Eugene E.: Strength Tests of Thin-Walled Duralumin Cylinders in Compression. NACA Rep. 473, 1933.

15. Southwell, R. V.: On the General Theory of Elastic Stability. Phil. Trans. Roy. Soc. (London), ser. A, vol. 213, 1914, pp. 187-244.

16. Batdorf, S. B., Schildcrout, Murry, and Stein, Manuel: Critical Stress of Thin-Walled Cylinders in Axial Compression. NACA TN 1343, 1947.

17. Leggett, D. M. A., and Jones, R. P. N.: The Behaviour of a Cylindrical Shell Under Axial Compression When the Buckling Load Has Been Exceeded. R. & M. No. 2190, British A.R.C., 1942.

18. Michielsen, Herman F.: The Behavior of Thin Cylindrical Shells After Buckling Under Axial Compression. Jour. Aero. Sci., vol. 15, no. 12, Dec. 1948, pp. 738-744.

19. Kempner, Joseph: Postbuckling Behavior of Axially Compressed Circular Cylindrical Shells. Jour. Aero. Sci., vol. 21, no. 5, May 1954, pp. 329-335.

20. Donnell, L. H., and Wan, C. C.: Effect of Imperfections on Buckling of Thin Cylinders and Columns Under Axial Compression. Jour. Appl. Mech., vol. 17, no. 1, Mar. 1950, pp. 73-83.

21. Osgood, William R.: The Crinkling Strength and the Bending Strength of Round Aircraft Tubing. NACA Rep. 632, 1938.

22. Moore, R. L., and Holt, Marshall: Beam and Torsion Tests of Aluminum-Alloy 61S-T Tubing. NACA TN 867, 1942.

23. Moore, R. L., and Clark, J. W.: Torsion, Compression, and Bending Tests of Tubular Sections Machined From 75S-T6 Rolled Round Rod. NACA RM 52I25, 1952.

24. Bijlaard, P. P.: Theory and Tests on the Plastic Stability of Plates and Shells. Jour. Aero. Sci., vol. 16, no. 9, Sept. 1949, pp. 529-541.

25. Stowell, Elbridge Z.: A Unified Theory of Plastic Buckling of Columns and Plates. NACA Rep. 898, 1948.

26. Lo, Hsu, Crate, Harold, and Schwartz, Edward B.: Buckling of Thin-Walled Cylinder Under Axial Compression and Internal Pressure. NACA TN 2021, 1950.

27. Brazier, L. G.: The Flexure of Thin Cylindrical Shells and Other "Thin" Sections. R. & M. No. 1081, British A.R.C., 1927. Also Proc. Roy. Soc. (London), ser. A, vol. 116, 1927, pp. 104-111.

28. Flügge, W.: Die Stabilität der Kreiszylinderschale Ing.-Archiv., Bd. 3, 1932, pp. 463-506.

29. Lundquist, Eugene E.: Strength Tests of Thin-Walled Duralumin Cylinders in Pure Bending. NACA TN 479, 1933.

30. Lundquist, Eugene E., and Burke, Walter F.: Strength Tests of Thin-Walled Duralumin Cylinders of Elliptic Section. NACA TN 527, 1935.

31. Heck, O. S.: The Stability of Orthotropic Elliptic Cylinders in Pure Bending. NACA TM 834, 1937.

32. Fralich, Robert W., Mayers, J., and Reissner, Eric: Behavior in Pure Bending of a Long Monocoque Beam of Circular-Arc Cross Section. NACA TN 2875, 1953.

33. Anderson, Roger A., Pride, Richard A., and Johnson, Aldie E., Jr.: Some Information on the Strength of Thick-Skin Wings With Multiweb and Multipost Stabilization. NACA RM L53F16, 1953.

34. Greenhill, A. G.: On the Strength of Shafting When Exposed to Torsion and to End Thrust. Proc. Institution Mech. Eng. (London), Apr. 1883.

35. Schwerin, E.: Die Torsionsstabilität des dünnwändigen Rohres. Proc. First Int. Cong. Appl. Mech. (Apr. 1924, Delft), Technische Boekhandel en Drukkerij J. Waltman, Jr. (Delft), 1925, pp. 255-265.

36. Lundquist, Eugene E.: Strength Tests on Thin-Walled Duralumin Cylinders in Torsion. NACA TN 427, 1932.

37. Leggett, D. M. A.: The Elastic Stability of a Long and Slightly Bent Rectangular Plate Under Uniform Shear. Proc. Roy. Soc. (London), ser. A., vol. 162, no. 908, Sept. 1, 1937, pp. 62-83.

38. Batdorf, S. B., Stein, Manuel, and Schildcrout, Murry: Critical Stress of Thin-Walled Cylinders in Torsion. NACA TN 1344, 1947.

39. Stang, Ambrose H., Ramberg, Walter, and Back, Goldie: Torsion Tests of Tubes. NACA Rep. 601, 1937.

40. Moore, R. L., and Paul, D. A.: Torsional Stability of Aluminum Alloy Seamless Tubing. NACA TN 696, 1939.

41. Moore, R. L., and Wescoat, C.: Torsion Tests of Stiffened Circular Cylinders. NACA WR W-89, 1944. (Formerly NACA ARR 4E31.)

42. Hopkins, H. G., and Brown, E. H.: The Effect of Internal Pressure on the Initial Buckling of Thin-Walled Circular Cylinders Under Torsion. R. & M. No. 2423, British A.R.C., 1946.

43. Crate, Harold, Batdorf, S. B., and Baab, George W.: The Effect of Internal Pressure on the Buckling Stress of Thin-Walled Circular Cylinders Under Torsion. NACA WR L-67, 1944. (Formerly NACA ARR L4E27.)

44. Gerard, G.: Critical Shear Stress of Plates Above the Proportional Limit. Jour. Appl. Mech., vol. 15, no. 1, Mar. 1948, pp. 7-12.

45. Sherwood, A. W.: The Strength of Thin-Wall Cylinders of D Cross Section in Combined Pure Bending and Torsion. NACA TN 904, Sept. 1943.

46. Kavanaugh, E. S., and Drinkwater, W. D.: Torsional Strength of Stiffened D-Tubes. NACA TN 2362, 1951.

47. Sturm, R. G.: A Study of the Collapsing Pressure of Thin-Walled Cylinders. Bull. No. 329, Eng. Exp. Station, Univ. of Ill., Nov. 1941.

48. Windenberg, D. F., and Trilling, C.: Collapse by Instability of Thin Cylindrical Shells Under External Pressure. Trans. A.S.M.E., vol. 56, no. 11, Nov. 1934, pp. 819-825.

49. Kempner, J., Pandalai, K. A. V., and Patel, S. A.: Postbuckling Behavior of Circular Cylindrical Shells Under Hydrostatic Pressure. PIBAL Rep. No. 256, Polytechnic Inst. of Brooklyn, May 1954.

50. Bridget, F. J., Jerome, C. C., and Vosseller, A. B.: Some New Experiments on Buckling of Thin-Wall Construction. Trans. A.S.M.E., vol. 56, no. 8, Aug. 1934, pp. 569-578.

51. Ballerstedt, W., and Wagner, H.: Versuch über die Festigkeit dünner unversteifter Zylinder. Luftfahrtforschung, Bd. 13, Nr. 9, Nov. 20, 1936, pp. 309-312.

52. Leggett, D. M. A.: The Initial Buckling of Slightly Curved Panels Under Combined Shear and Compression. R. & M. No. 1972, British A.R.C., 1943.

53. Kromm, A.: The Limit of Stability of a Curved Plate Strip Under Shear and Axial Stresses. NACA TM 898, 1939.

54. Bruhn, Elmer F.: Tests on Thin-Walled Celluloid Cylinders to Determine the Interaction Curves Under Combined Bending, Torsion, and Compression or Tension Loads. NACA TN 951, 1945.

55. Batdorf, S. B., Stein, Manuel, and Schildcrout, Murry: Critical Combinations of Torsion and Direct Axial Stress for Thin-Walled Cylinders. NACA TN 1345, 1947.

56. Lundquist, Eugene E.: Strength Tests of Thin-Walled Duralumin Cylinders in Combined Transverse Shear and Bending. NACA TN 523, 1935.

57. Redshaw, S. C.: The Elastic Instability of a Thin Curved Panel Subjected to An Axial Thrust, Its Axial and Circumferential Edges Being Simply Supported. R. & M. No. 1565, British A.R.C., 1933.

58. Sechler, E. E., and Dunn, L. G.: Airplane Structural Analysis and Design. John Wiley & Sons, Inc., 1942.

59. Stowell, Elbridge Z.: Critical Compressive Stress for Curved Sheet Supported Along All Edges and Elastically Restrained Against Rotation Along the Unloaded Edges. NACA WR L-691, 1943. (Formerly NACA RB 3107.)

60. Cox, H. L., and Clenshaw, W. J.: Compression Tests on Curved Plates of Thin Sheet Duralumin. R. & M. No. 1894, British A.R.C., 1941.

61. Crate, Harold, and Levin, L. Ross: Data on Buckling Strength of Curved Sheet in Compression. NACA WR L-557, 1943. (Formerly NACA ARR 3J04.)

62. Jackson, K. V., and Hall, A. H.: Curved Plates in Compression. Rep. AR-1 (MM-180), Nat. Res. Council, 1947.

63. Welter, Georges: Influence of Different Factors on Buckling Loads of Curved Thin Aluminum-Alloy Sheet for Monocoque Construction. Jour. Aero. Sci., vol. 13, no. 4, Apr. 1946, pp. 204-208, 217.

64. Welter, Georges: The Effect of the Radius of Curvature and Preliminary Artificial Eccentricities on Buckling Loads of Curved Thin Aluminum-Alloy Sheets for Monocoque Constructions. Jour. Aero. Sci., vol. 13, no. 11, Nov. 1946, pp. 593-596, 604. (See also letter to the ed. by H. L. Cox and reply by Georges Welter, Jour. Aero. Sci., vol. 14, no. 6, June 1947, pp. 333-335.)

65. Schuette, E. H.: Buckling of Curved Sheet in Compression and Its Relation to the Secant Modulus. Jour. Aero. Sci., vol. 15, no. 1, Jan. 1948, pp. 18-22.

66. Cox, H. L., and Pribram, E.: The Elements of the Buckling of Curved Plates. Jour. R.A.S., vol. 52, no. 453, Sept. 1948, pp. 551-565.

67. Batdorf, S. B., Schildcrout, Murry, and Stein, Manuel: Critical Combinations of Shear and Longitudinal Direct Stress for Long Plates with Transverse Curvature. NACA TN 1347, 1947.

68. Gerard, George: Handbook of Structural Stability, Part IV - Failure of Plates and Composite Elements. NACA TN 3784, 1957.

69. Eastman, E. J., McDonald, J. C., and Moore, A. A.: The Relation of Stress to Strain in Magnesium Base Alloys. Jour. Aero. Sci., vol. 12, no. 3, July 1945, pp. 273-280.

70. Rafel, Norman, and Sandlin, Charles W., Jr.: Effect of Normal Pressure on the Critical Compressive and Shear Stress of Curved Sheet. NACA WR L-57, 1944. (Formerly NACA ARR L5B10.)

71. Rafel, Norman: Effect of Normal Pressure on the Critical Compressive Stress of Curved Sheet. NACA WR L-258, 1942. (Formerly NACA RB.)

72. Zoelly, R.: Dissertation, Zürich, 1915.

73. Schwerin, E.: Zur Stabilität der dünnwandigen Hohlkugel unter gleichmassigem Aussendruck. Z.a.M.M., Bd. 2, Heft 2, Apr. 1922, pp. 81-91.

74. Van der Neut, A.: Dissertation, Delft, 1932.

75. Kaplan, A., and Fung, Y. C.: A Nonlinear Theory of Bending and Buckling of Thin Elastic Shallow Spherical Shells. NACA TN 3212, 1954.

76. Loo, T. T.: Effects of Large Deflections and Imperfections on Buckling of Thin Cylinders and Columns Under Axial Compression. Ph. D. Thesis, Ill. Inst. of Tech., 1952.

77. Klein, B.: Parameters Predicting the Initial and Final Collapse Pressures of Uniformly Loaded Spherical Shells. Reader's Forum, Jour. Aero. Sci., vol. 22, no. 1, Jan. 1955, pp. 69-70.

78. Batdorf, S. B., Schildcrout, Murry, and Stein, Manuel: Critical Shear Stress of Long Plates With Transverse Curvature. NACA TN 1346, 1947.

79. Batdorf, S. B., Stein, Manuel, and Schildcrout, Murry: Critical Shear Stress of Curved Rectangular Panels. NACA TN 1348, 1947.

80. Rafel, Norman: Effect of Normal Pressure on the Critical Shear Stress of Curved Sheet. NACA WR L-416, 1943. (Formerly NACA RB.)

81. Kuhn, Paul, and Levin, L. Ross: An Empirical Formula for the Critical Shear Stress of Curved Sheets. NACA WR L-58, 1944. (Formerly NACA ARR L5A05.)

82. Chiarito, Patrick T.: Some Strength Tests of Stiffened Curved Sheets Loaded in Shear. NACA WR L-259, 1944. (Formerly NACA RB L4D29.)

83. Brown, E. H., and Hopkins, H. G.: The Initial Buckling of a Long and Slightly-Bowed Panel Under Combined Shear and Normal Pressure. R. & M. No. 2766, British A.R.C., 1949.

84. Schildcrout, Murry, and Stein, Manuel: Critical Combinations of Shear and Direct Axial Stress for Curved Rectangular Panels. NACA TN 1928, 1949.

TABLE 1

MEMBRANE STRESS STATES WHEN BUCKLING OCCURS FOR VARIOUS CASES

Element	Loading	Superimposed transverse membrane stresses	Correlation of test data and linear theory
Column	Compression	None	Satisfactory
Flat plate	Compression Shear Bending	Tension	Satisfactory
Cylinder and cylindrical plate	Compression Bending Torsion or shear Lateral pressure	Compression Compression Tension Tension	Unsatisfactory Unsatisfactory Satisfactory Satisfactory
Sphere and spherical plate	Lateral pressure	Compression	Unsatisfactory

TABLE 2

RATIO OF BENDING- TO AXIAL-COMPRESSIVE-BUCKLING STRESS FOR MATCHED CIRCULAR CYLINDERS

[Data of Donnell (ref. 8); average γ for all tests, 1.46]

Steel cylinders		Brass cylinders	
Number	$\gamma = \sigma_{b_{cr}}/\sigma_{c_{cr}}$ (a)	Number	$\gamma = \sigma_{b_{cr}}/\sigma_{c_{cr}}$ (a)
1	1.36	1	1.49
2	1.10	2	2.62
3	1.18	3	1.18
4	.96	4	1.99
5	1.50	5	1.95
6	1.69	6	2.26
7	1.02	7	1.28
8	1.67	8	2.18
9	.86	9	1.29
10	1.04	10	1.34
11	1.37	11	.80
	Av. 1.25		Av. 1.67

[a] $\sigma_{b_{cr}}$, bending-buckling stress; $\sigma_{c_{cr}}$, compressive-buckling stress.

TABLE 3

DATA FOR CIRCULAR-ARC SECTIONS IN BENDING

[All specimens were fabricated from 7075-T6 aluminum alloy and were 120 in. long]

Specimen	H/t	H/c	r/t	Z_L	$\sigma_{exp}/\sigma_{emp}$
1	3.3	0.04	667	146	1.43
2	7.6	.08	333	293	1.16
3	10.5	.10	250	390	1.15

TABLE 4

GRADIENT FACTORS FOR CIRCULAR-ARC SECTIONS

C_1 (from table 3)	C_2 (from fig. 7, using U = 0.00015)	$\gamma = C_1/C_2$
0.408	0.270	1.51
.331	.250	1.32
.329	.395	.83

TABLE 5

INTERACTION EQUATIONS FOR CIRCULAR CYLINDERS

UNDER COMBINED LOADINGS

Loading	Interaction equation	Applicable range (a)
Axial compression and bending	$R_c + R_b = 1$	All values of Z_L, all edge restraints
Axial compression and torsion	$R_c + R_t^2 = 1$	Using theoretical σ_{cr} and τ_{cr}, $Z_L < 1$, SS; $Z_L < 5$, C
		Using empirical σ_{cr} and τ_{cr}, $1 < Z_L < 7.7(r/t)^2$, SS; $5 < Z_L < 7.7(r/t)^2$, C
Axial tension and torsion	$0.4R_c + R_t = 1$	Using theoretical τ_{cr}, $-1 < R_c < 0$, $30 < Z_L < 7.7(r/t)^2$, both SS and C
Bending and torsion	$R_b^{1.5} + R_t^2 = 1$	All values of Z_L, all edge restraints

[a] SS, simply supported edges; C, clamped edges.

TABLE 6

PLATE DIMENSIONS FOR TEST SPECIMENS OF VARIOUS INVESTIGATORS

[All dimensions are in inches]

Dimension	Cox and Clenshaw (ref. 60)	Crate and Levin (ref. 61)	Jackson and Hall (ref. 62)	Schuette (ref. 65)
L	24	24	18	3 to 25
r	18, 36, ∞	11.4 to 121 and ∞	24, 48, ∞	3.25 to 21
b	4, 6, 8, 10, 12	[a]8.7	3 to 7	3.2 to 26
t	0.018 to 0.067	0.065 to 0.128	0.018 to 0.039	0.015 to 0.248

[a]Average value.

TABLE 7

IMPERFECTION PARAMETERS FOR TEST SPECIMENS

OF KAPLAN AND FUNG (ref. 75)

Specimen	r/t	σ_{cr}/σ_{cl}	d/t	a_o	U_o
1	316	0.464	635	0.249	2.17×10^{-4}
2	319	.425	645	.446	3.78
3	309	.439	635	.358	3.22
4	219	.373	640	.592	6.25
5	211	.414	635	.363	3.93
6	628	.708	1,210	.050	.17
7	602	.563	1,210	.156	.55
8	517	.521	1,230	.184	.73
9	384	.587	1,160	.118	.65
10	382	.517	1,250	.176	.99
11	372	.448	1,250	.386	2.30
12	851	.262	2,050	.292	.84
13	691	.369	2,000	.354	1.34
14	732	.315	2,050	.325	1.24
15	615	.356	1,950	.694	3.15
16	591	.402	1,950	.292	1.44
17	621	.332	2,220	.624	4.45
18	207	.404	635	.403	4.39
19	186	.442	635	.136	1.60
20	549	.654	1,160	.082	.32
21	359	.556	1,190	.114	.67
22	722	.379	2,000.	.323	1.17
23	606	.554	1,950	.148	.71
					[a]2.00

[a]Average value.

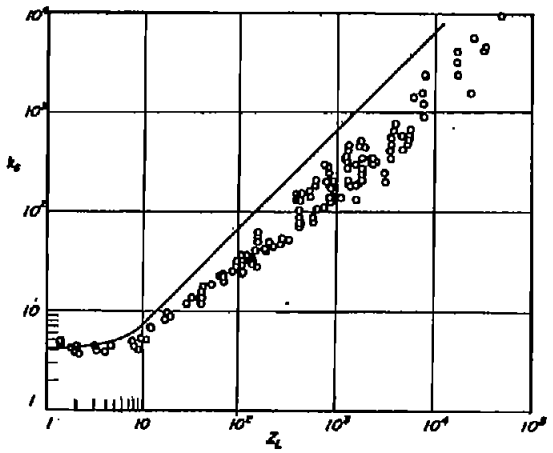

(a) Axial compression.

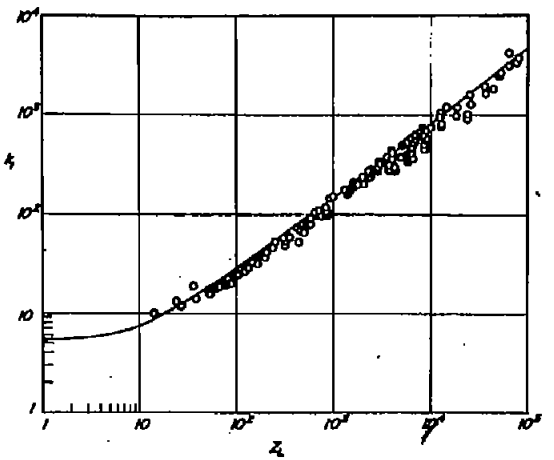

(b) Torsion.

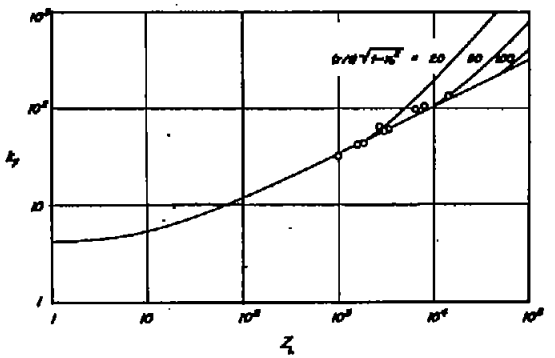

(c) External radial pressure.

Figure 1.- Comparison of linear buckling theory and test data for circular cylinders under axial compression, torsion, and external radial pressure.

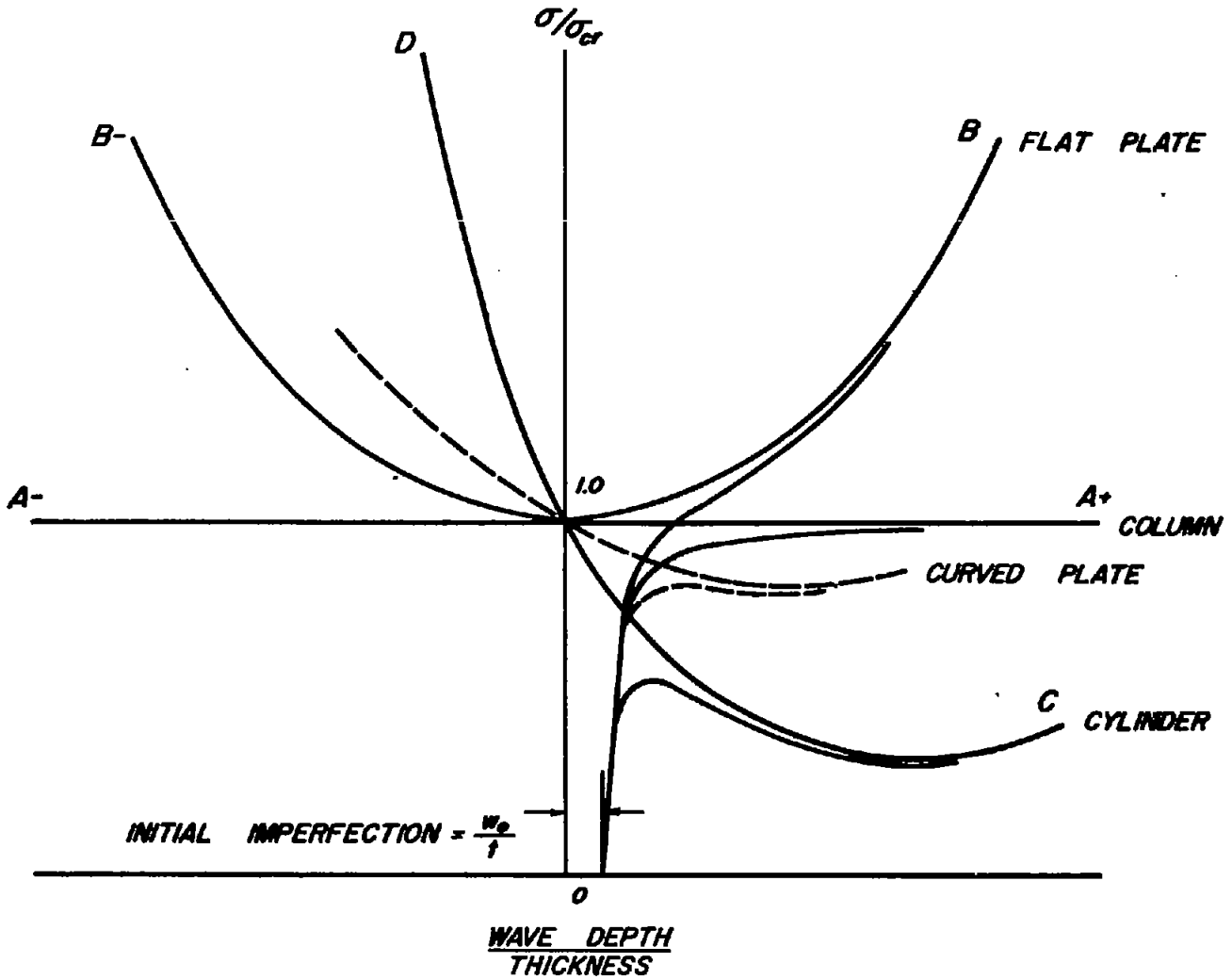

Figure 2.- Buckling-stress ratio as a function of buckle wave depth for axially compressed columns, plates, and cylinders.

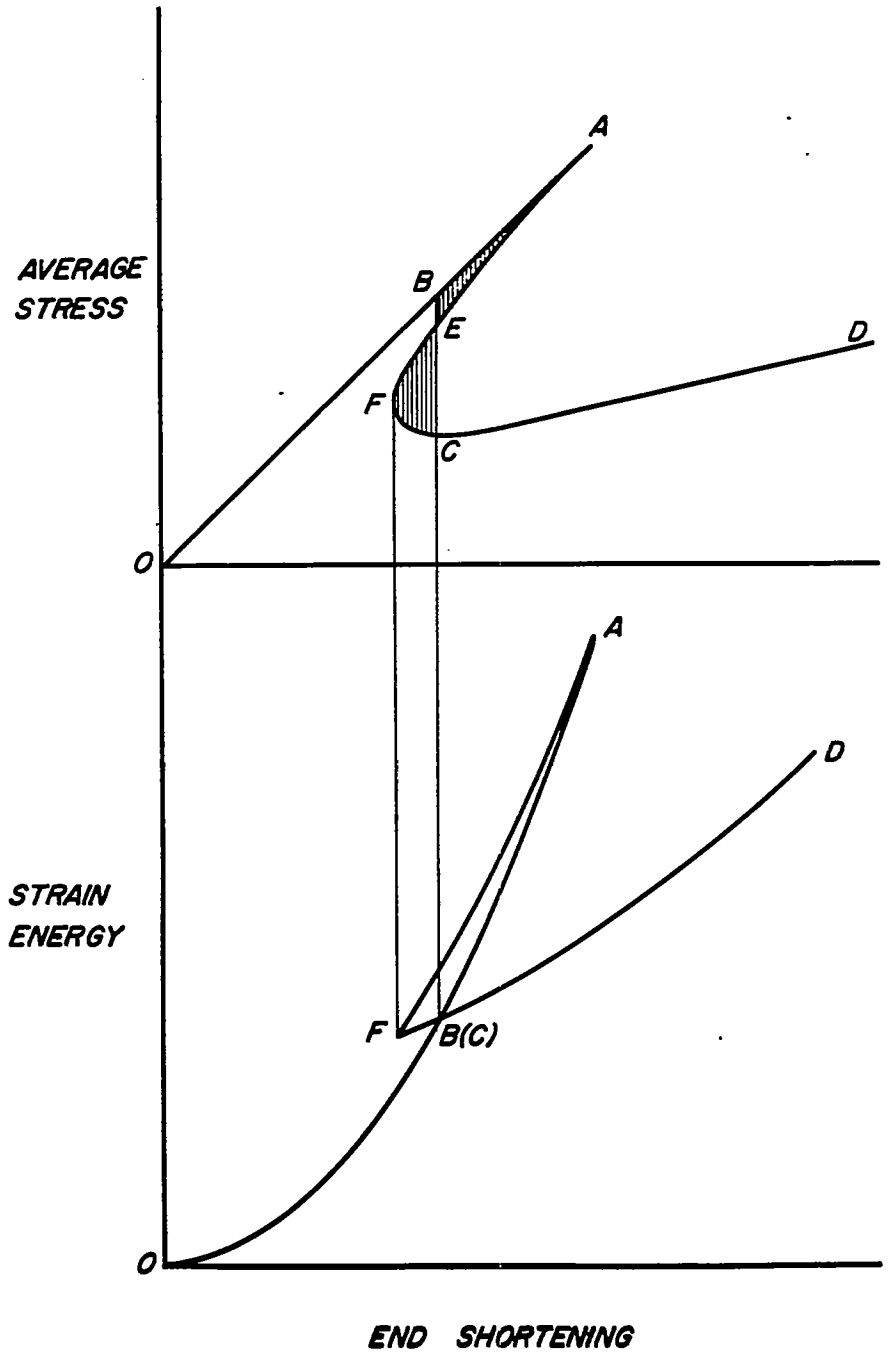

(a) Rigid testing machine.

Figure 3.- Theoretical behavior of axially compressed circular cylinder in rigid and dead-weight testing machines according to theory of Tsien (ref. 12).

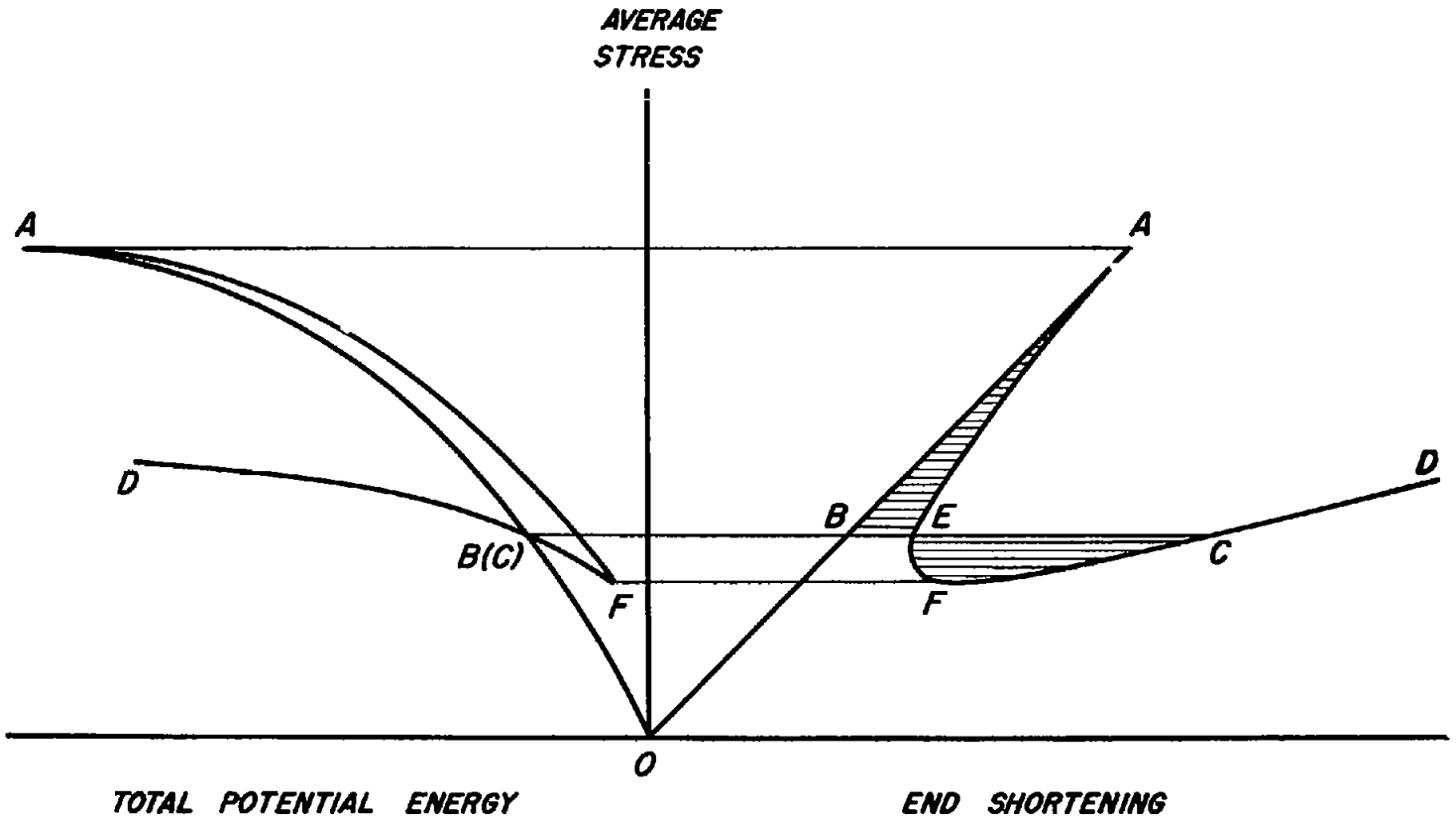

(b) Dead-weight testing machine.

Figure 3.- Concluded.

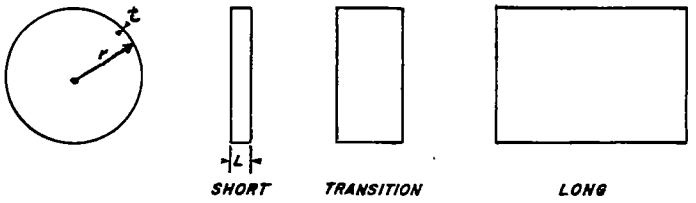

(a) Cylinder. $\sigma_{cr} = \frac{k\pi^2 E}{12\left(1 - \nu_e^2\right)}\left(\frac{t}{L}\right)^2$; $Z_L = \frac{L^2}{rt}\left(1 - \nu_e^2\right)^{1/2}$;

$k = f_{cylinder}\left(Z_L, r/t, L/r\right)$.

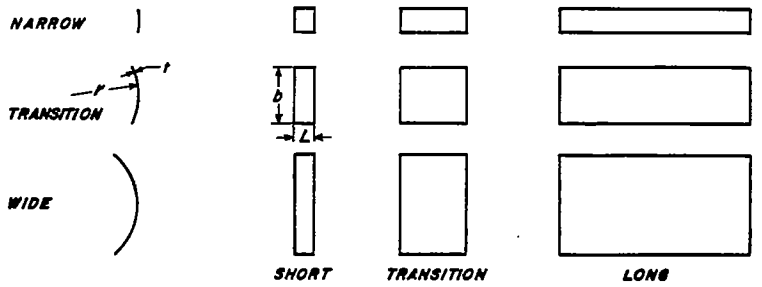

(b) Curved plate. $\sigma_{cr} = \frac{k\pi^2 E}{12\left(1 - \nu_e^2\right)}\left(\frac{t}{b}\right)^2$; $Z_b = \frac{b^2}{rt}\left(1 - \nu_e^2\right)^{1/2}$;

$k = f_{plate}\left(Z_b, r/t, L/r, r/b\right)$.

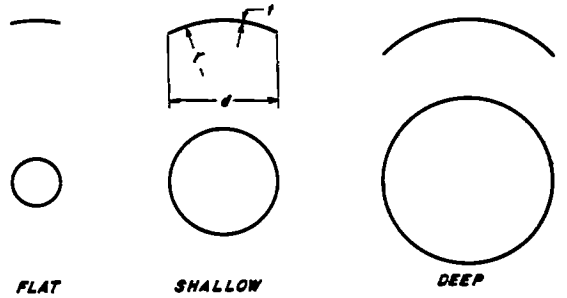

(c) Spherical cap. $\sigma_{cr} = \frac{k\pi^2 E}{12\left(1 - \nu_e^2\right)}\left(\frac{t}{d}\right)^2$; $Z_d = \frac{d^2}{rt}\left(1 - \nu_e^2\right)^{1/2}$;

$k = f_{cap}\left(Z_d, r/t, d/r\right)$.

Figure 4.- Geometrical parameters and ranges of behavior for cylinders, curved plates, and spherical caps.

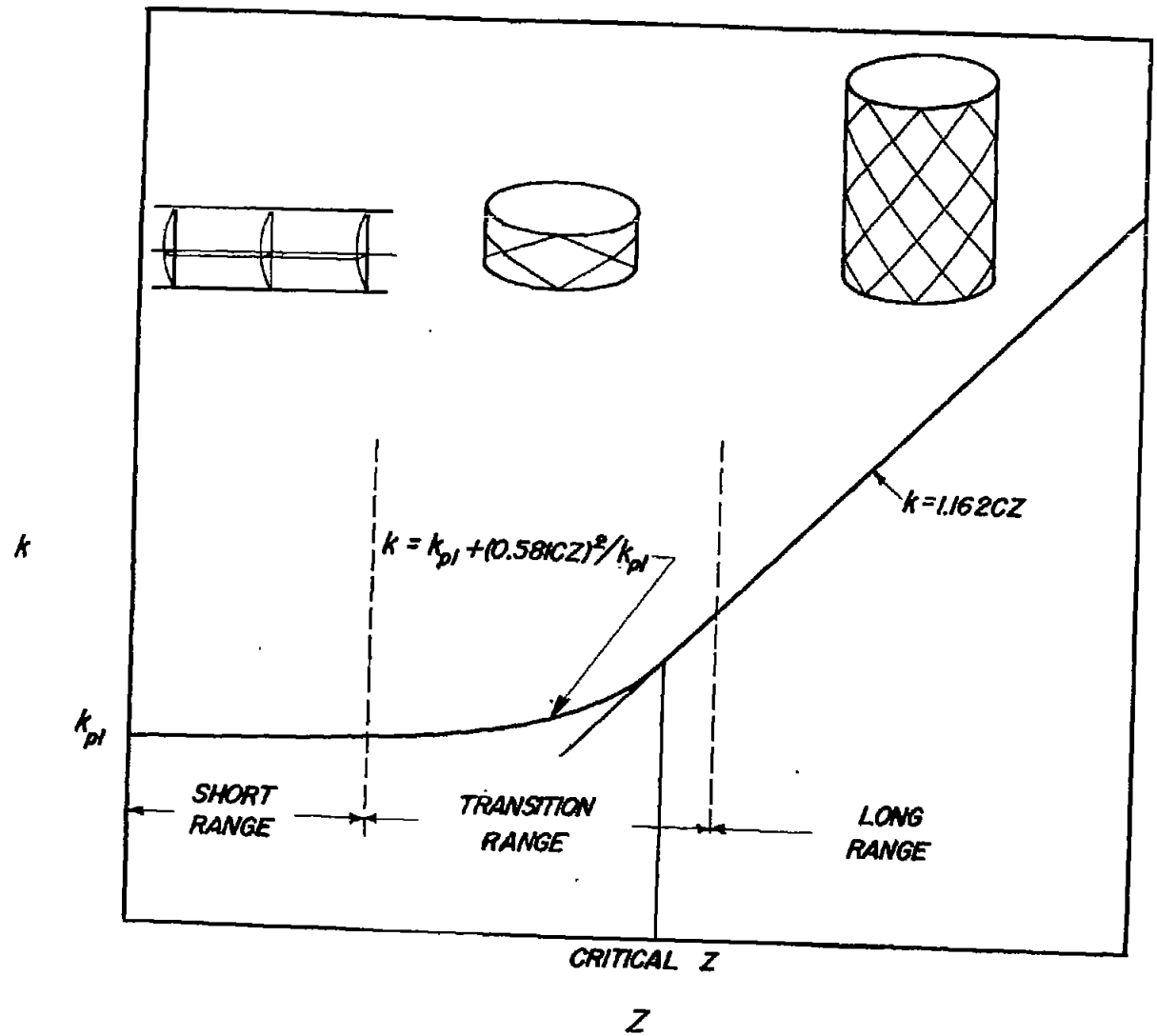

Figure 5.- Method of construction of curve for k as a function of Z. Typical buckle patterns shown for cylinder in each range of Z.

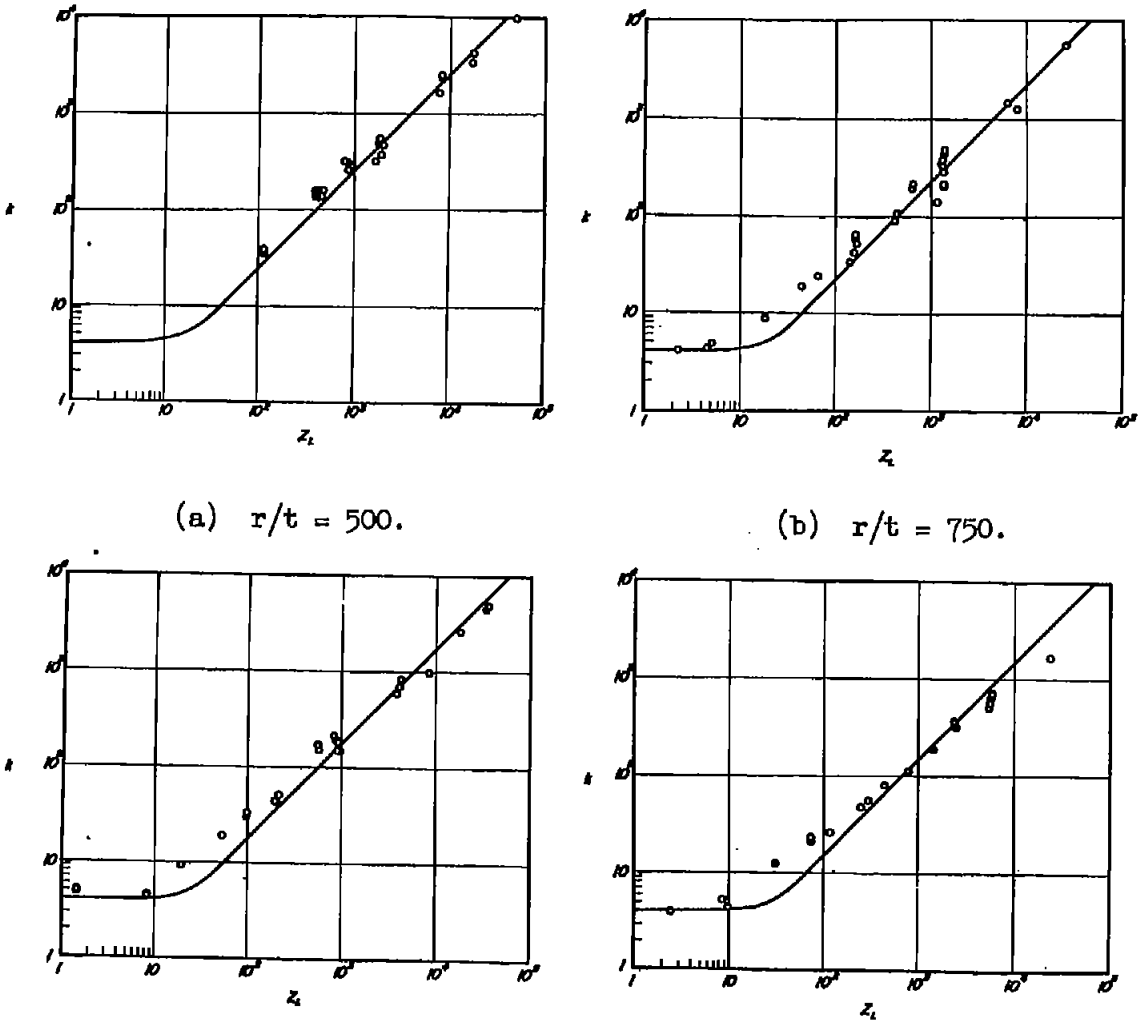

(a) r/t = 500.

(b) r/t = 750.

(c) r/t = 1,000.

(d) r/t = 1,250.

Figure 6.- Buckling test data and corresponding empirical curve for clamped axially compressed circular cylinders.

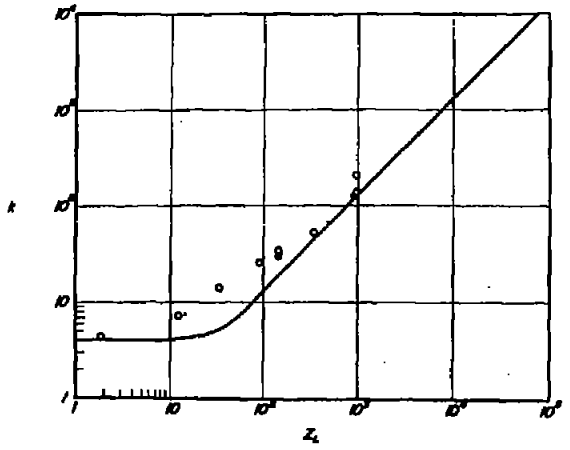

(e) r/t = 1,600.

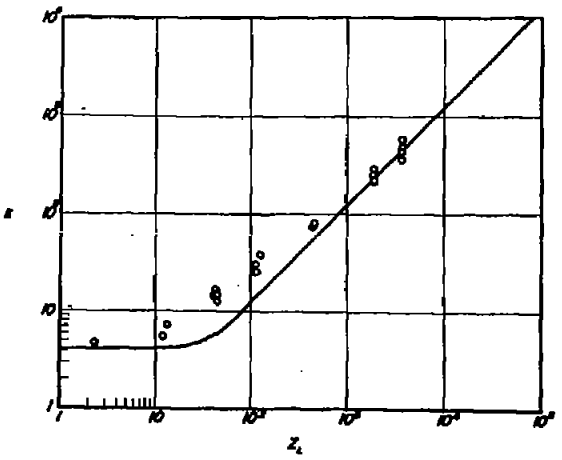

(f) r/t = 2,000.

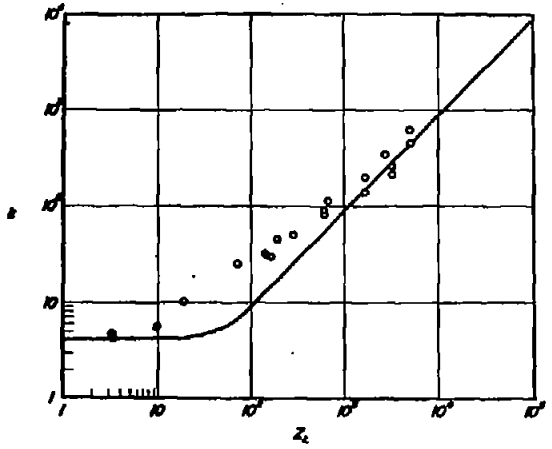

(g) r/t = 3,000.

Figure 6.- Concluded.

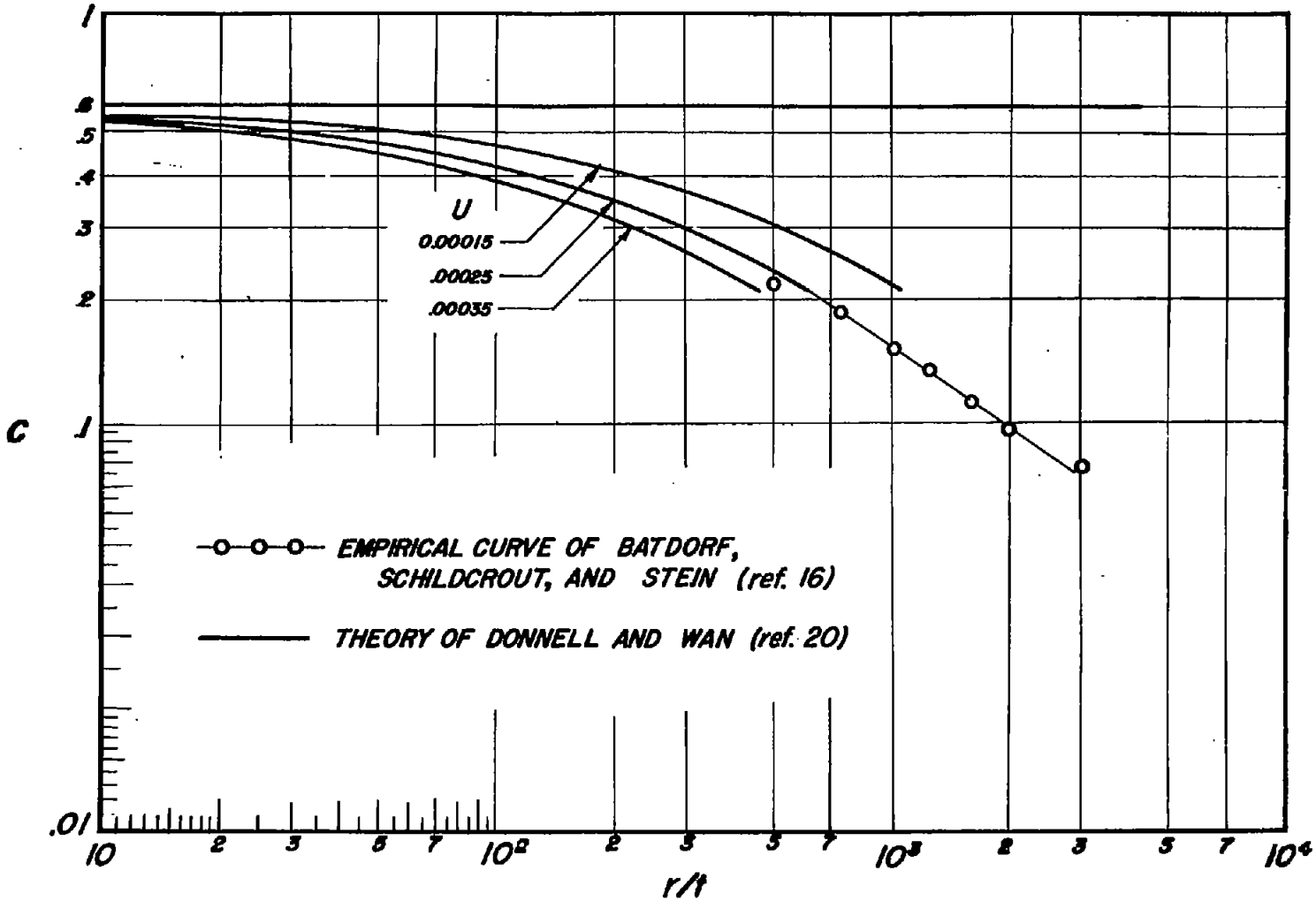

Figure 7.- Modified classical buckling coefficient as a function of r/t for axially compressed cylinders.

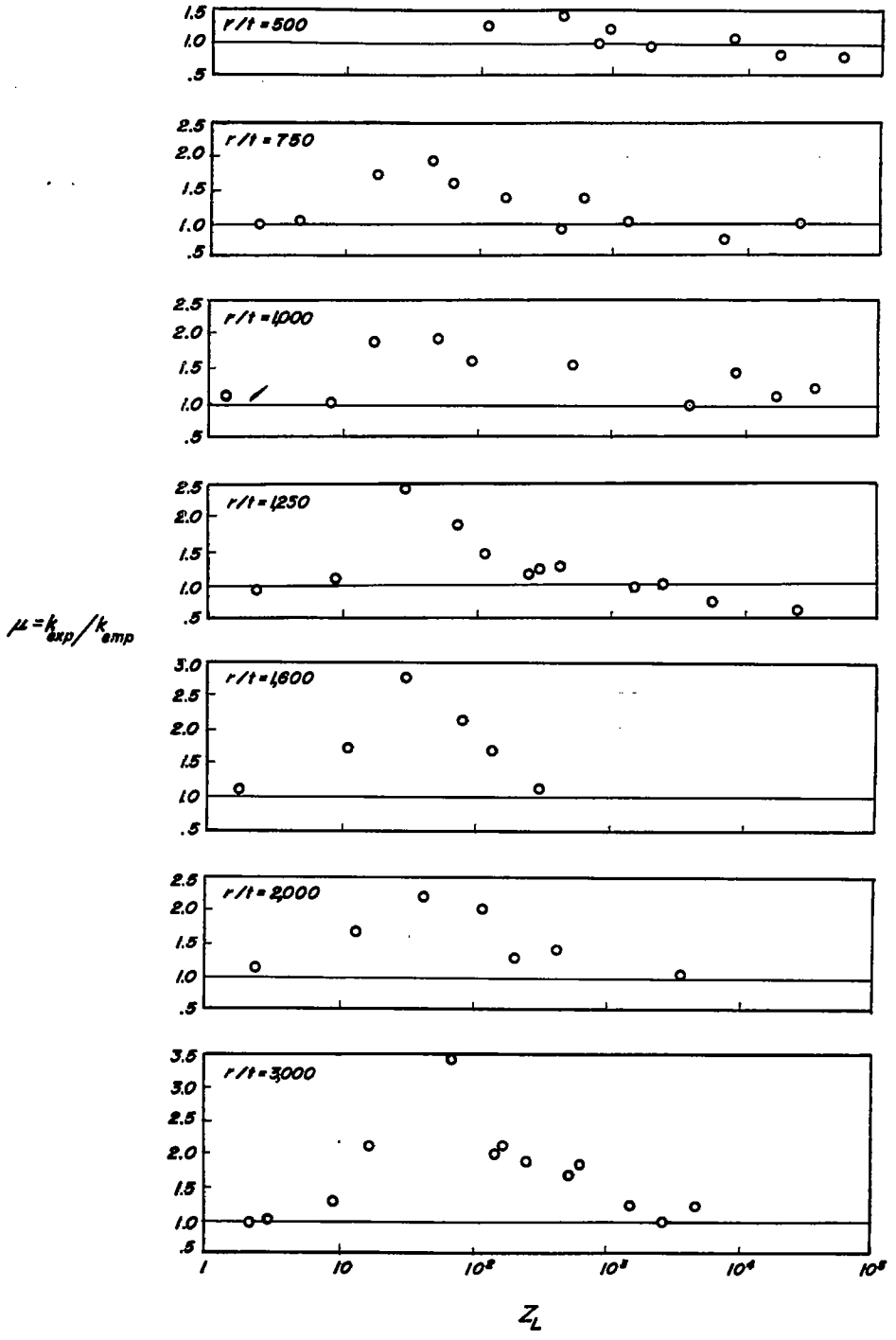

Figure 8.- Magnification factor for axially compressed cylinders derived from figure 6.

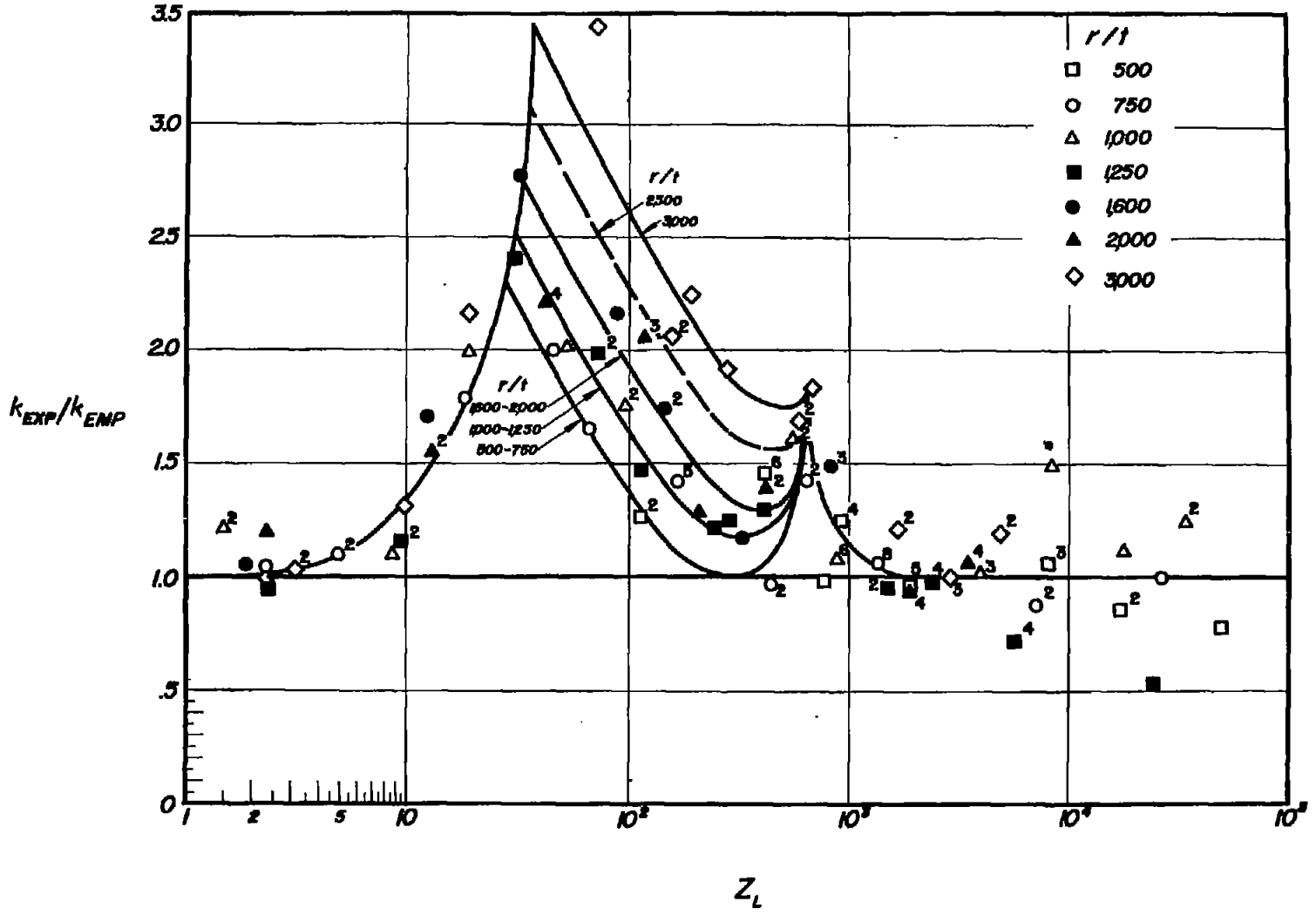

Figure 9.- Composite chart of magnification factors for axially compressed cylinders.

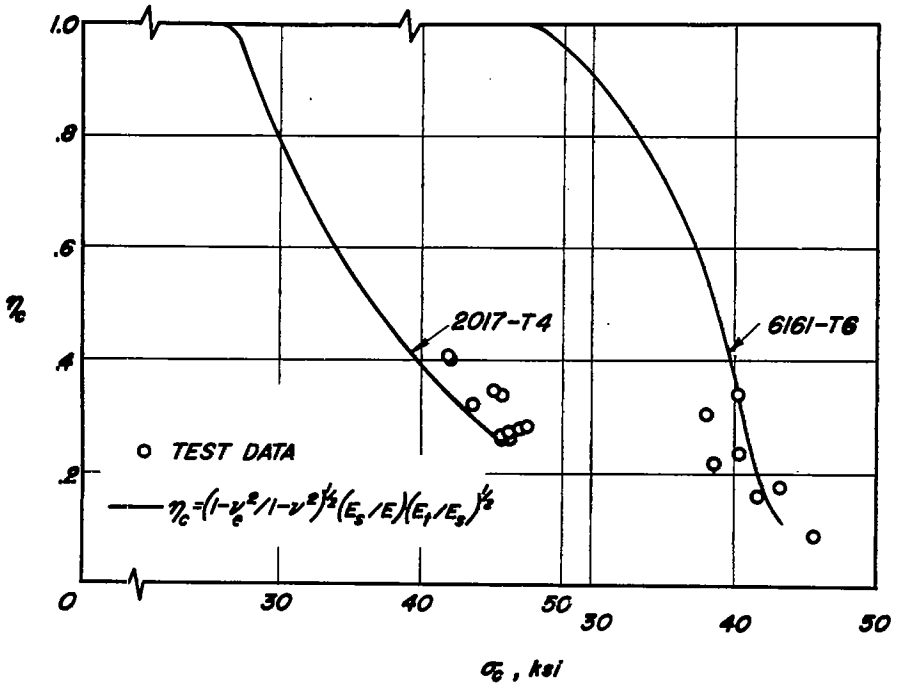

(a) Data in plastic range.

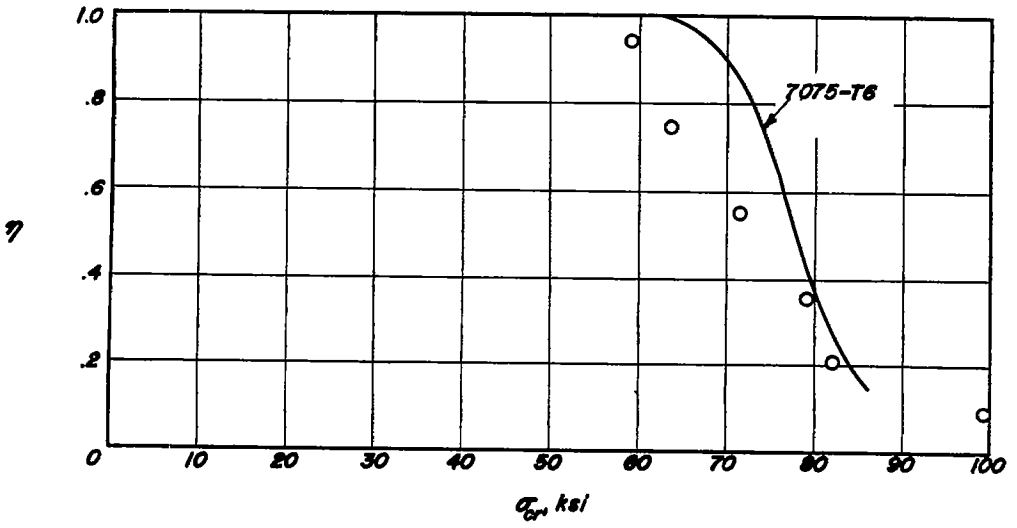

(b) Data in yield region.

Figure 10.- Plasticity-reduction factors for axially compressed long circular cylinders of aluminum alloy. Comparison of test data and theory using values of C from figure 7.

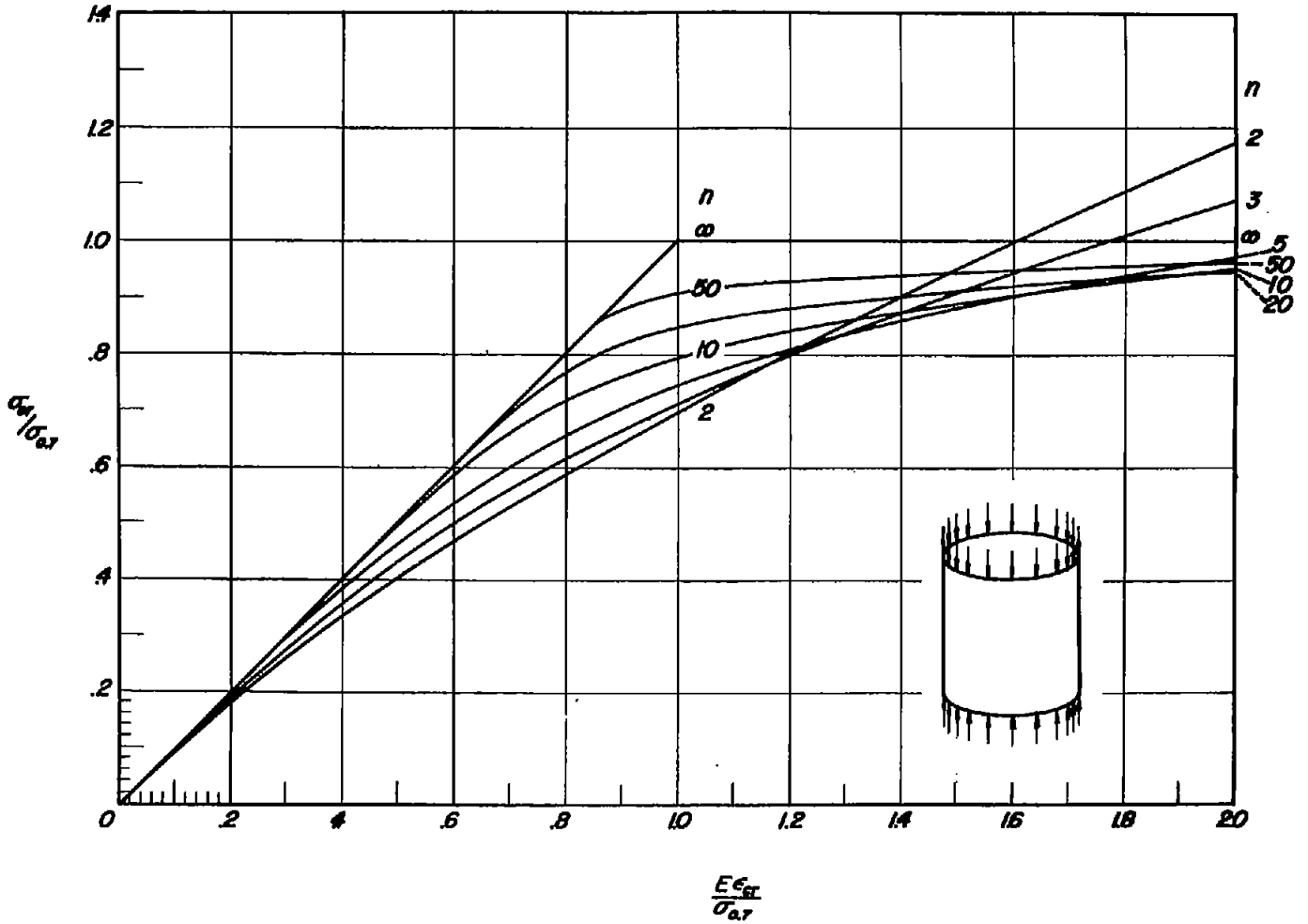

Figure 11.- Nondimensional buckling chart for axially compressed long circular cylinders.

$$\eta = \left(E_s/E\right)\left[\left(E_t/E\right)\left(1 - \nu_e^2\right)\Big/\left(1 - \nu^2\right)\right]^{1/2}.$$

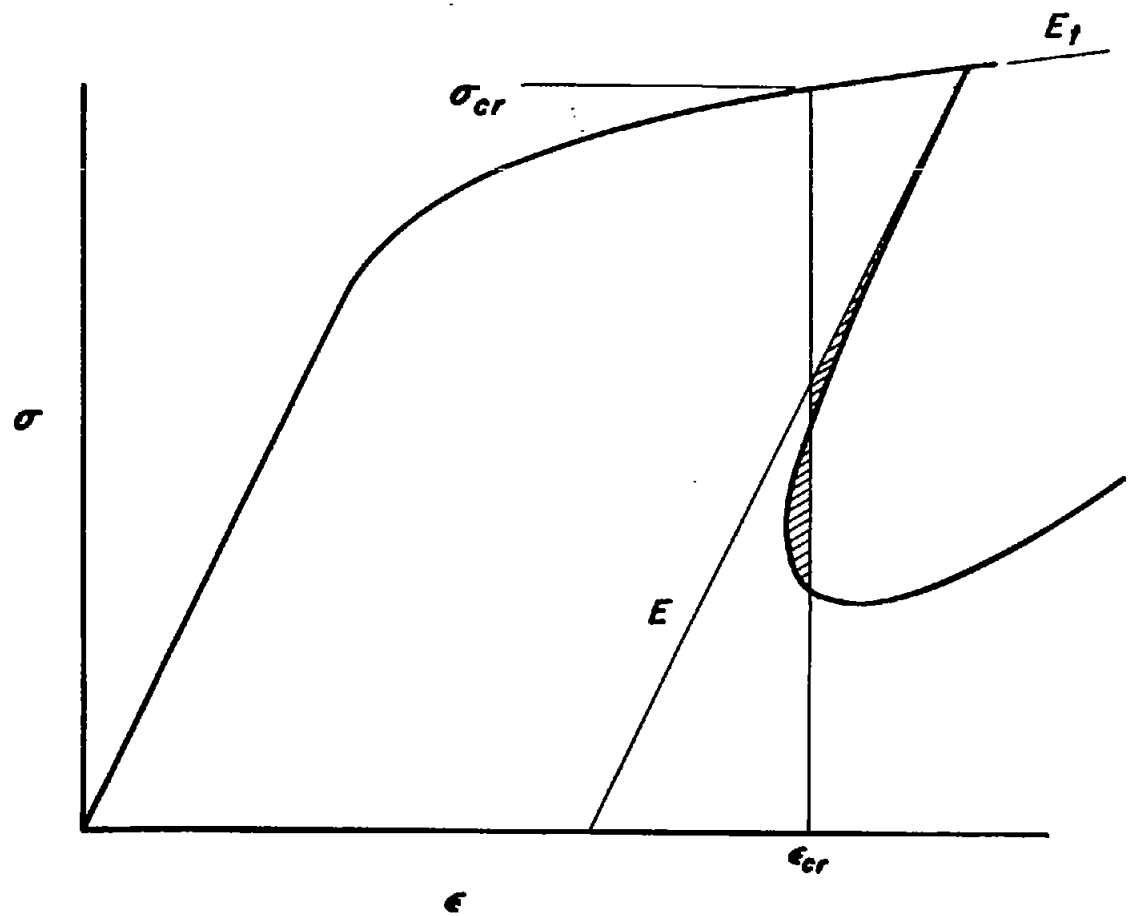

Figure 12.- Hypothetical buckling behavior of axially compressed circular cylinders in inelastic range.

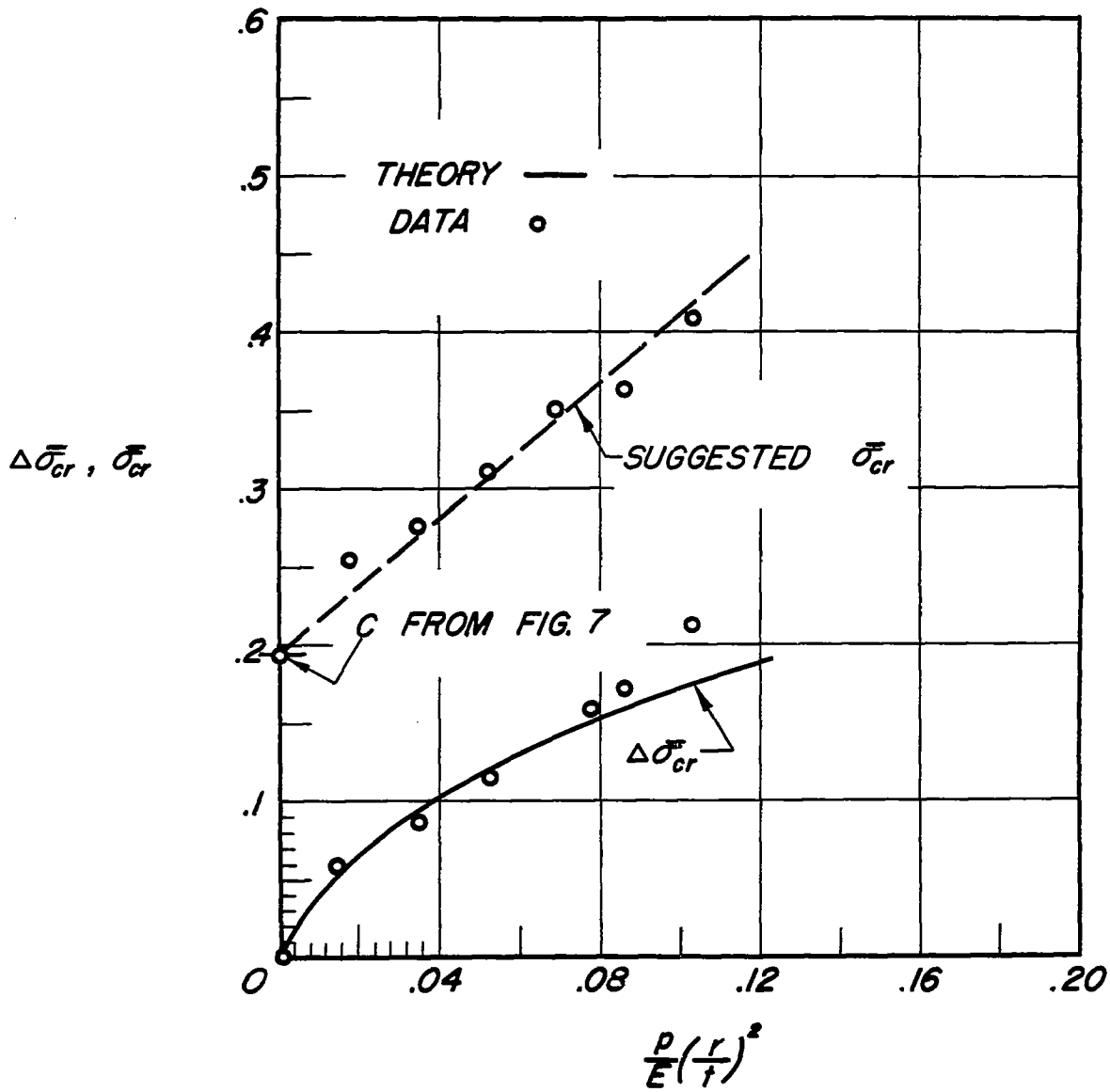

Figure 13.- Effect of internal pressure on axial-compressive-buckling stress of circular cylinders. $\bar{\sigma}_{cr} = \frac{\sigma_{cr} r}{Et}$.

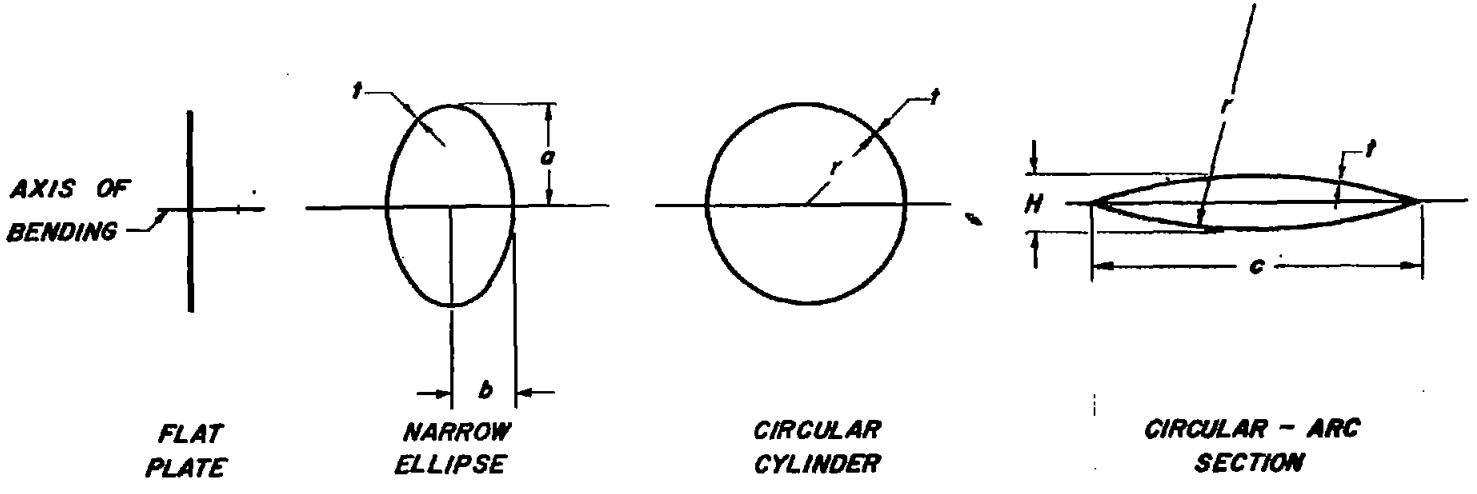

Figure 14.- Elliptic-cylinder geometry.

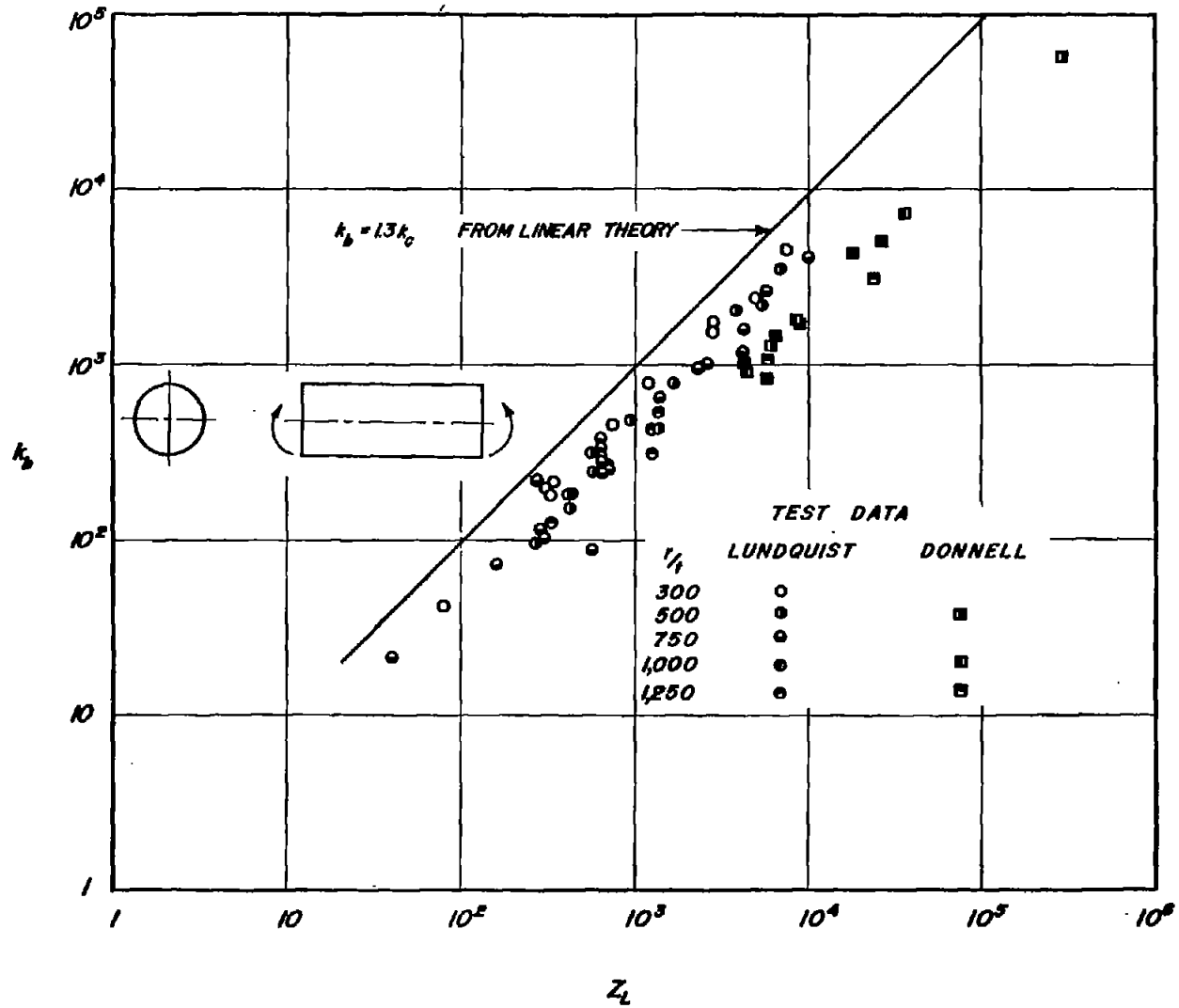

Figure 15.- Comparison of linear theory with bending-buckling data for circular cylinders. Data from Lundquist, reference 29; Donnell, reference 8.

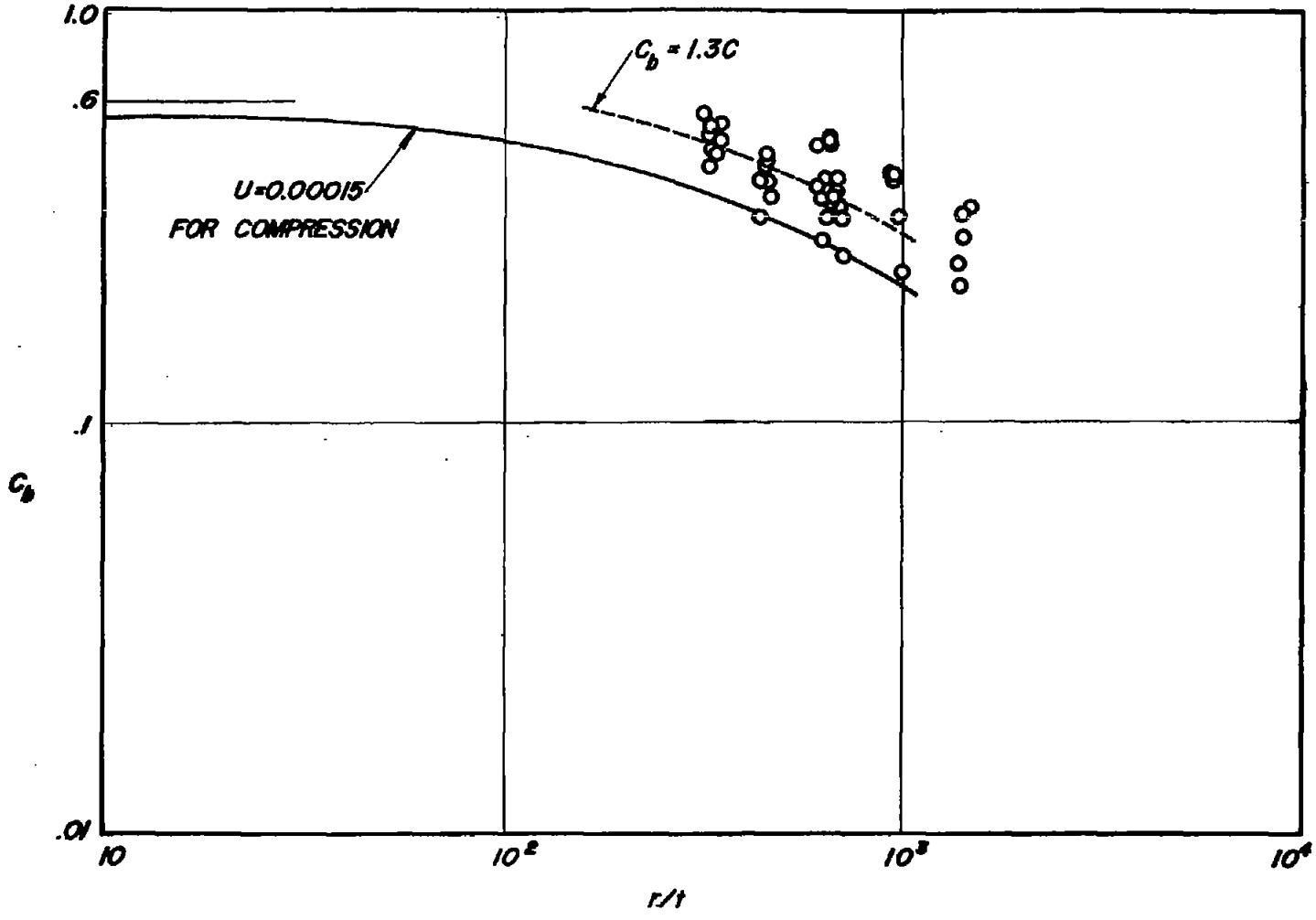

(a) Data of Lundquist for Duralumin sheet (ref. 29).

Figure 16.- Test data for long circular cylinders in bending.

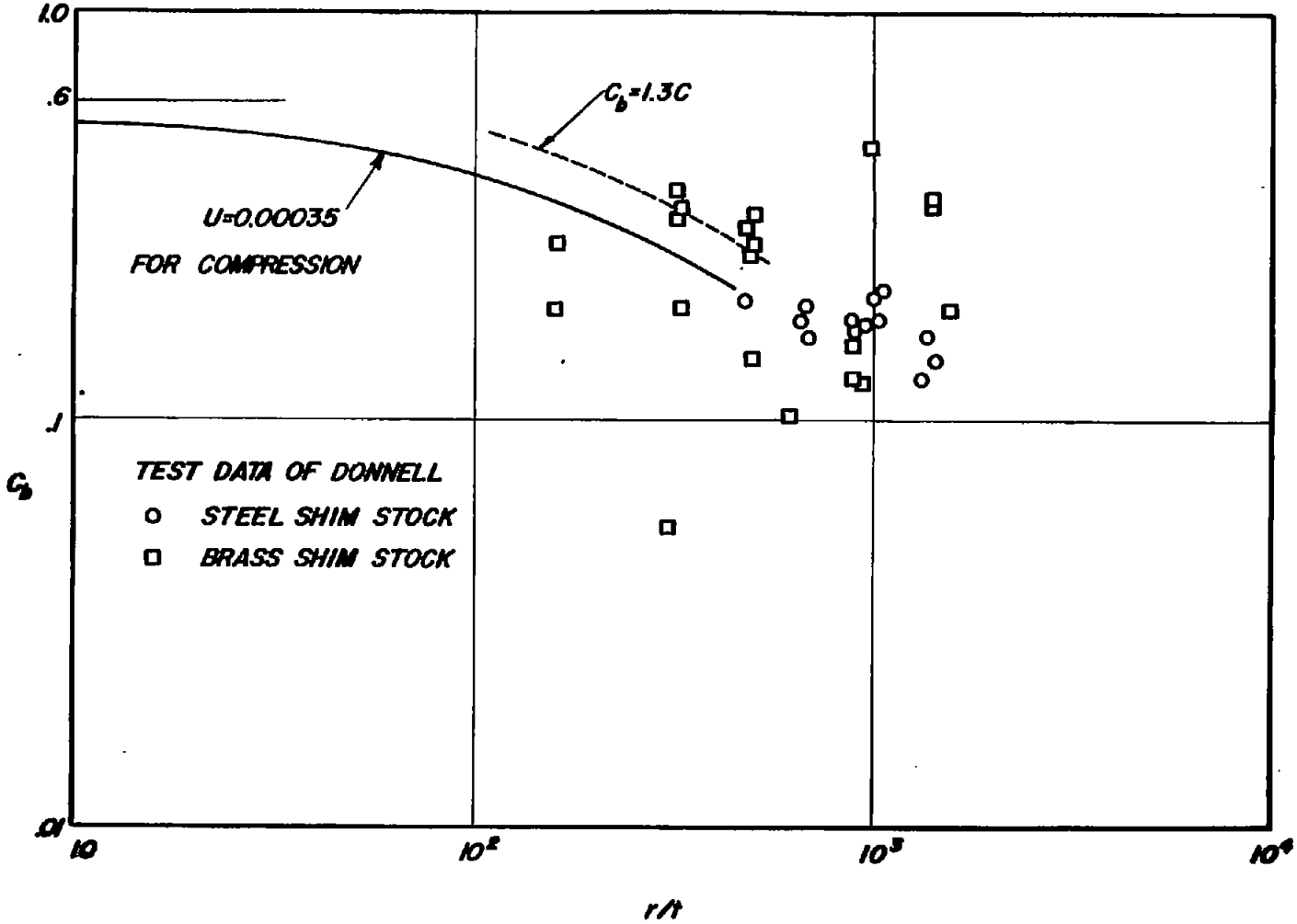

(b) Data of Donnell (ref. 8).

Figure 16.- Concluded.

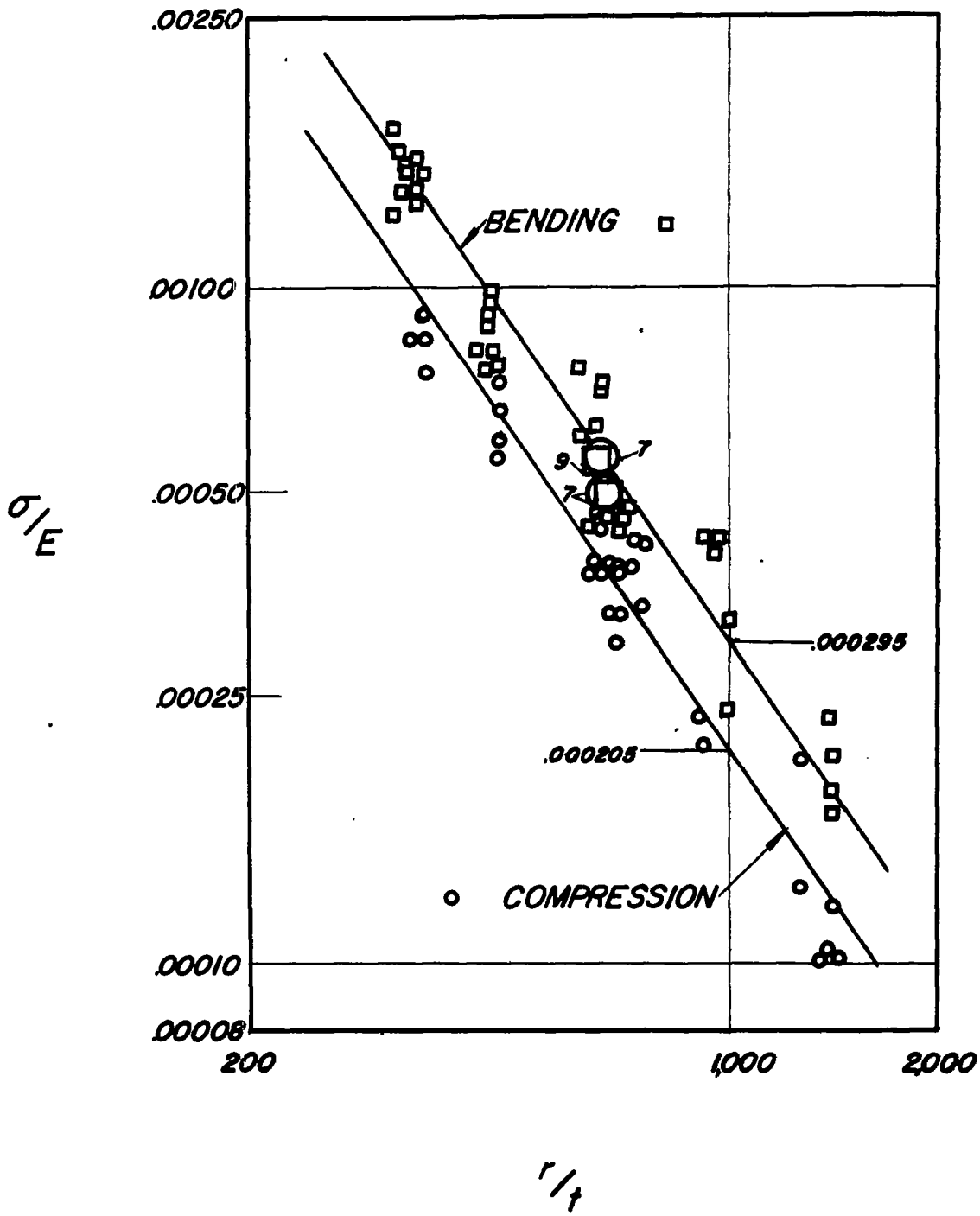

Figure 17.- Test data of Lundquist for long circular cylinders in axial compression and in bending (refs. 14 and 29).

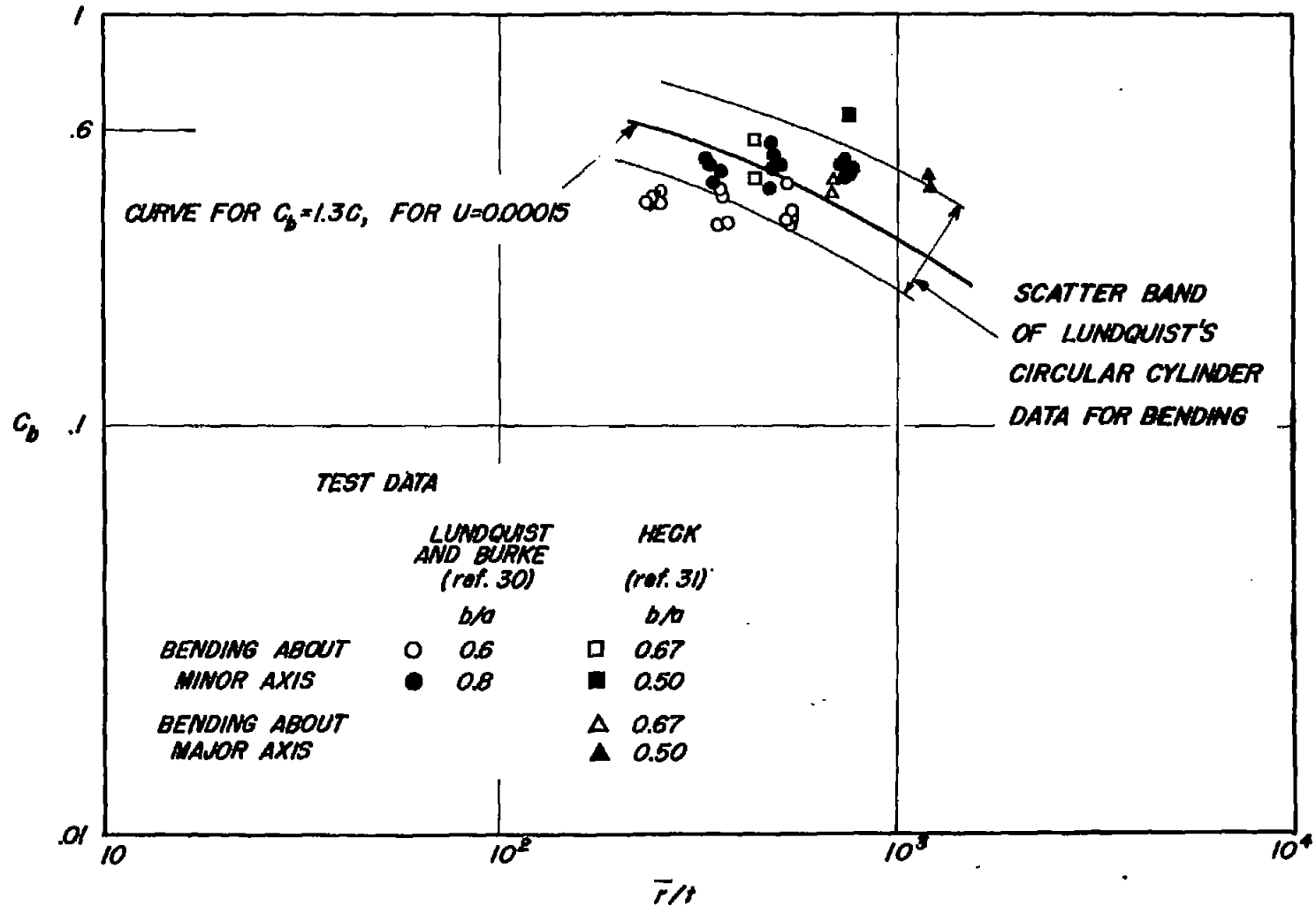

Figure 18.- Test data for long elliptic cylinders in bending.

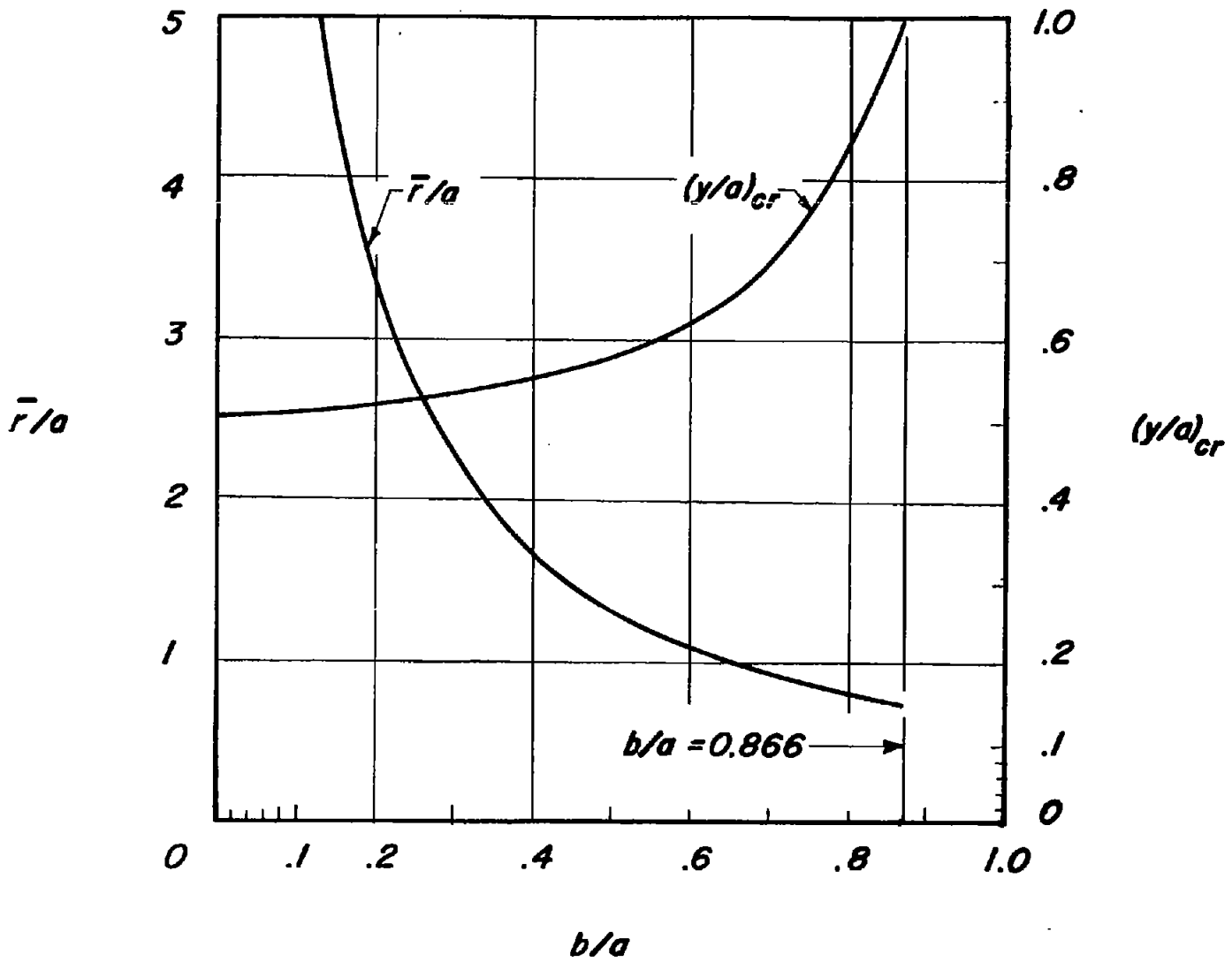

Figure 19.- Location and magnitude of critical radius of elliptic cylinder.

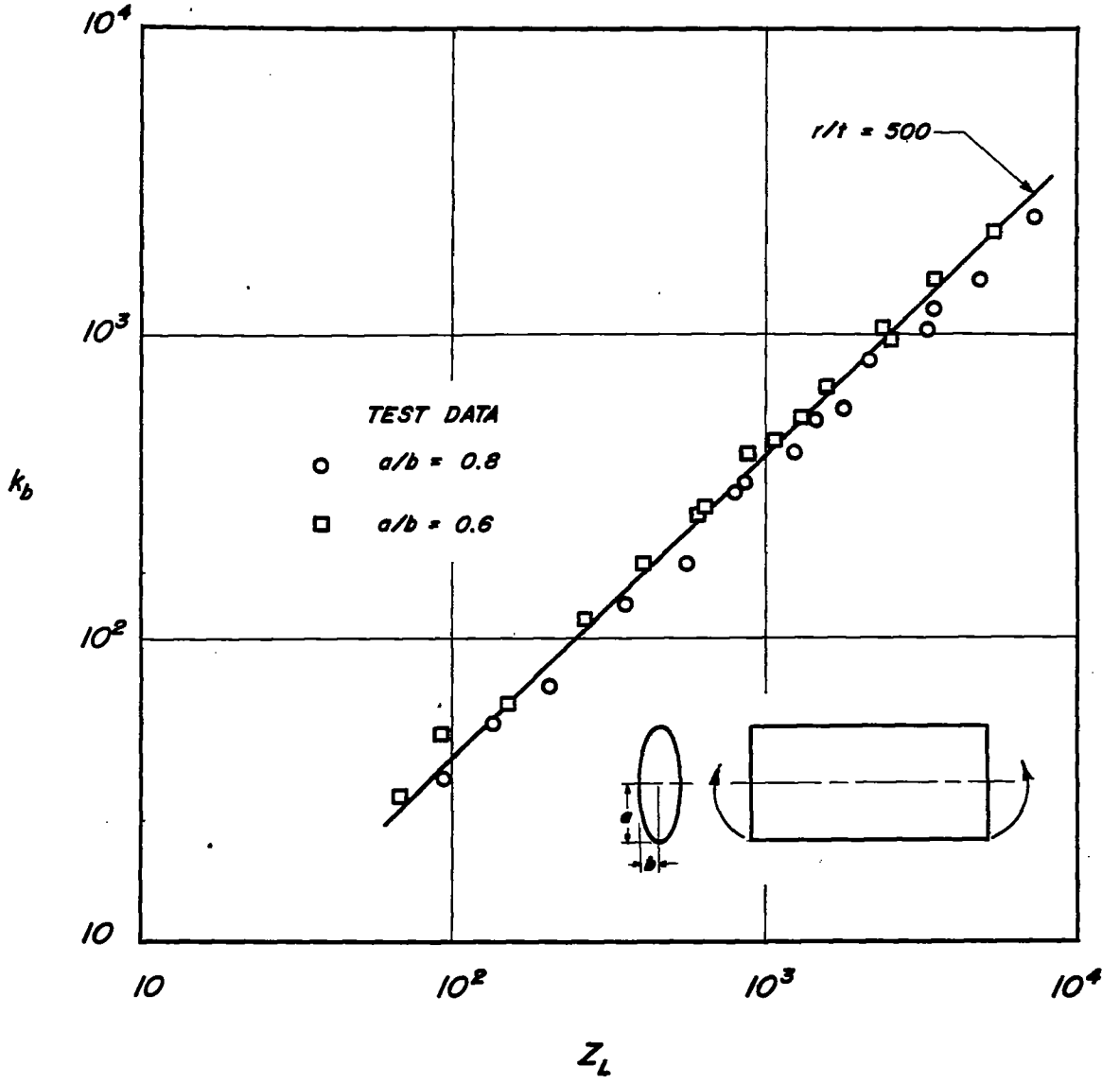

Figure 20.- Comparison of test data on elliptic cylinders with empirical curve for $\bar{r}/t = 500$. For test data, $250 < \bar{r}/t < 750$.

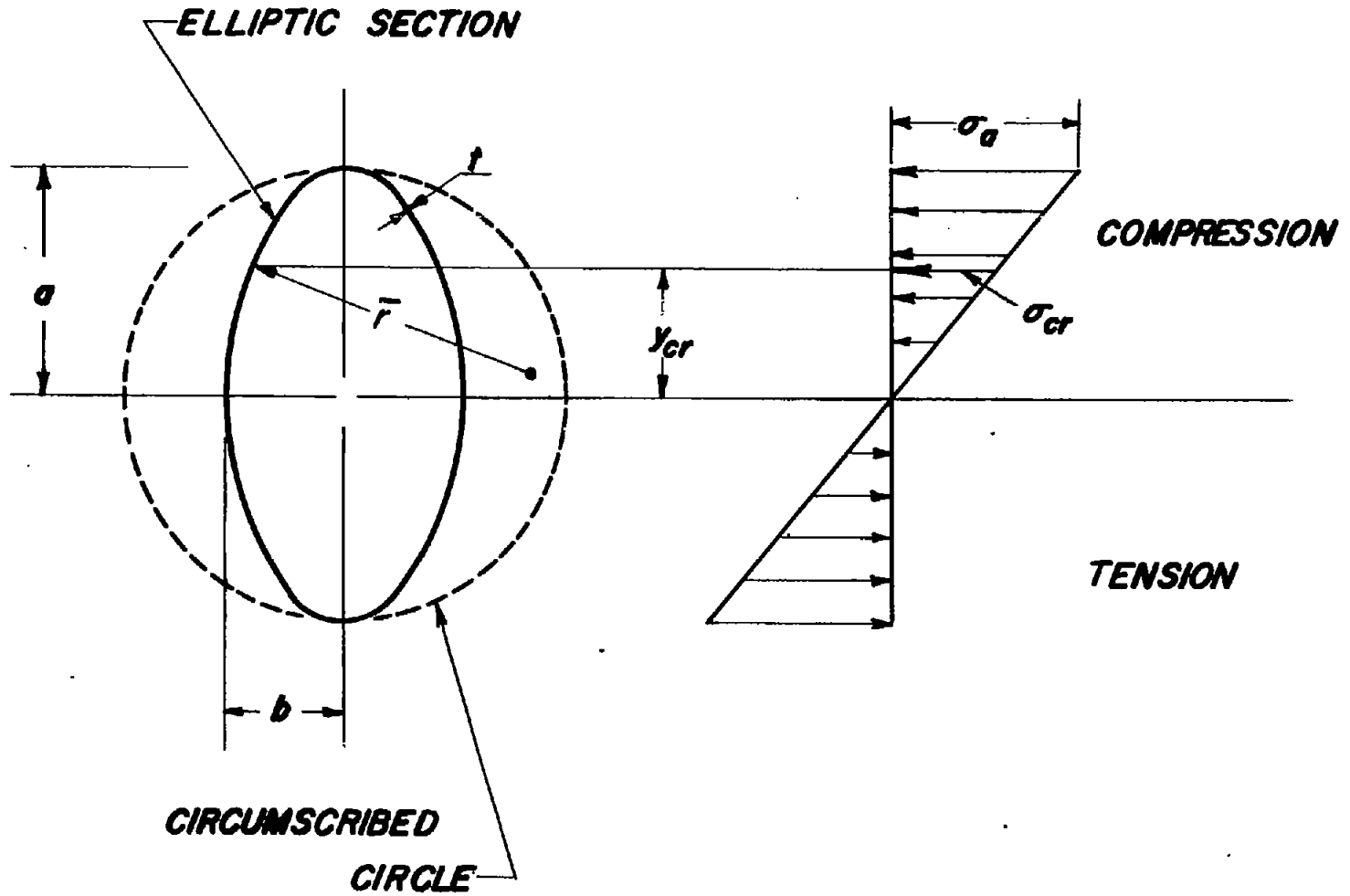

Figure 21.- Location of critical radius of curvature for elliptic cylinders in bending.

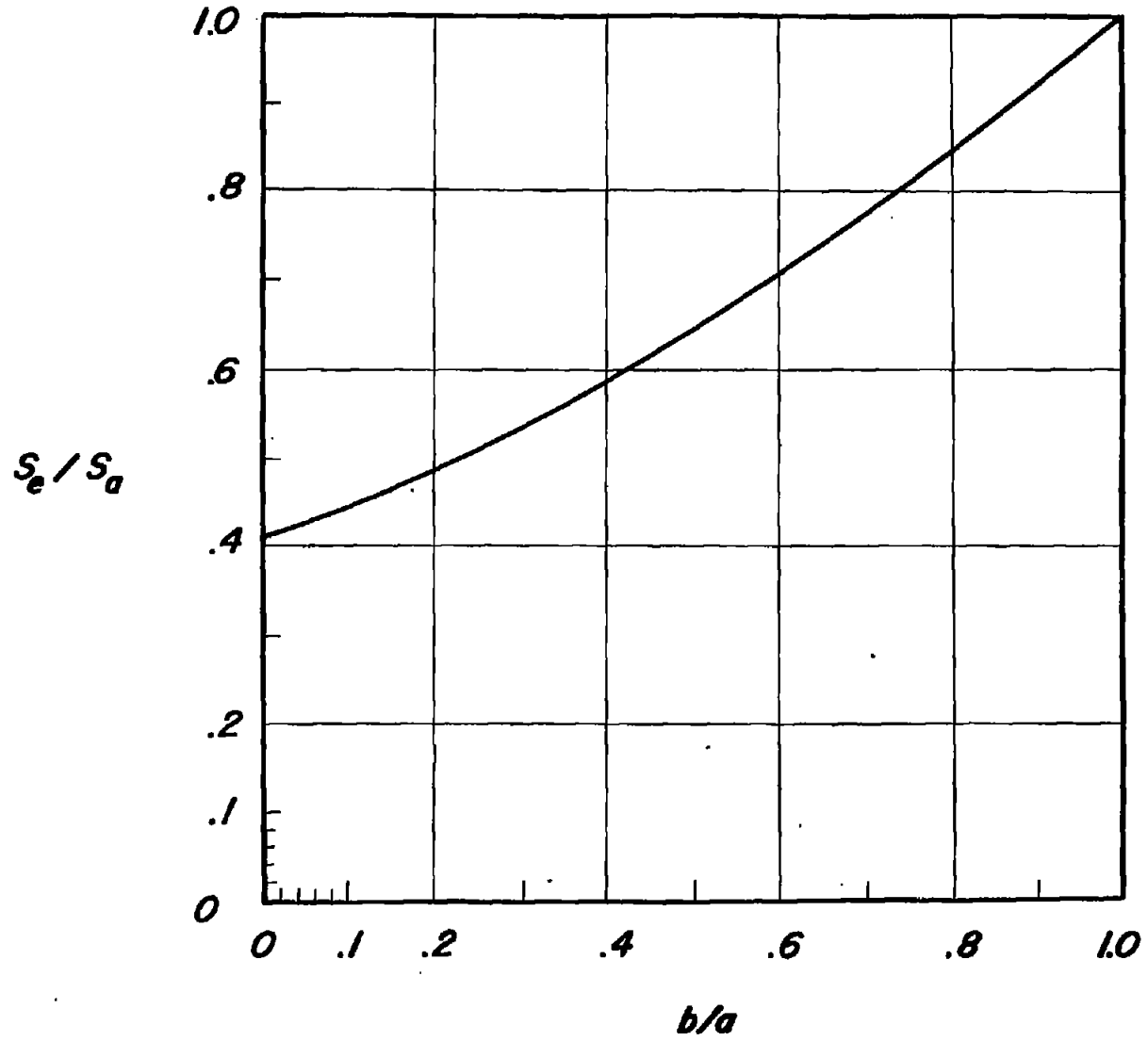

Figure 22.- Section modulus of elliptic cylinder.

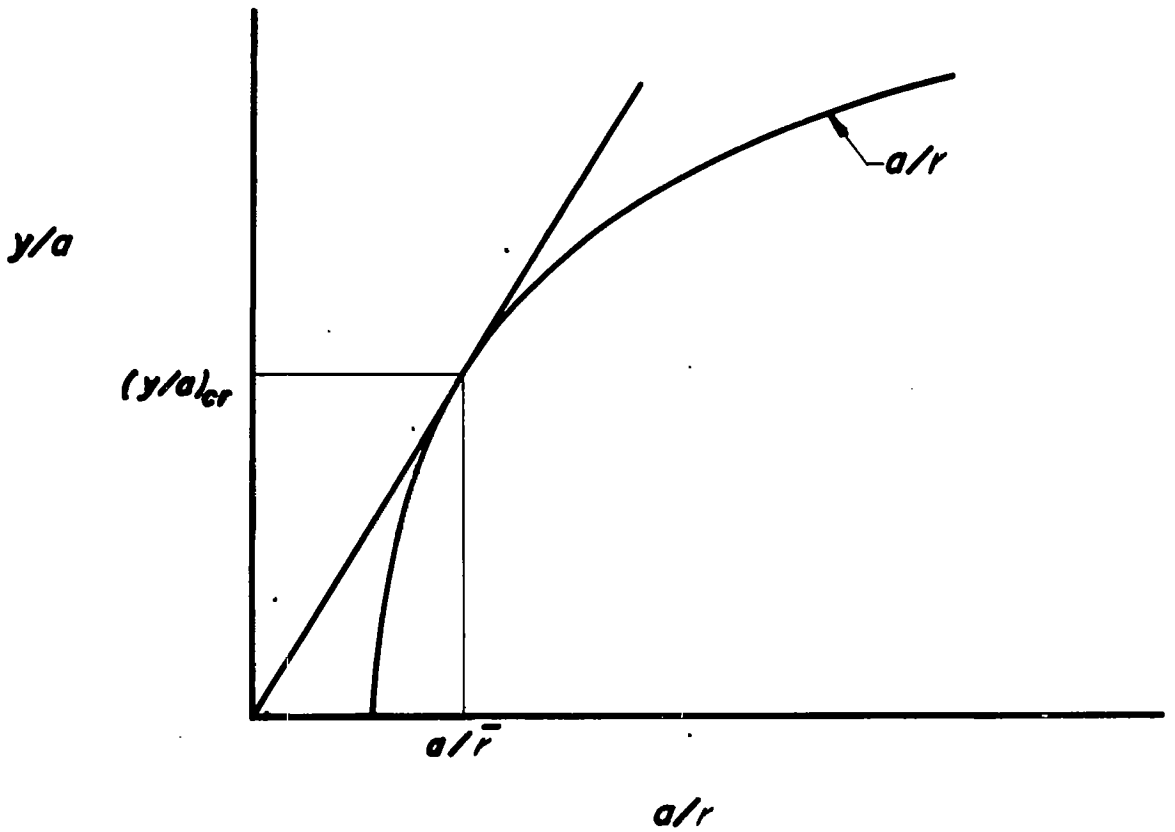

Figure 23.- Method for determining location and magnitude of critical radius of curvature.

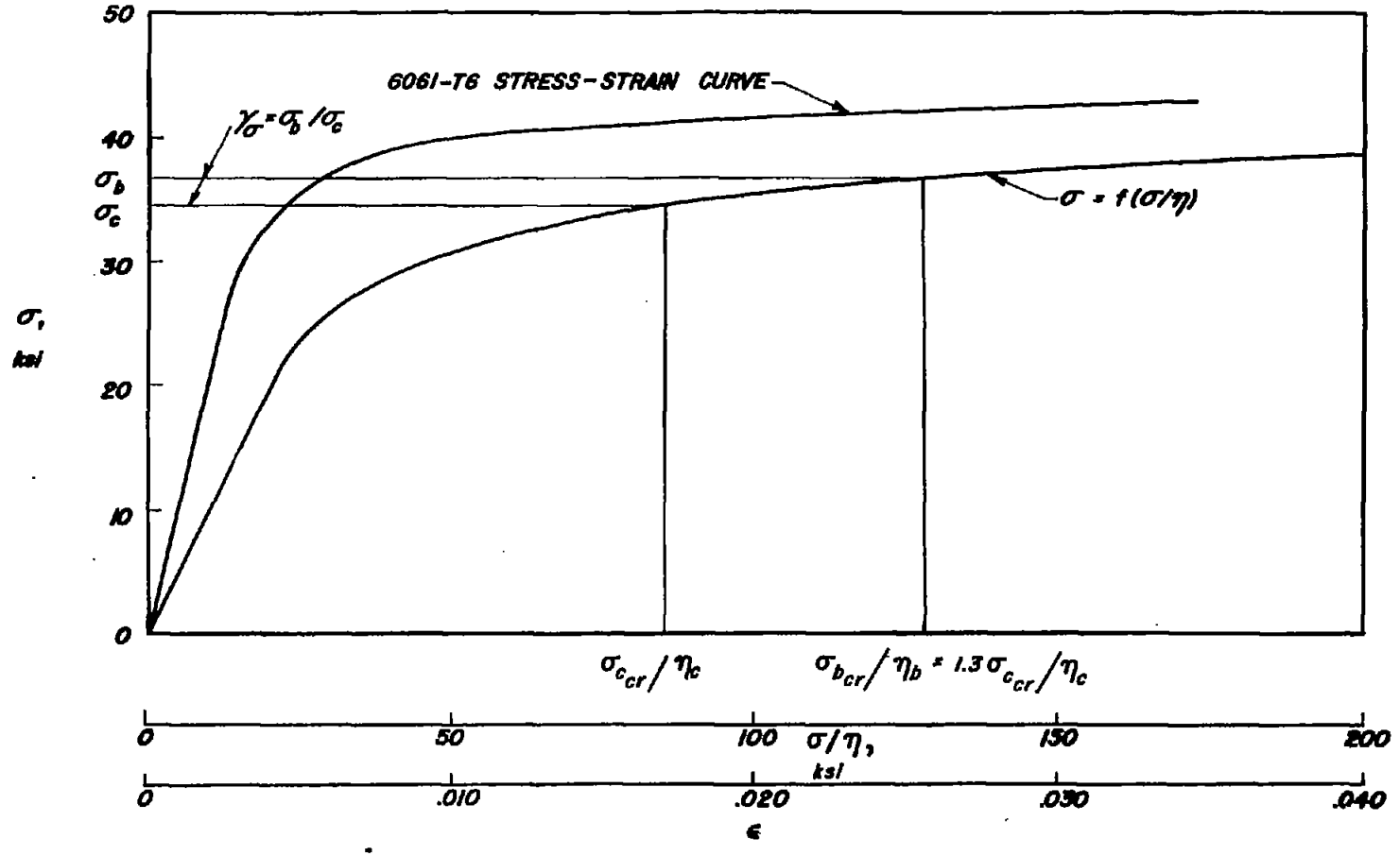

Figure 24.- Stress-strain curve for 6061-T6 aluminum alloy and derived curve of σ as a function of σ/η.

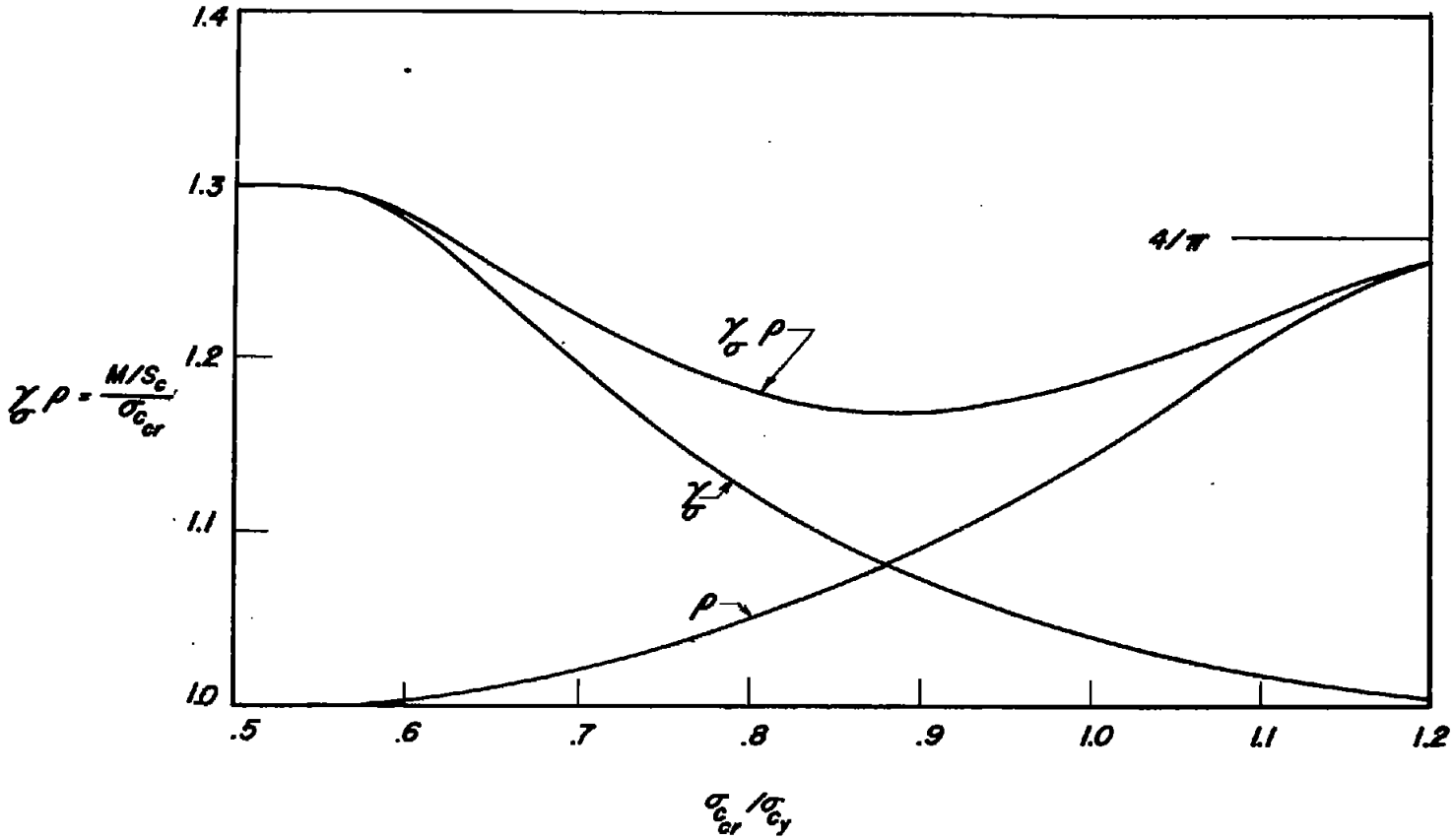

(a) Theoretical variation based on 6061-T6 aluminum-alloy data of figure 24.

Figure 25.- Variation of $(M/Sc)/\sigma_{c_{cr}}$ for long circular cylinders in bending.

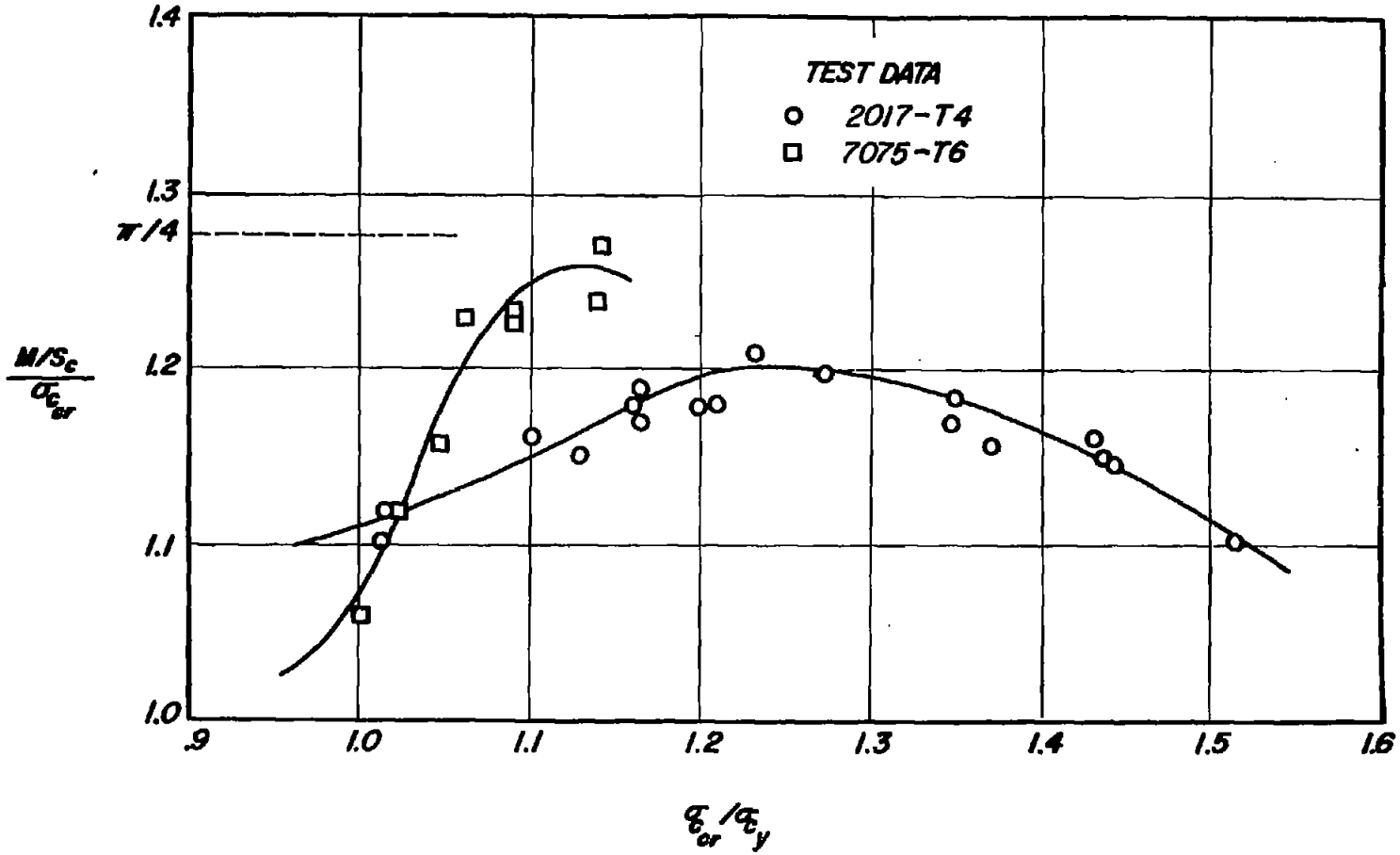

(b) Experimental variation.

Figure 25.- Concluded.

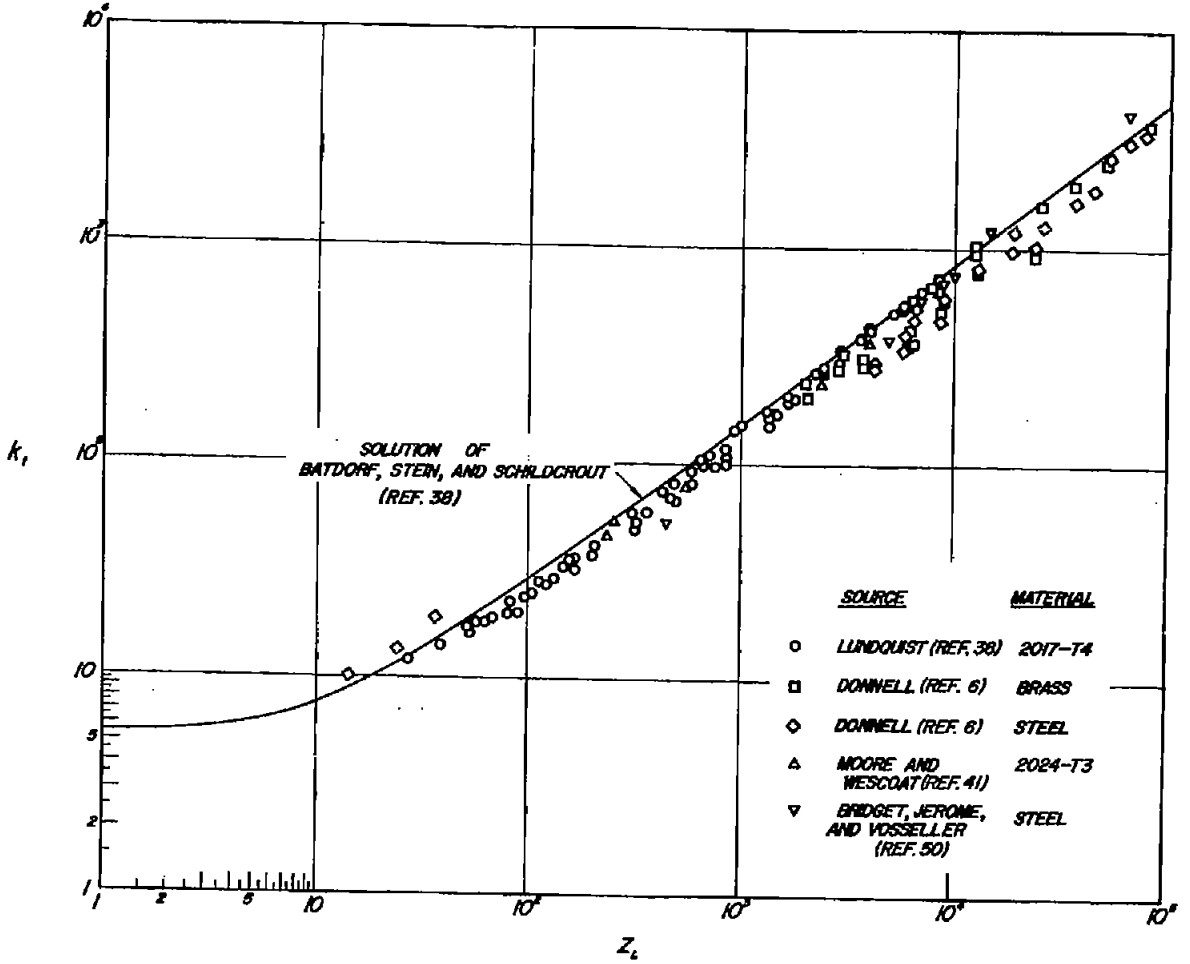

Figure 26.- Comparison of test data and theory for simply supported circuler cylinders in torsion.

$$\tau_{cr} = \frac{k_t \pi^2 E}{12\left(1 - \nu_e^2\right)} \left(\frac{t}{L}\right)^2; \quad Z_L = \frac{L^2}{rt}\left(1 - \nu_e^2\right)^{1/2}.$$

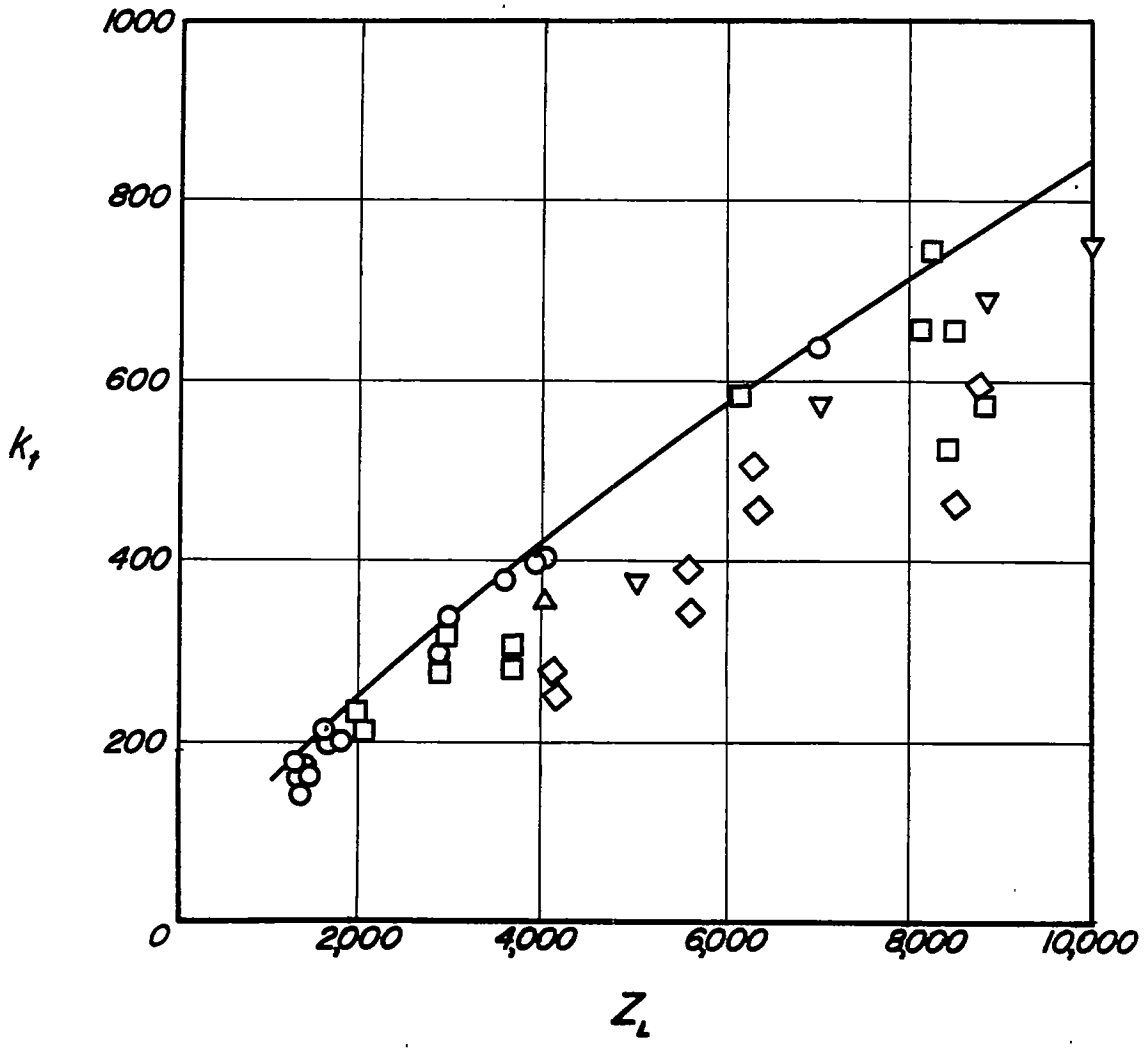

Figure 27.- Enlargement of a section of figure 26 on a linear scale.

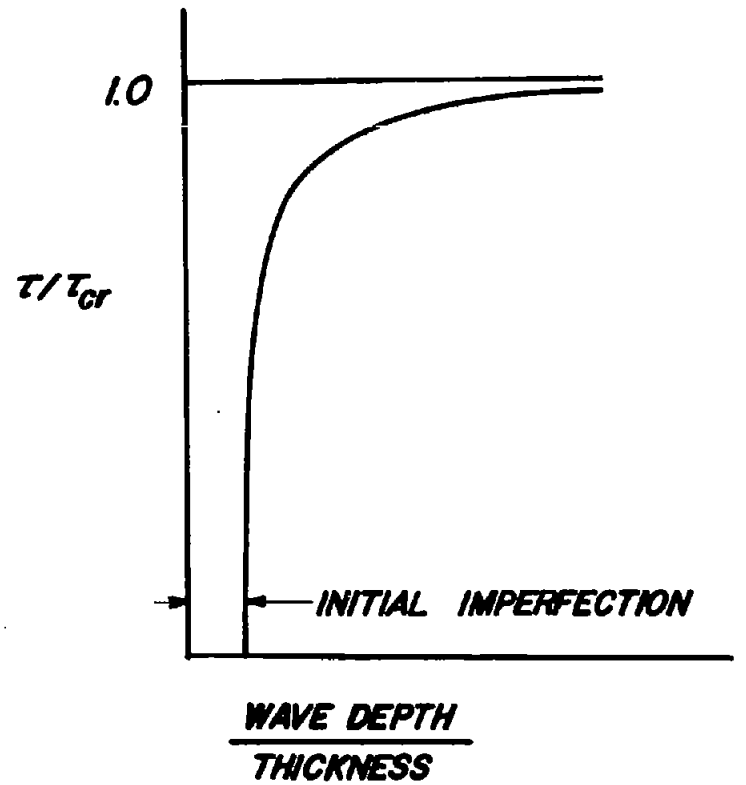

Figure 28.- Buckling stress as a function of buckle wave depth for circular cylinders in torsion. Curve taken from test data.

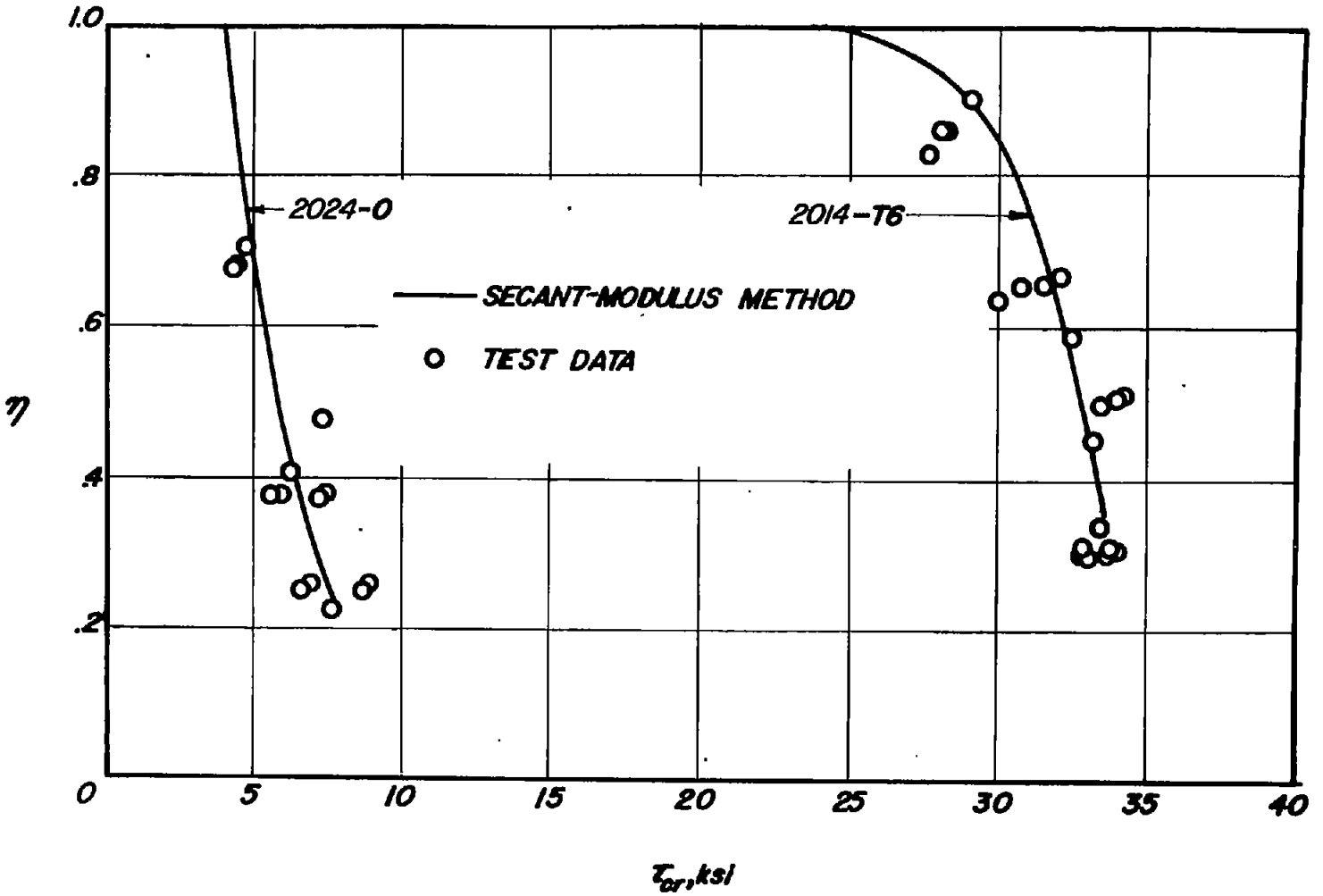

Figure 29.- Comparison of test data with plasticity-reduction factor for long flat plates in shear. Data from reference 44.

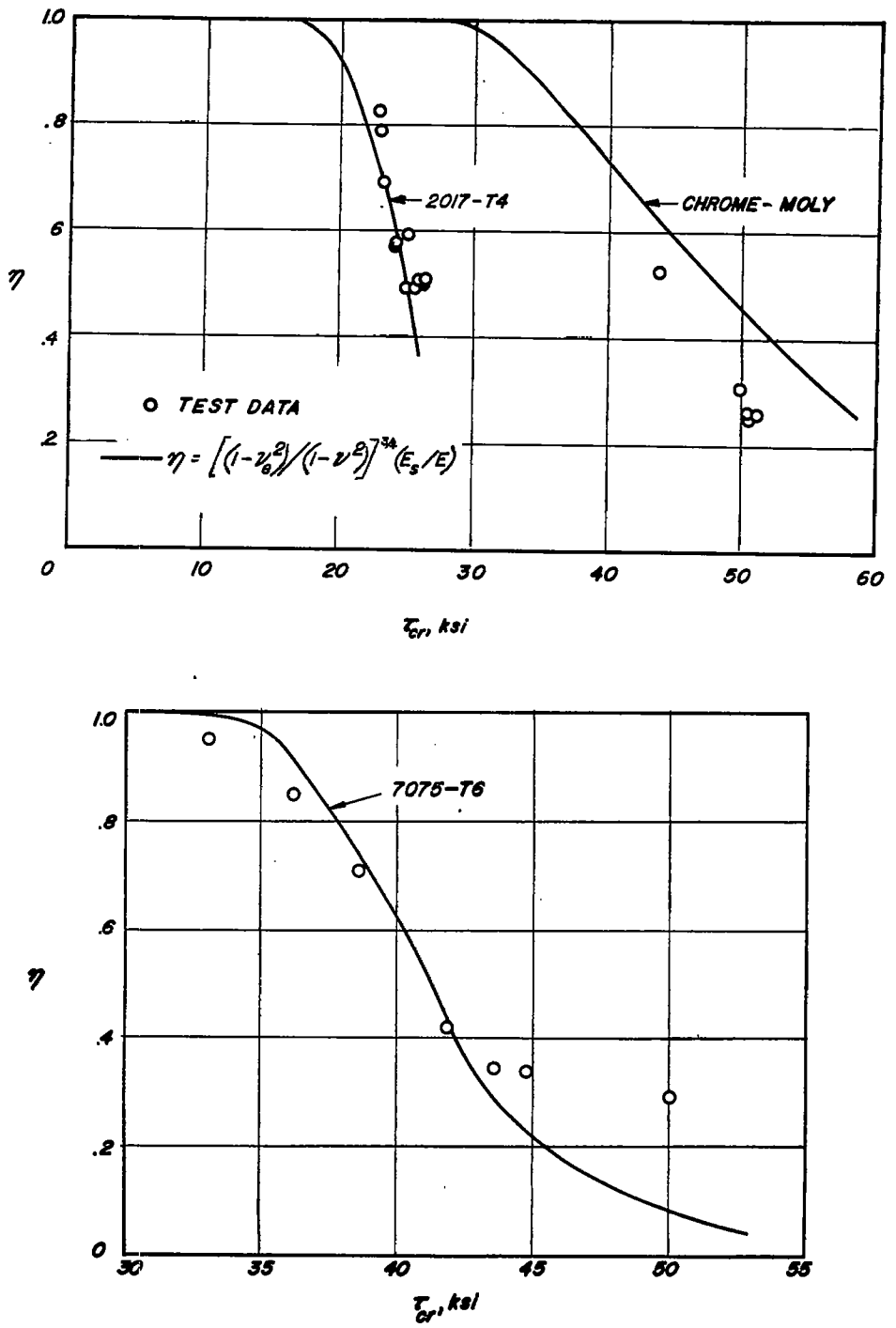

Figure 30.- Comparison of test data with theoretical plasticity-reduction factor for long cylinders in torsion.

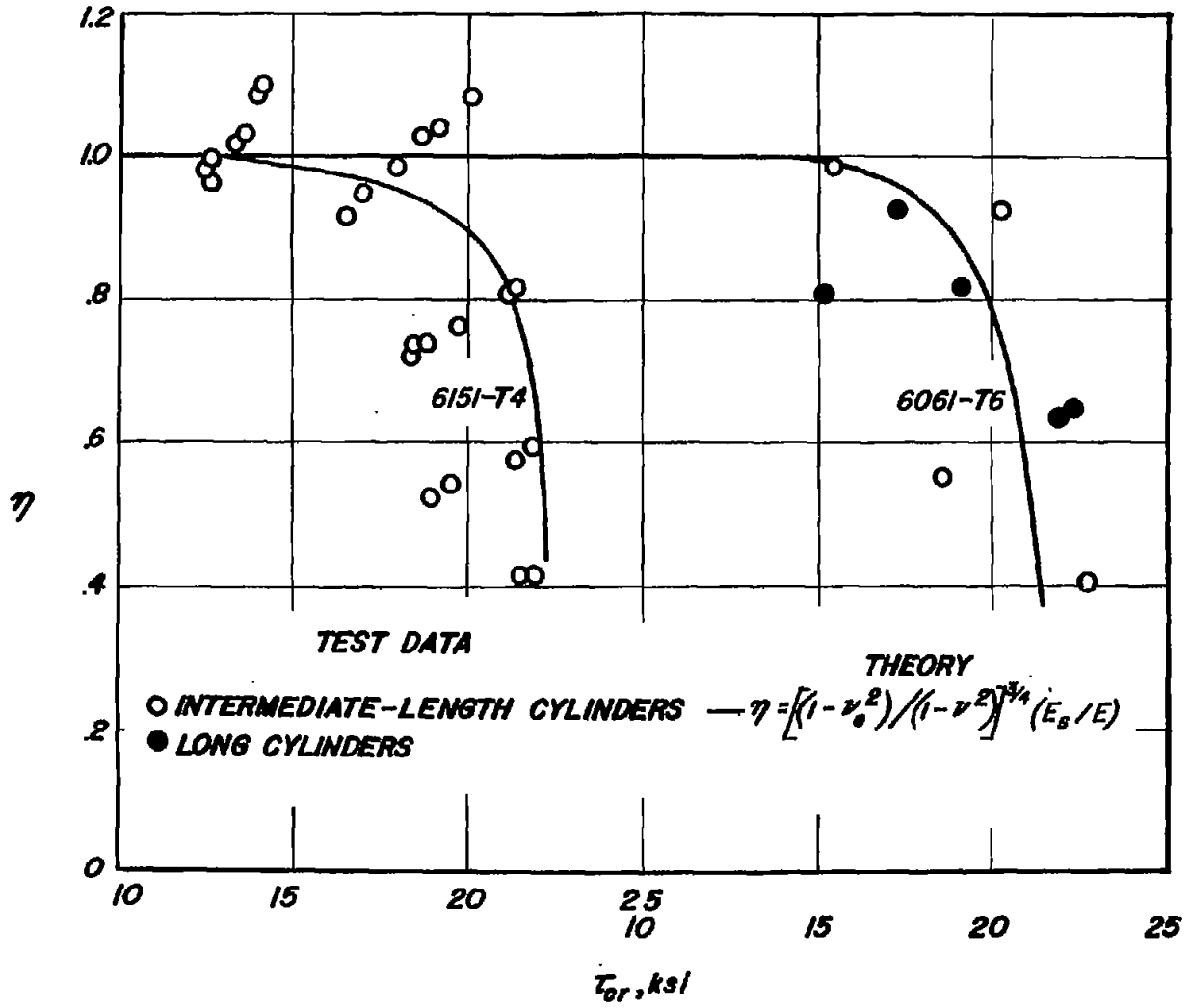

Figure 31.- Comparison of test data for intermediate-length cylinders with theory for long cylinders in torsion.

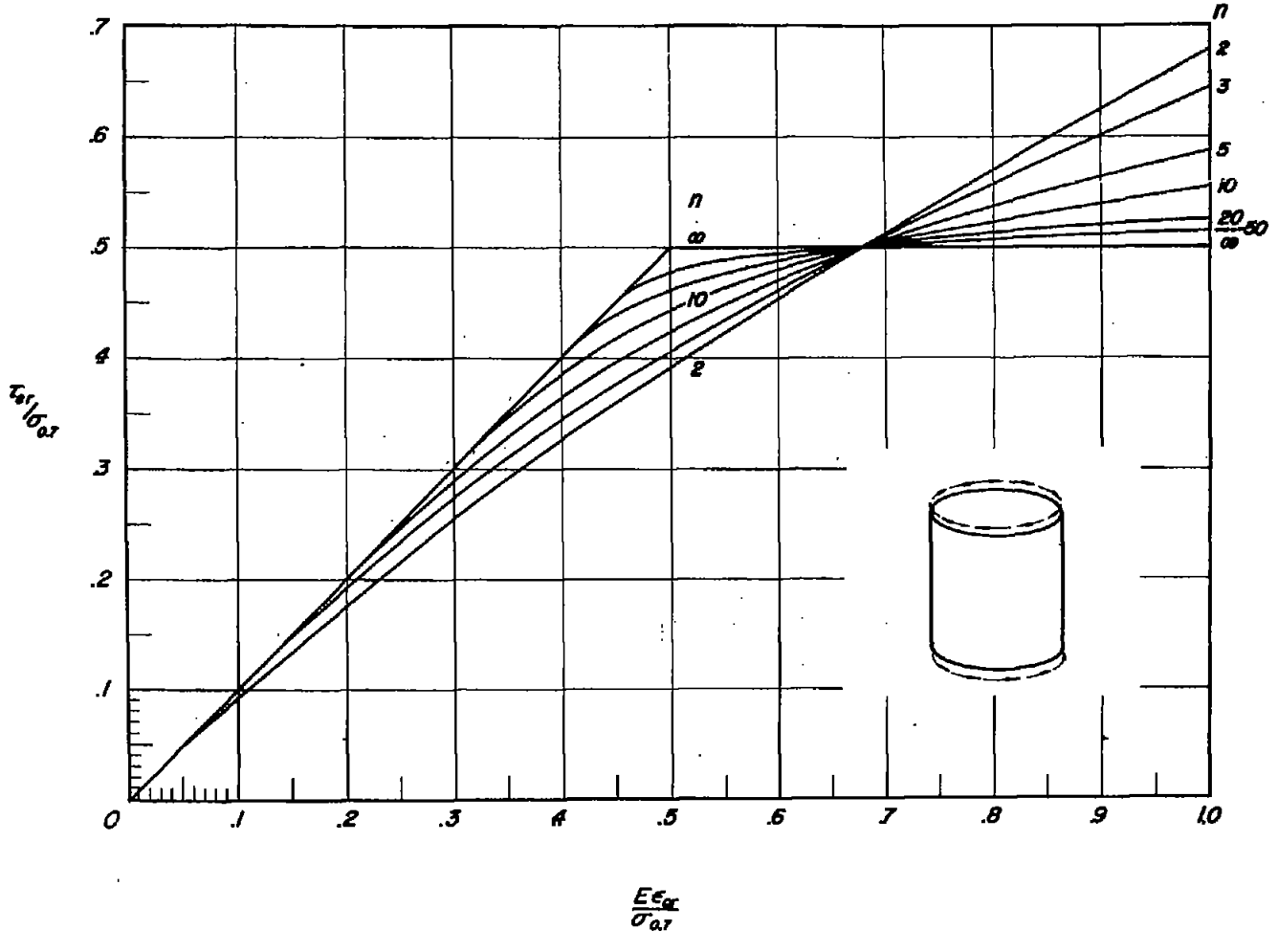

Figure 32.- Nondimensional-buckling-stress curves for long cylinders in torsion.

$$\eta = \left(E_s/E\right)\left[\left(1 - \nu_e^2\right)/\left(1 - \nu^2\right)\right]^{3/4}.$$

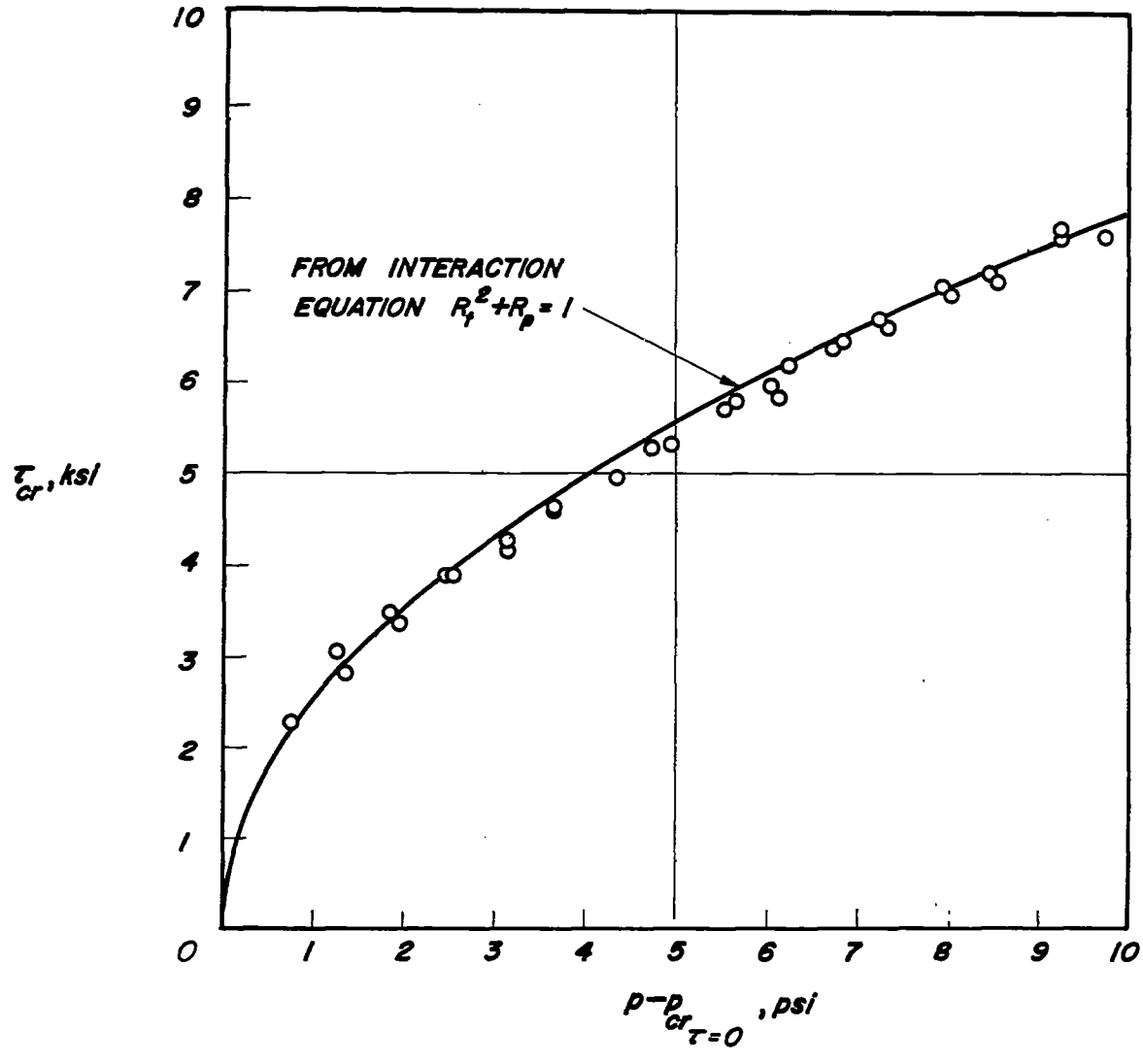

Figure 33.- Effect of internal pressure on torsional-buckling stress of long cylinders. Test results are from reference 43.

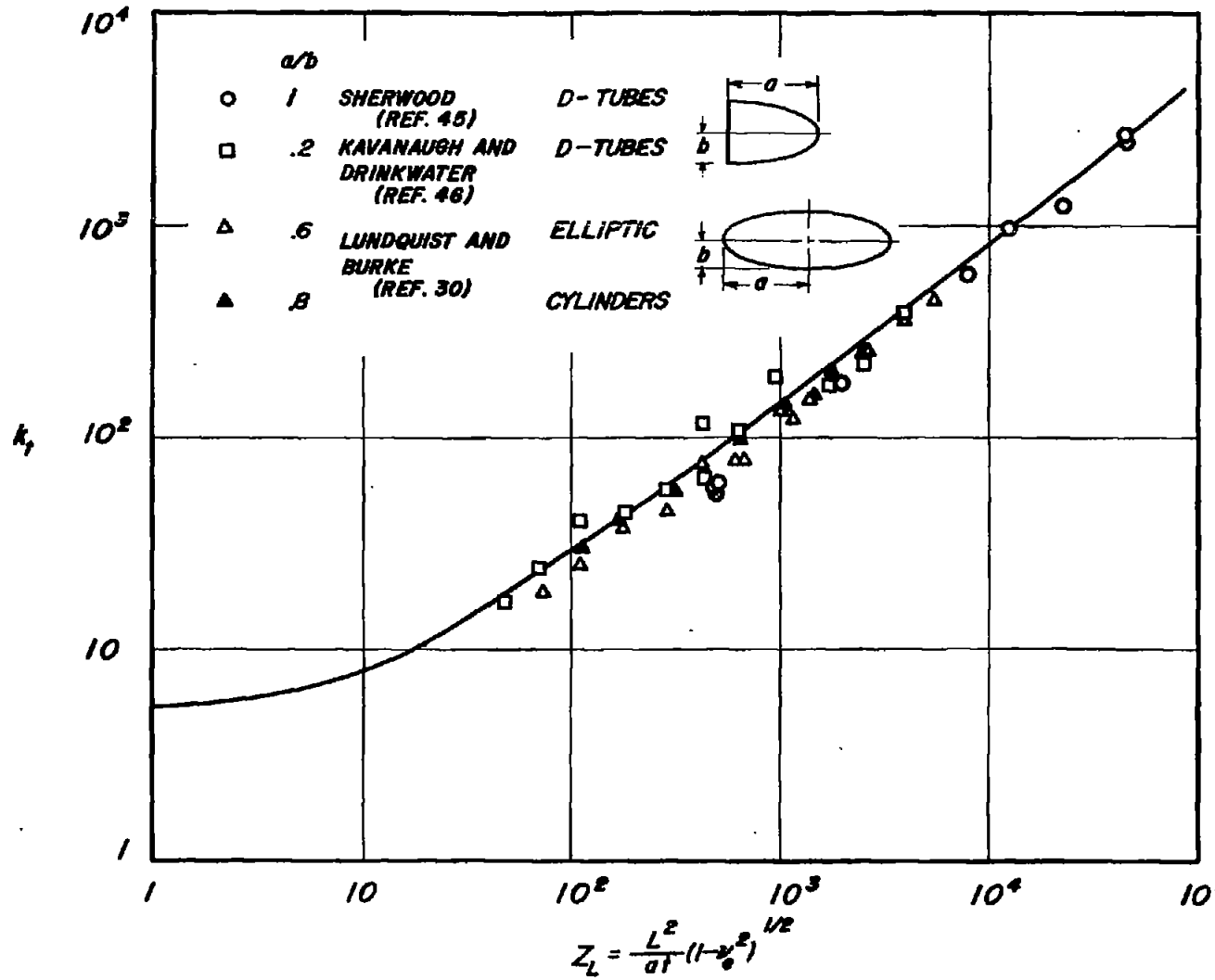

Figure 34.- Comparison of buckling test data on elliptic cylinders and D-tubes with theory for circular cylinders in torsion.

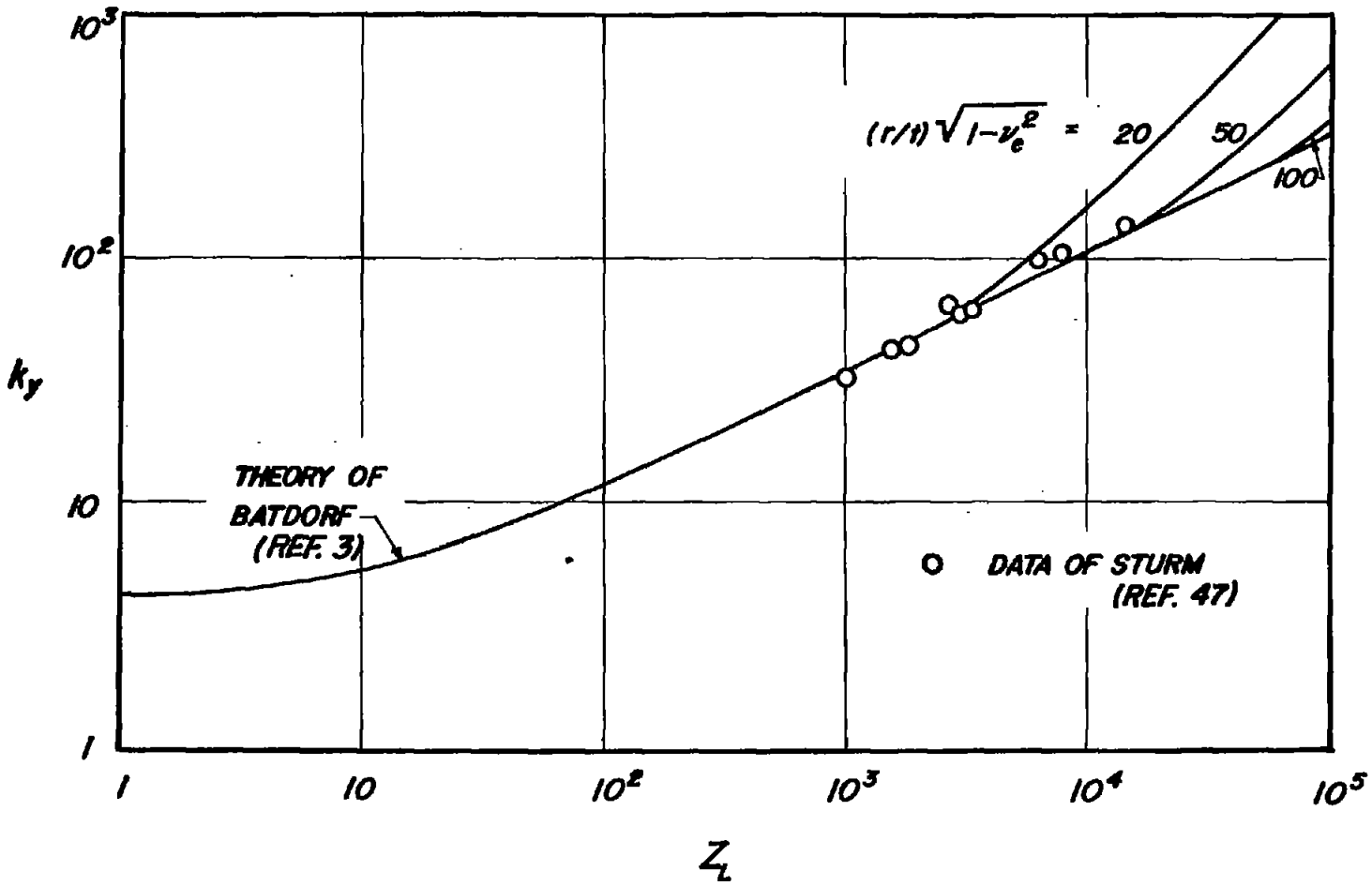

(a) Buckling under external radial pressure. $\sigma_{cr} = \dfrac{k_y \pi^2 E}{12\left(1 - \nu_e^2\right)} \left(\dfrac{t}{L}\right)^2$.

Figure 35.- Comparison of test data with theory for buckling of circular cylinders.

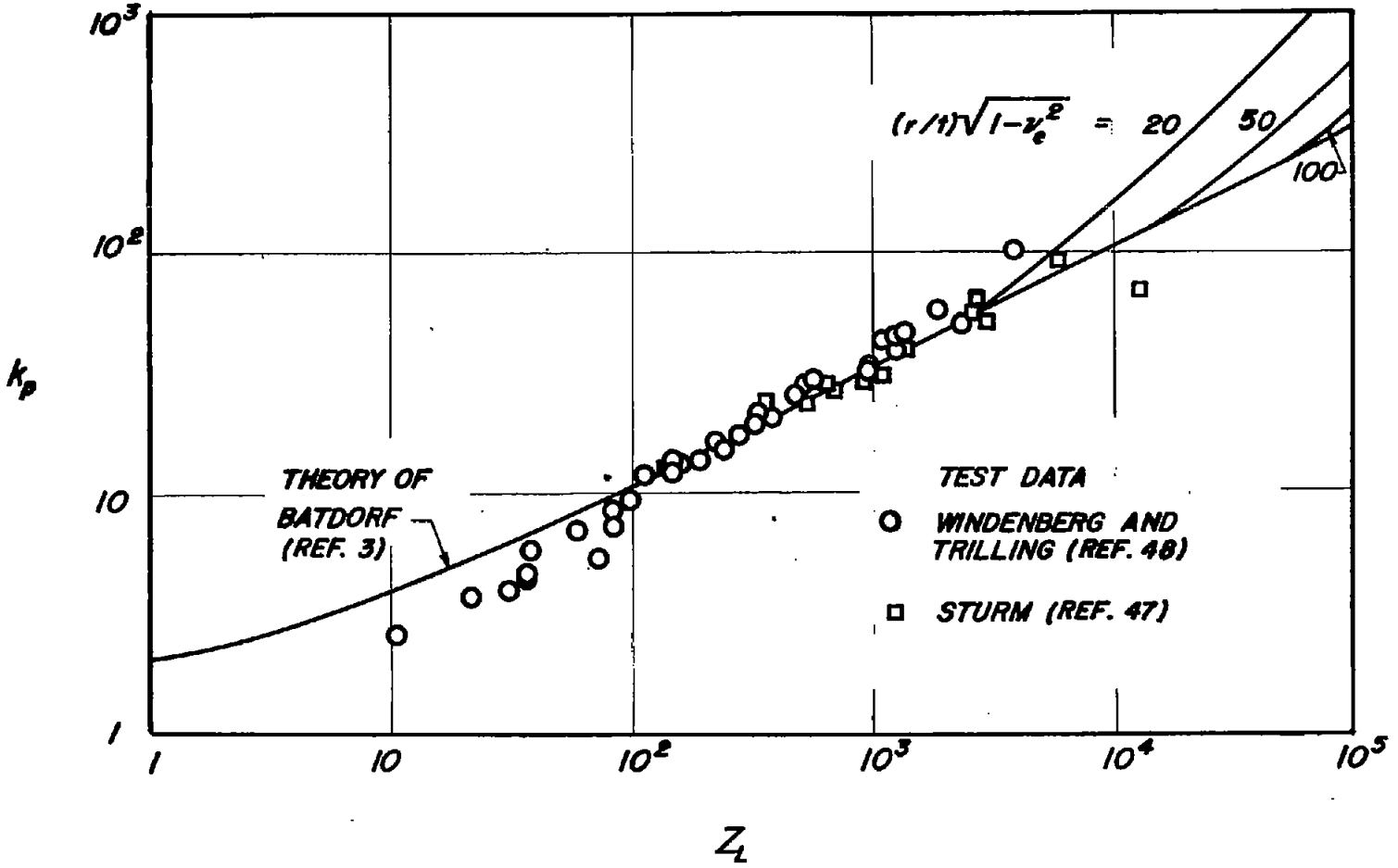

(b) Buckling under external hydrostatic pressure. $\sigma_{cr} = \frac{k_p \pi^2 E}{12\left(1 - \nu_e^2\right)} \left(\frac{t}{L}\right)^2$.

Figure 35.- Concluded.

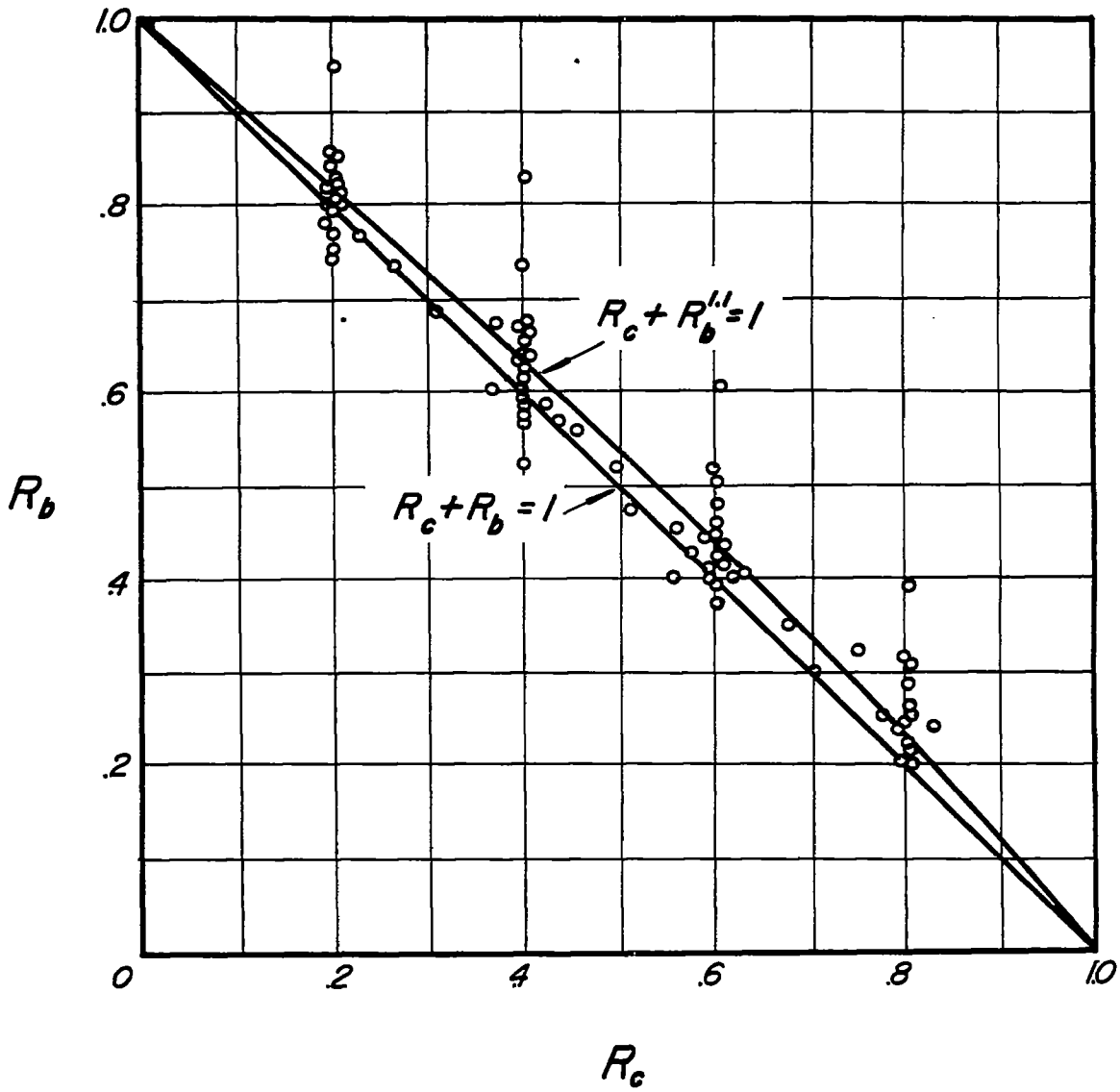

(a) Combined bending and compression.

Figure 36.- Interaction curves and test data for combined stresses on circular cylinders. Test data from Bruhn (ref. 54).

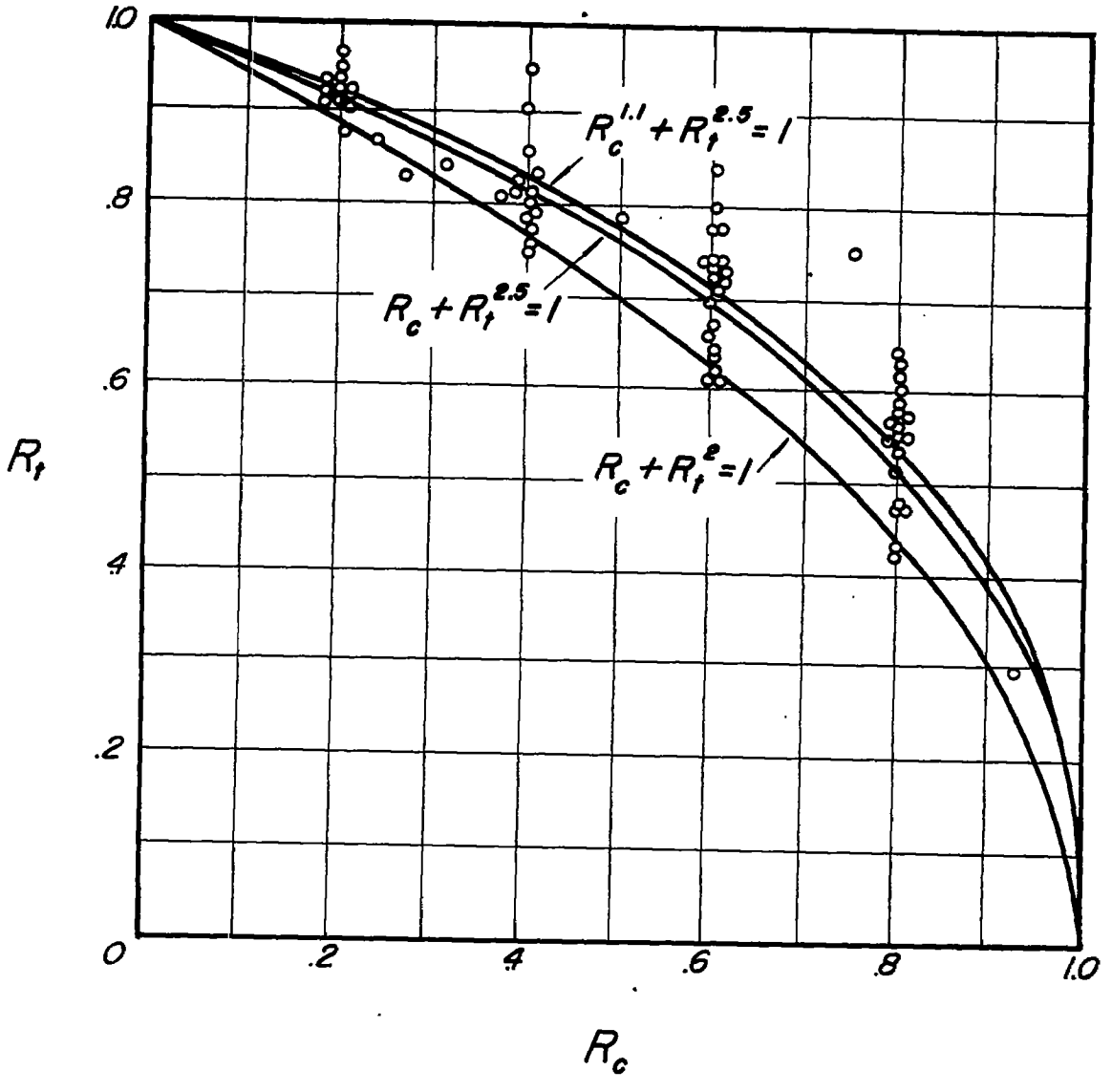

(b) Combined compression and torsion.

Figure 36.- Continued.

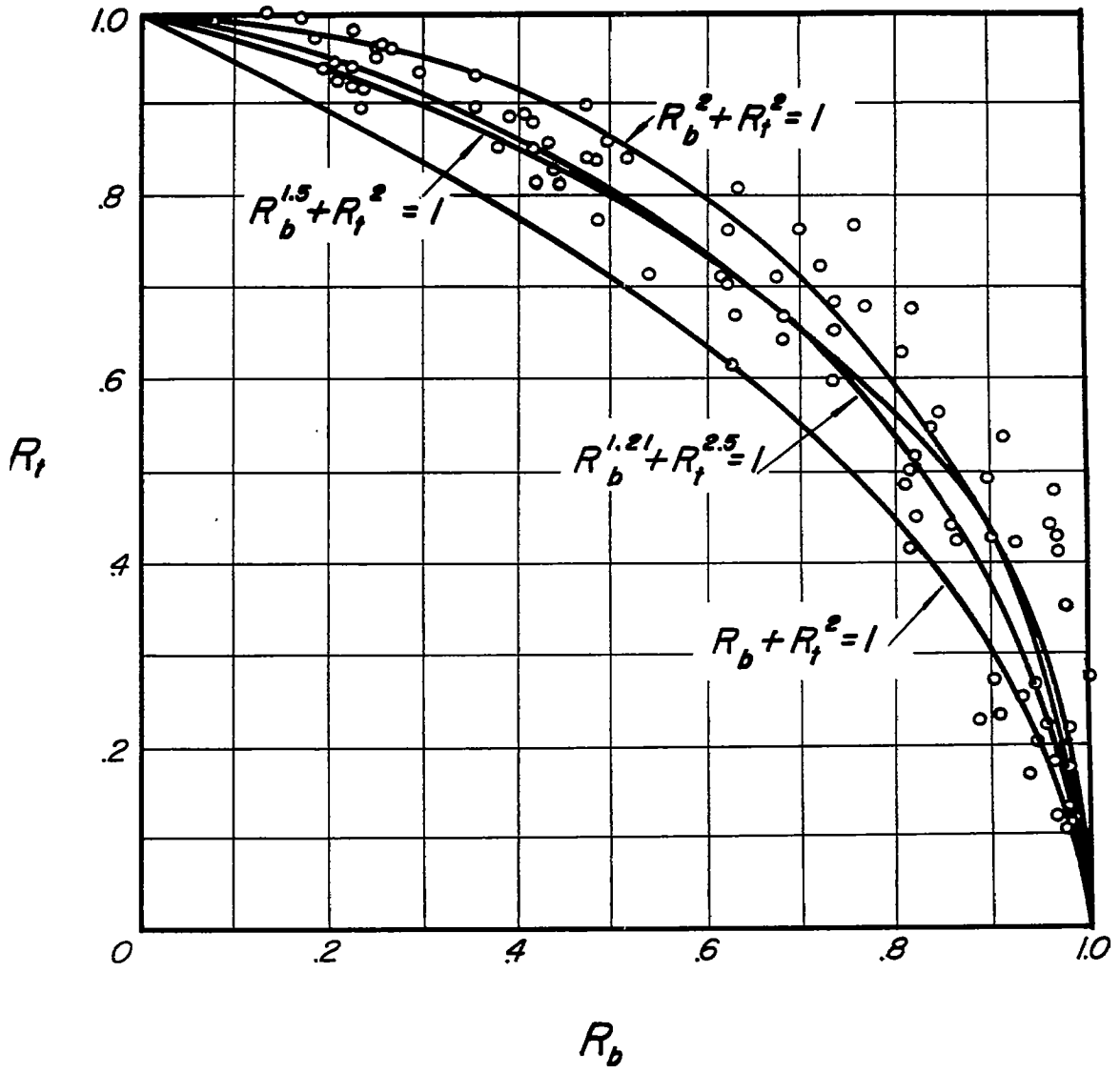

(c) Combined torsion and bending.

Figure 36.- Concluded.

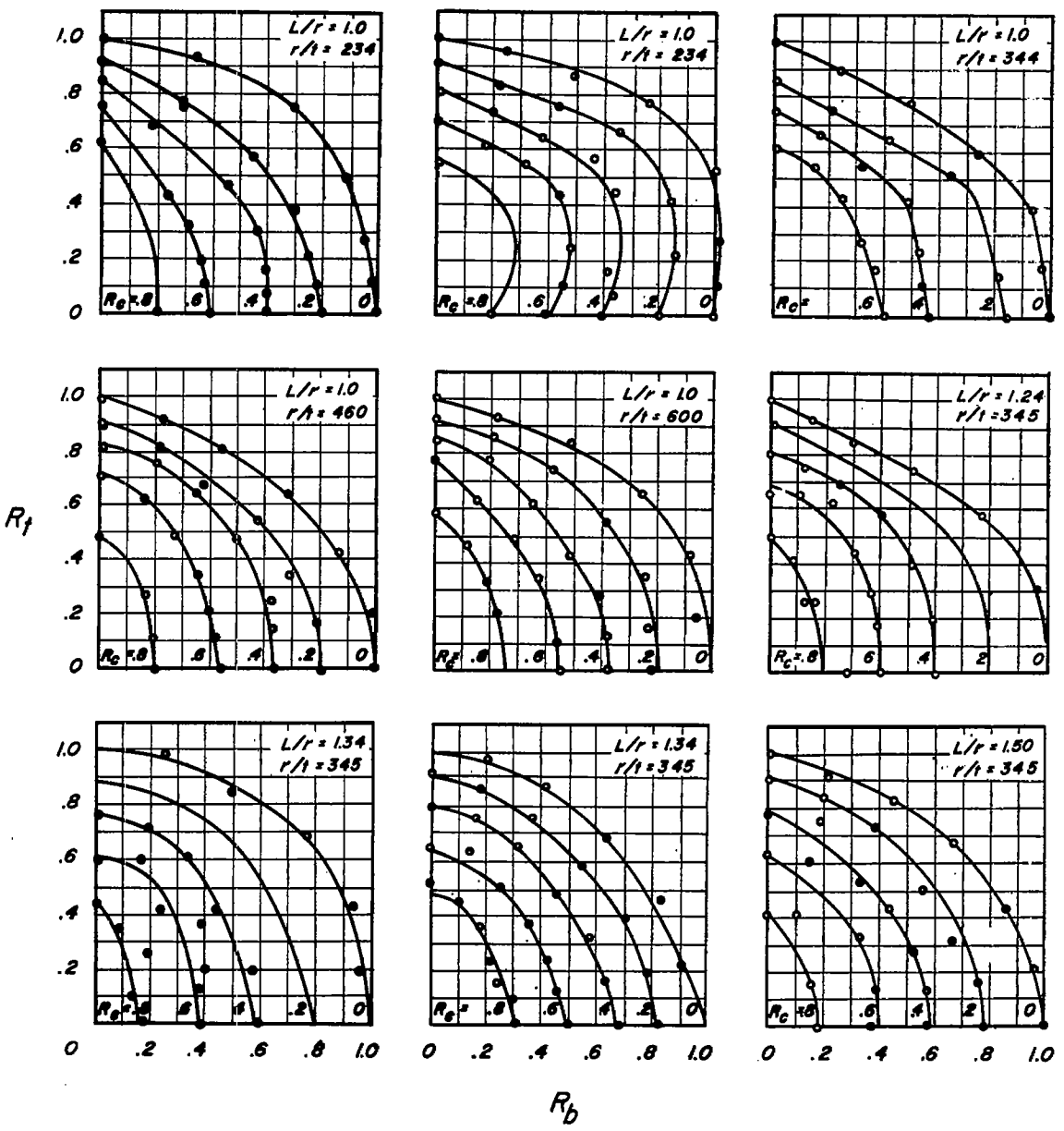

(a) $1 < L/r < 1.5$.

Figure 37.- Interaction curves for combined compression, bending, and torsion on circular cylinders of different proportions.

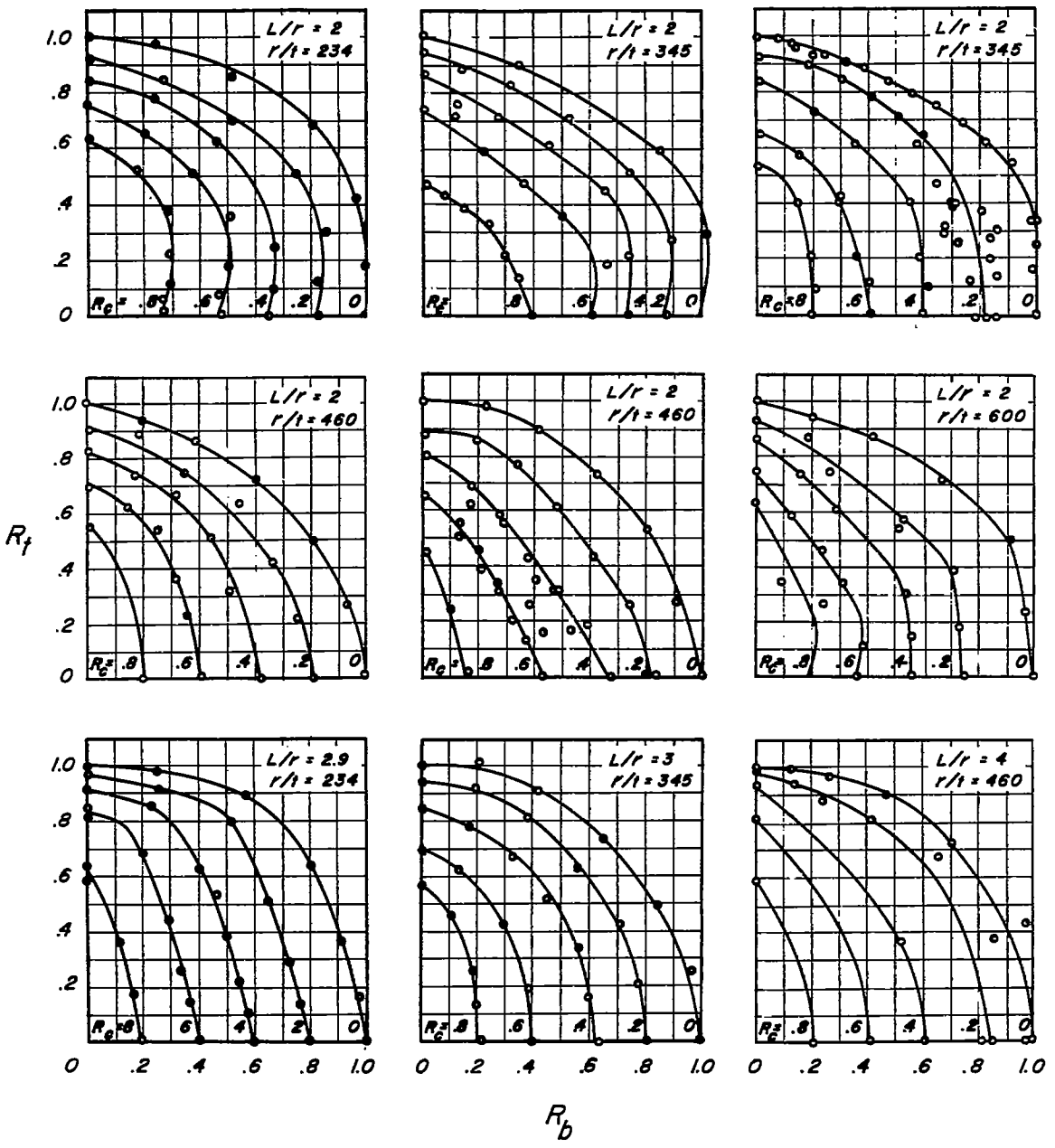

(b) $2 < L/r < 4$.

Figure 37.- Concluded.

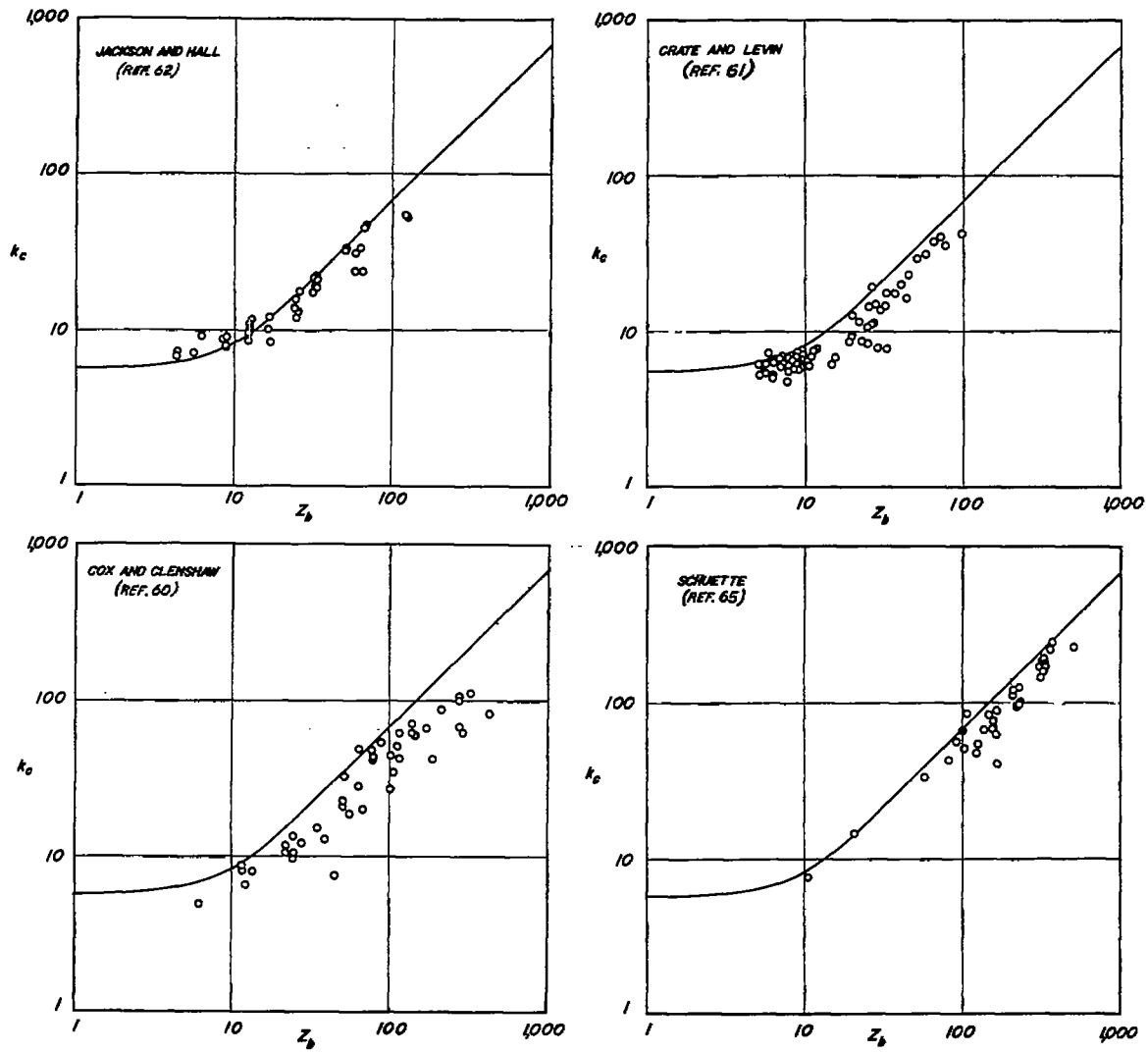

(a) Comparison of test data with linear theory.

Figure 38.- Comparison of test data with theory for axially compressed curved plates.

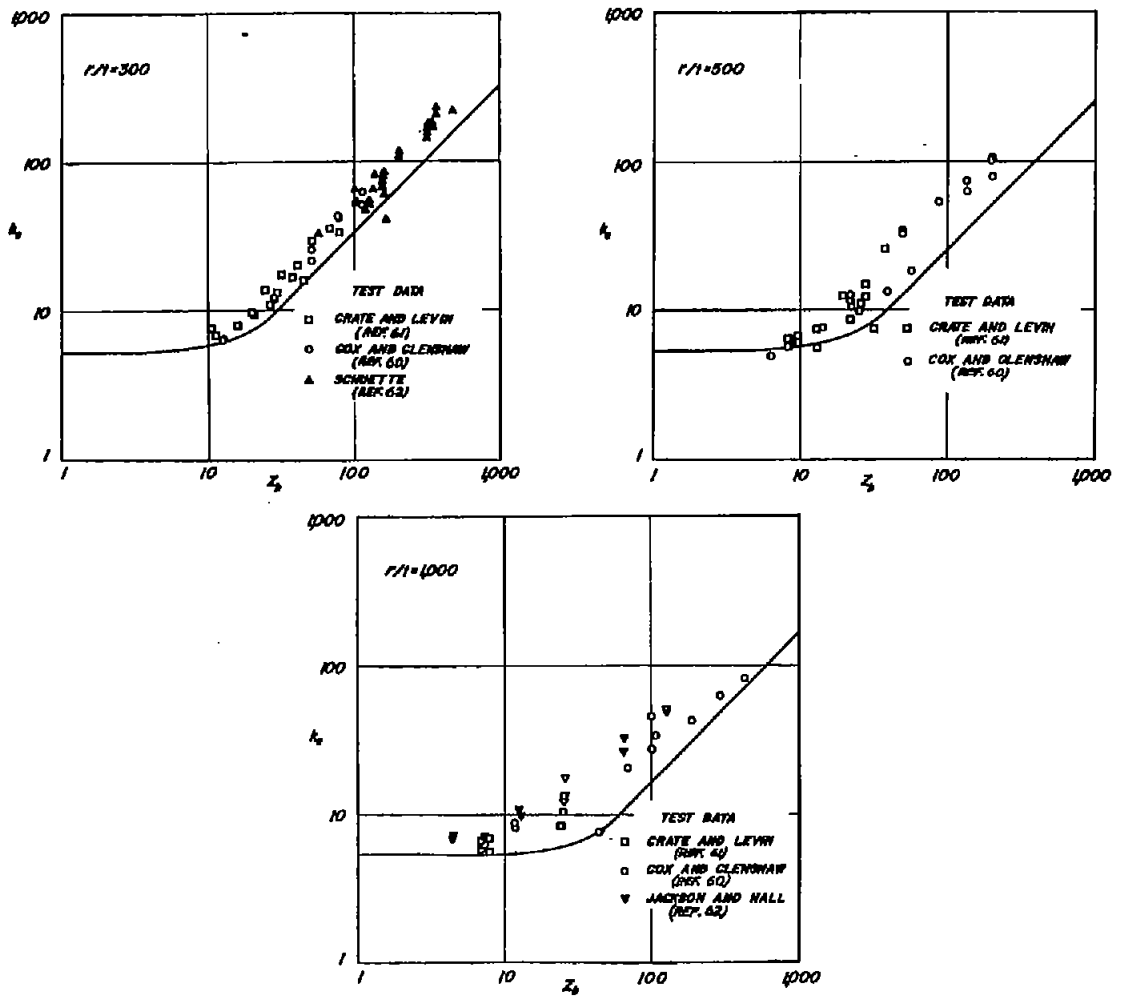

(b) Comparison of selected test data with empirical theory grouped according to r/t values using figure 5 with $k_{pl} = 5.7$.

Figure 38.- Concluded.

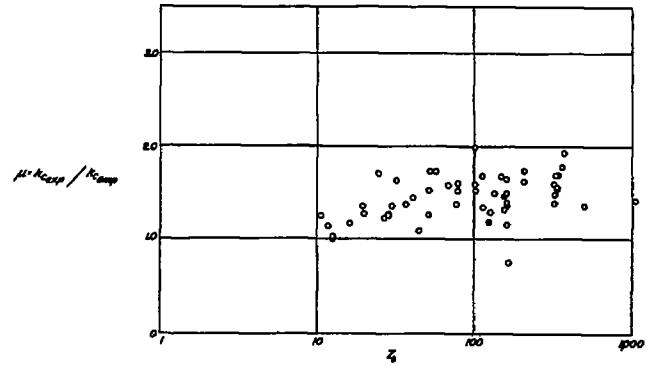

(a) r/t = 300.

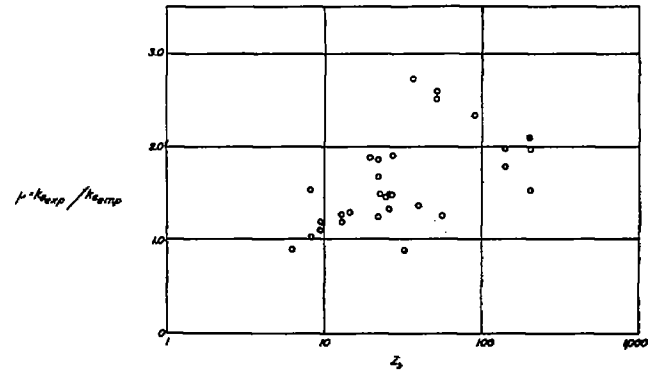

(b) r/t = 500.

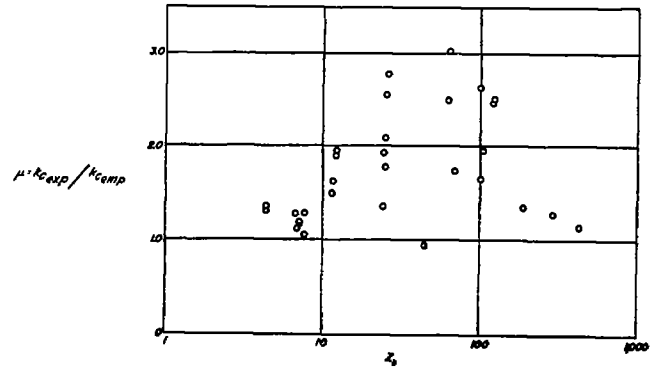

(c) r/t = 1,000.

Figure 39.- Summary of magnification factors for axially compressed curved plates of figure 38(b).

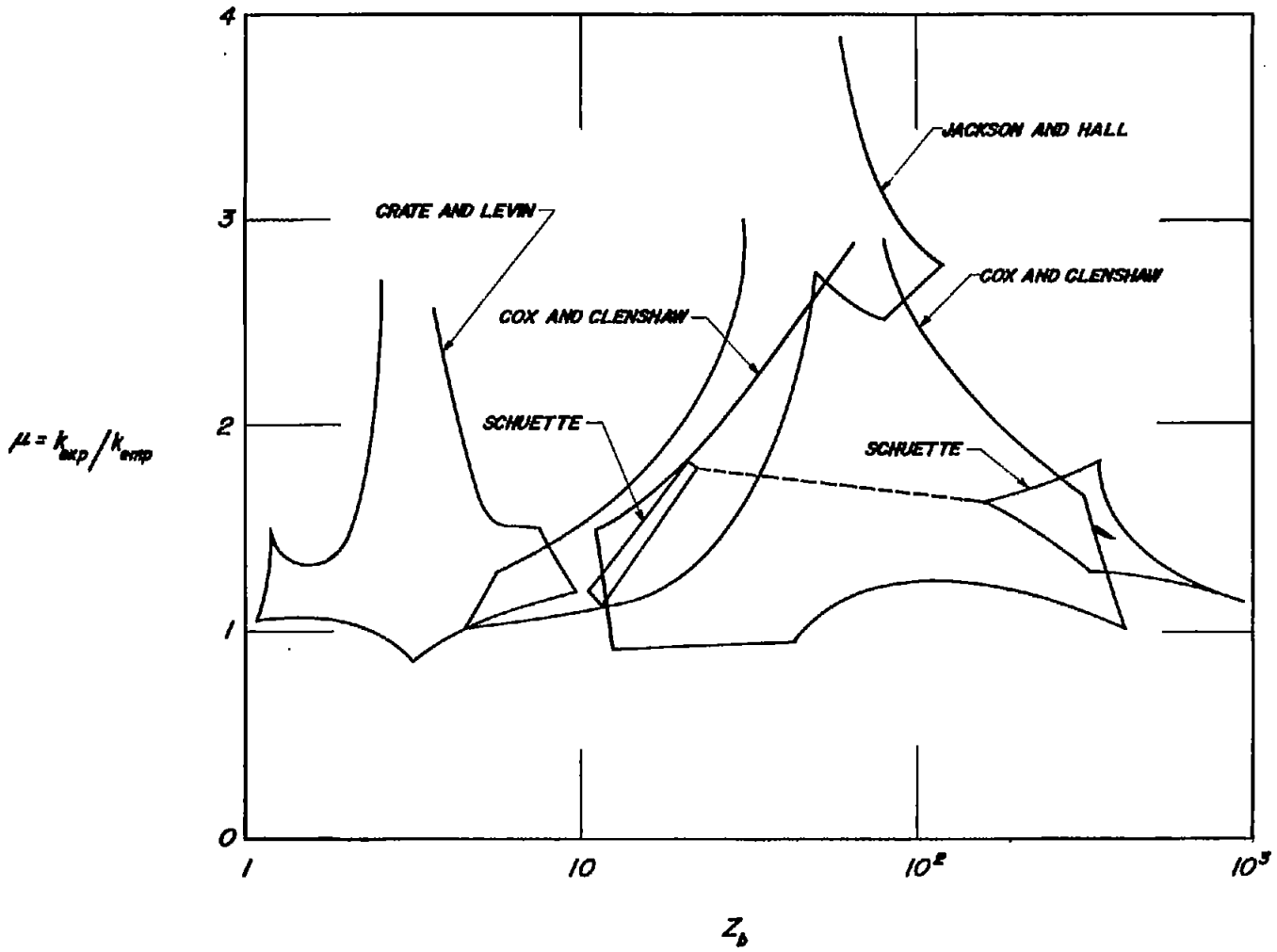

Figure 40.- Ranges of magnification factors for test data of figure 38(a). Data from Crate and Levine, reference 61; Cox and Clenshaw, reference 60; Jackson and Hall, reference 62; and Schuette, reference 65.

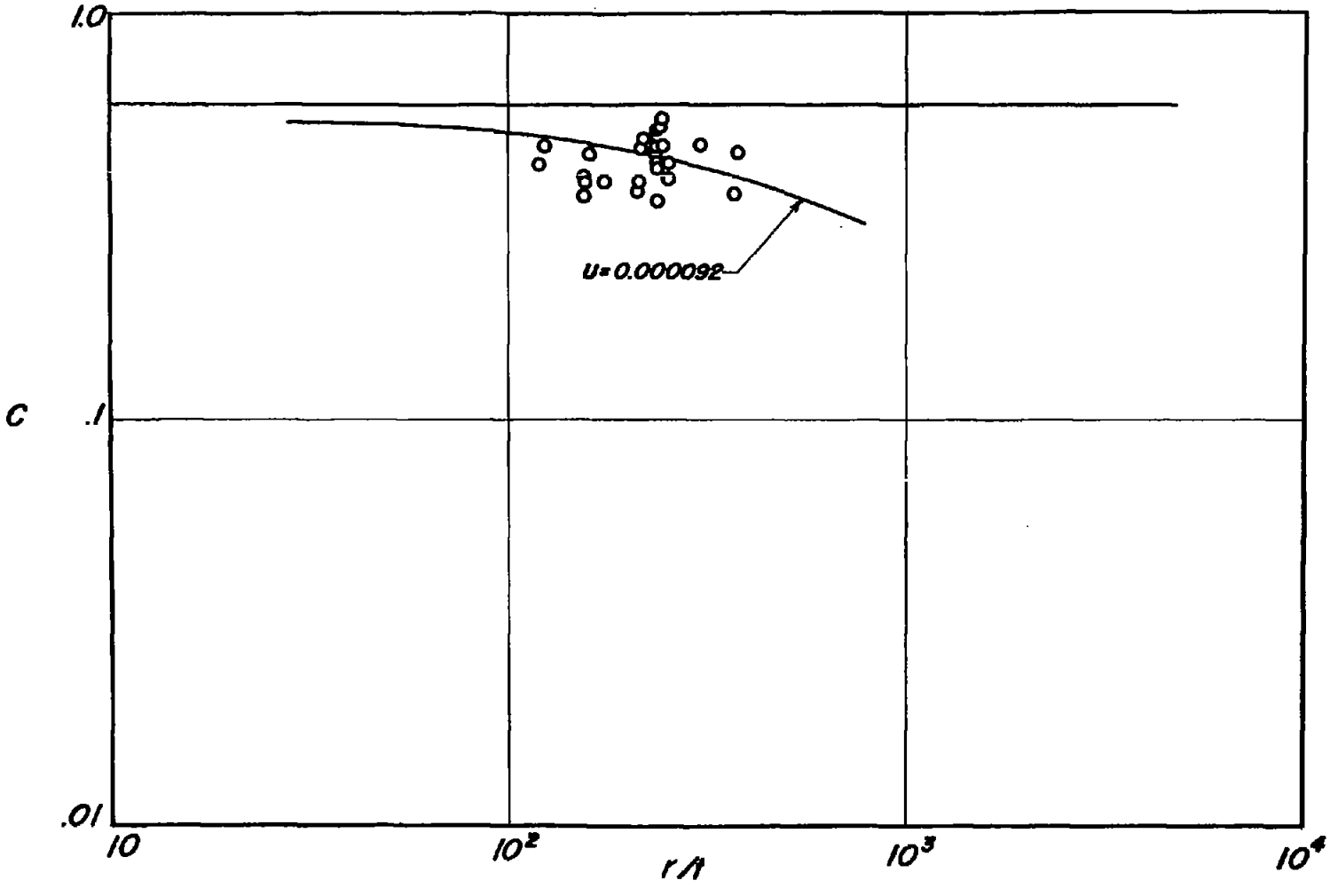

Figure 41.- Theoretical variation of C as a function of r/t for U = 0.000092 and comparison with elastic data of Schuette (ref. 65) for axially compressed curved plates.

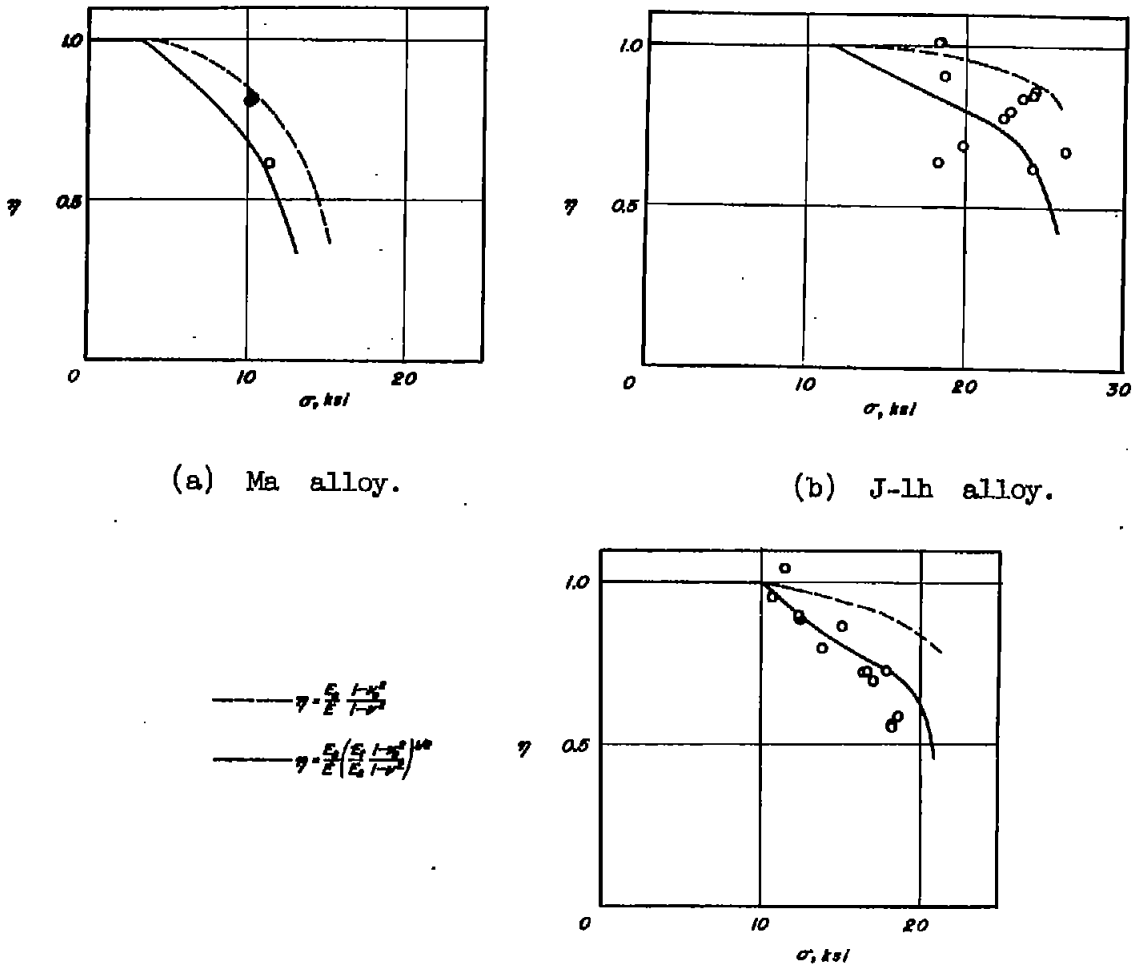

(a) Ma alloy.

(b) J-1h alloy.

(c) Mh Alloy.

Figure 42.- Comparison of test data for axially compressed curved plates with plasticity-reduction factor for axially compressed circular cylinders. Data for magnesium-alloy plates.

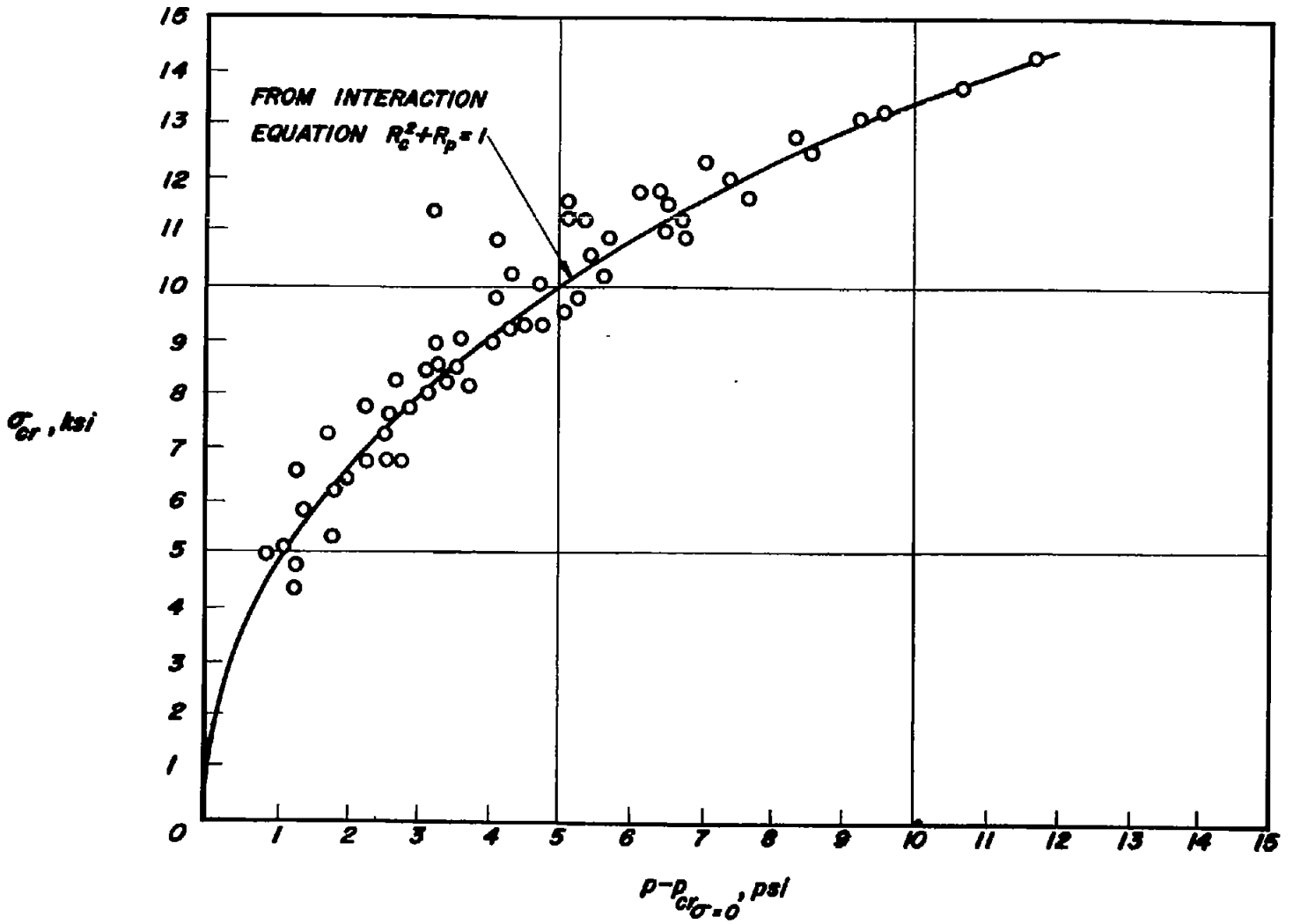

Figure 43.- Effect of internal pressure on axial-compressive-buckling stress of curved plates. Test data are from Rafel and Sandlin (ref. 70).

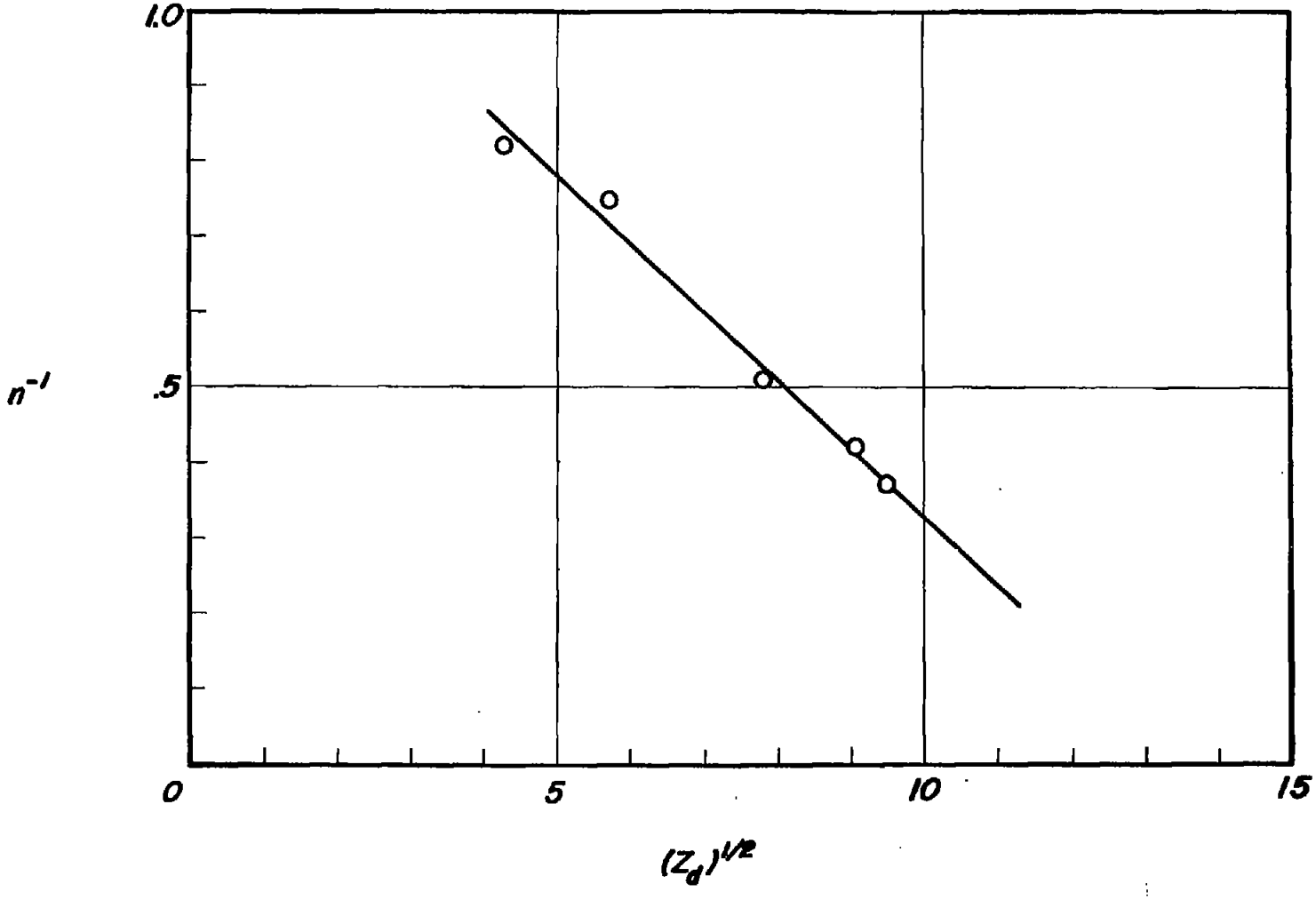

Figure 44.- Relation between number of buckles and Z_d for spherical plates under external pressure tested by Kaplan and Fung. Test points are for test data of Kaplan and Fung (ref. 75).

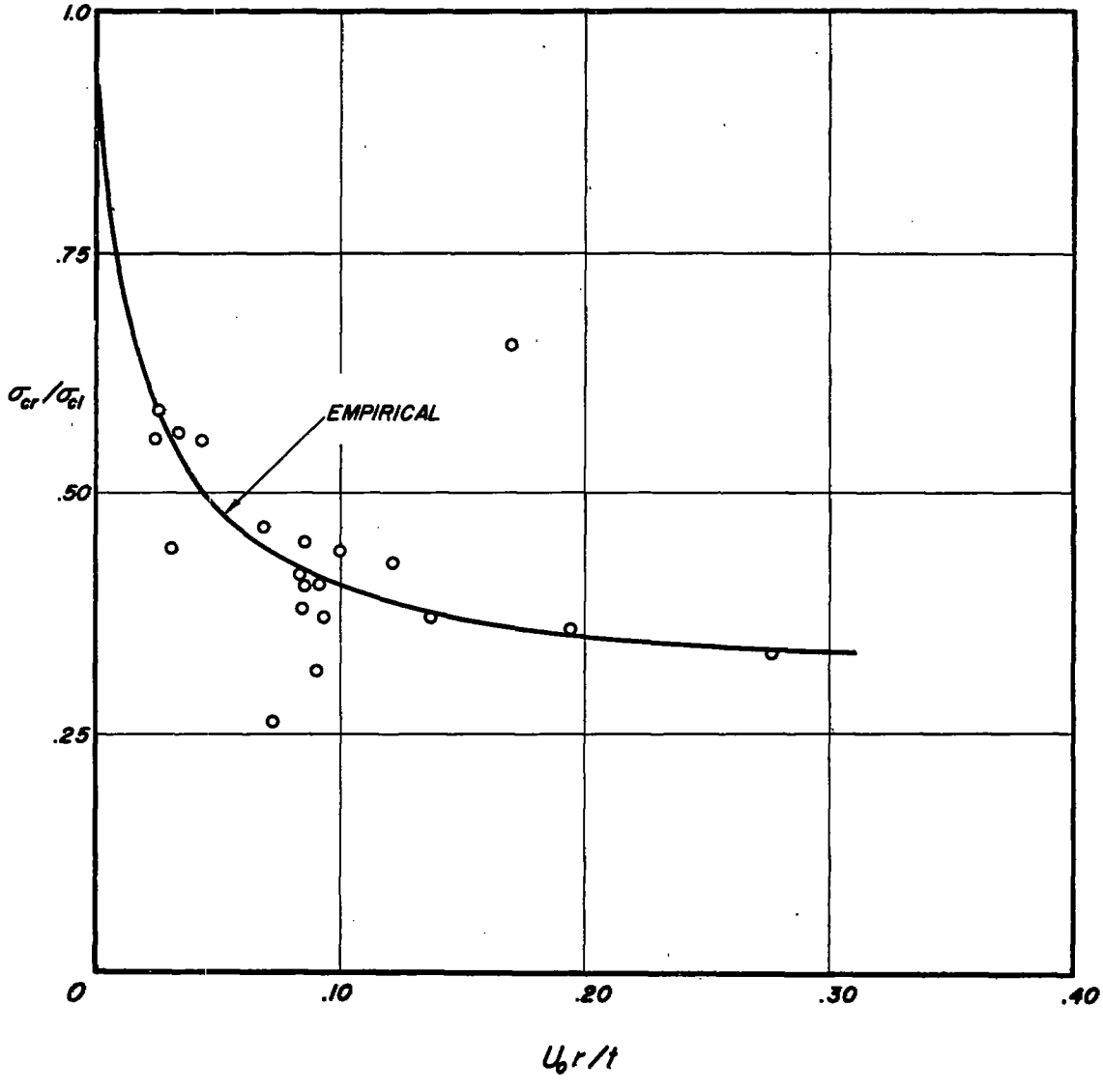

Figure 45.- Empirical curve fitted through spherical-plate test data of Kaplan and Fung (from ref. 75) to obtain relation between σ_{cr}/σ_{cl} and $U_o r/t$. $\sigma_{cl} = 0.6Et/r$.

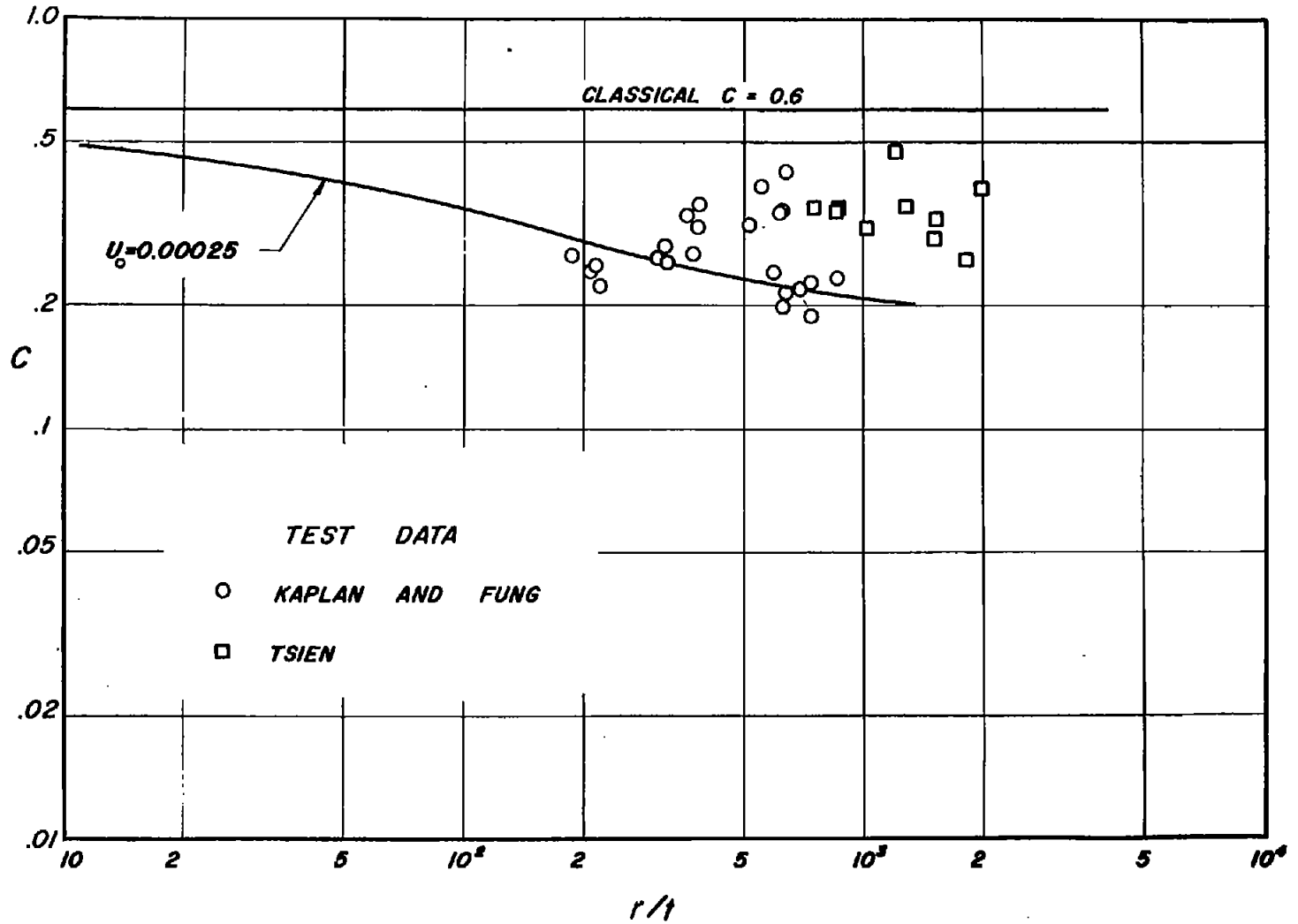

Figure 46.- C as a function of r/t derived from figure 45 using $U_o = 0.00025$. Test data of Kaplan and Fung (ref. 75) and of Tsien (ref. 12) shown for comparison.

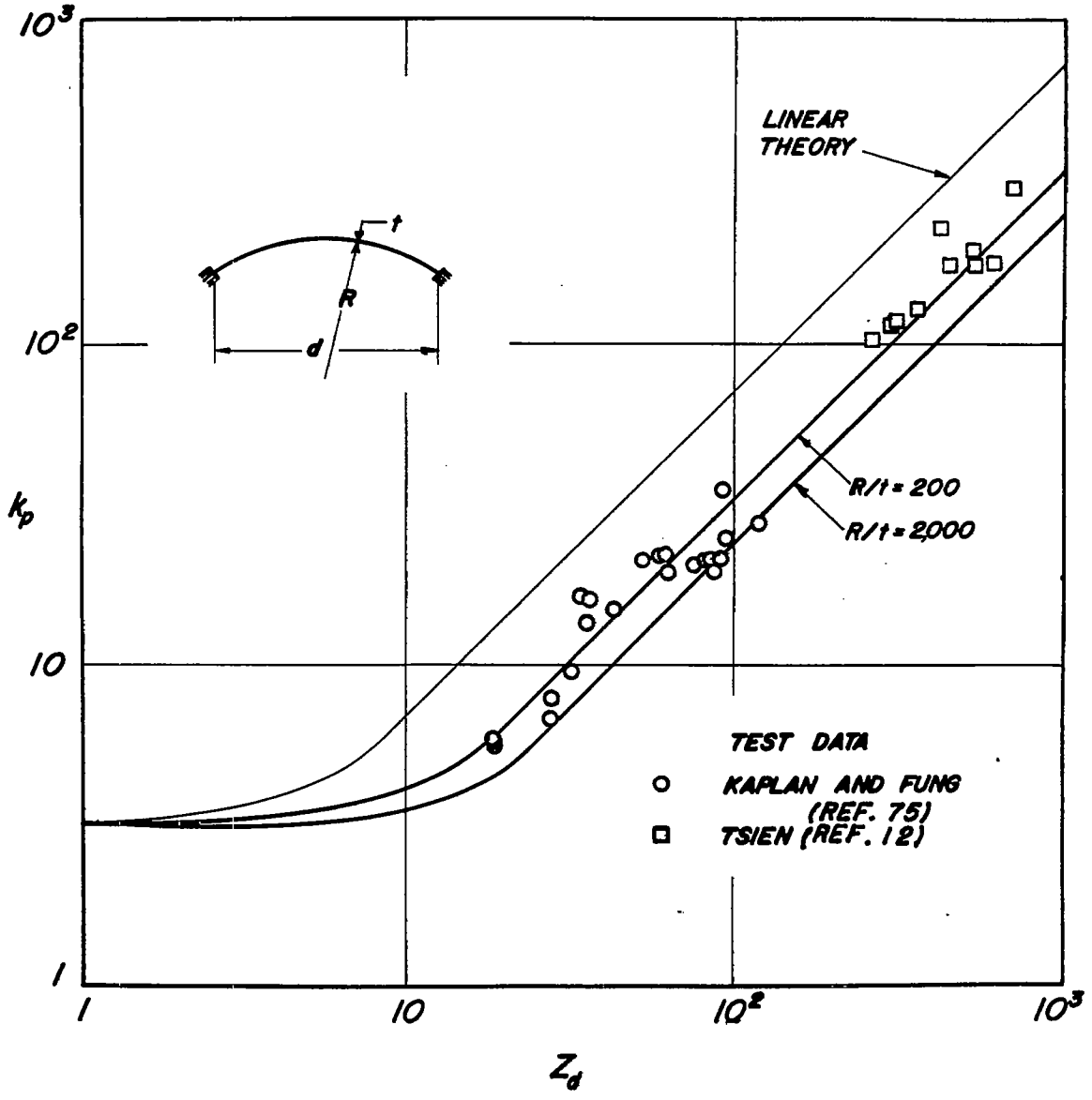

Figure 47.- Test data for spherical plates under external pressure compared with empirical theory. $\sigma_{cr} = \frac{k_p \pi^2 E}{12\left(1 - \nu_e^2\right)} \left(\frac{t}{d}\right)^2$.

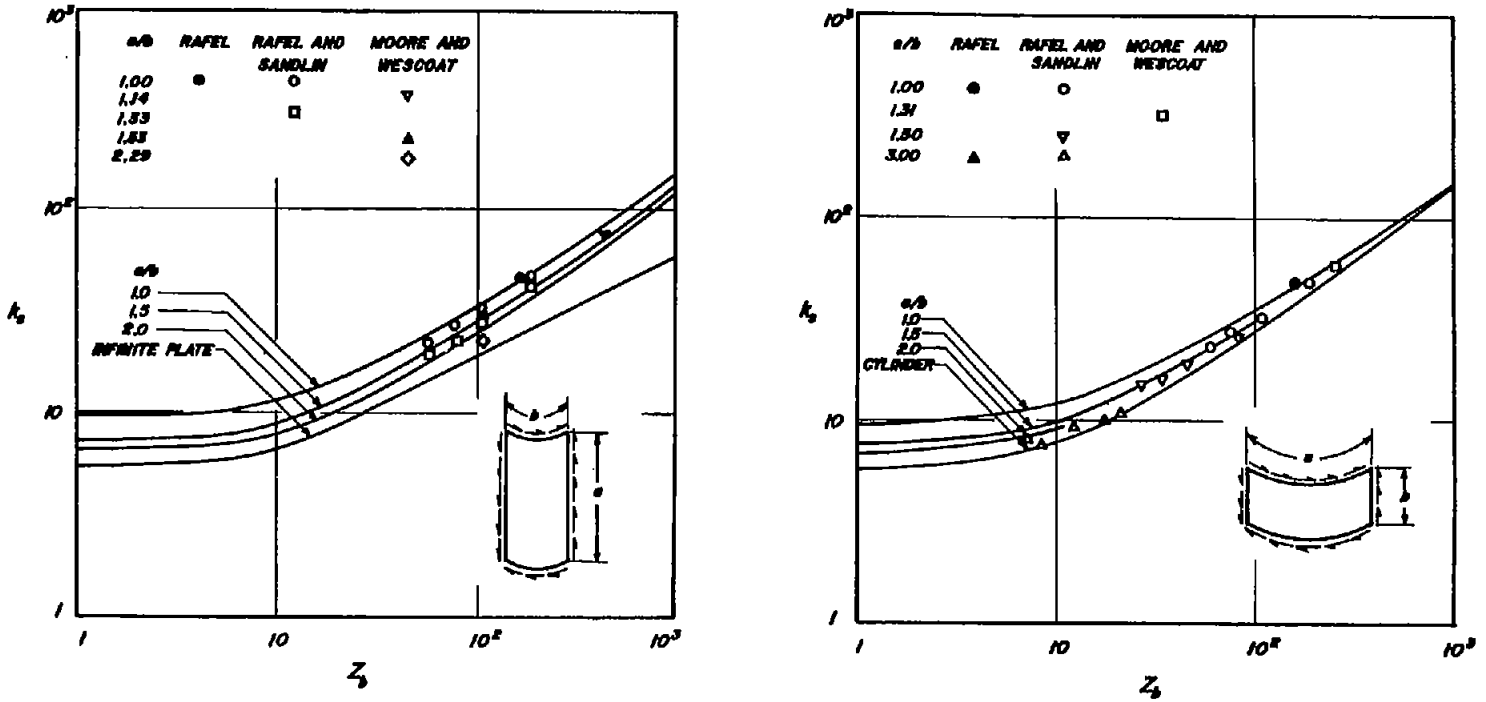

(a) Plates slightly affected by initial eccentricities. Test data from Rafel (ref. 80), Rafel and Sandlin (ref. 70), and Moore and Wescoat (ref. 41).

Figure 48.- Comparison of test data with theory for critical shear stress of simply supported curved plates affected by initial eccentricities. Theoretical curves from work of Batdorf, Stein, and Schildcrout (refs. 67, 78, and 79).

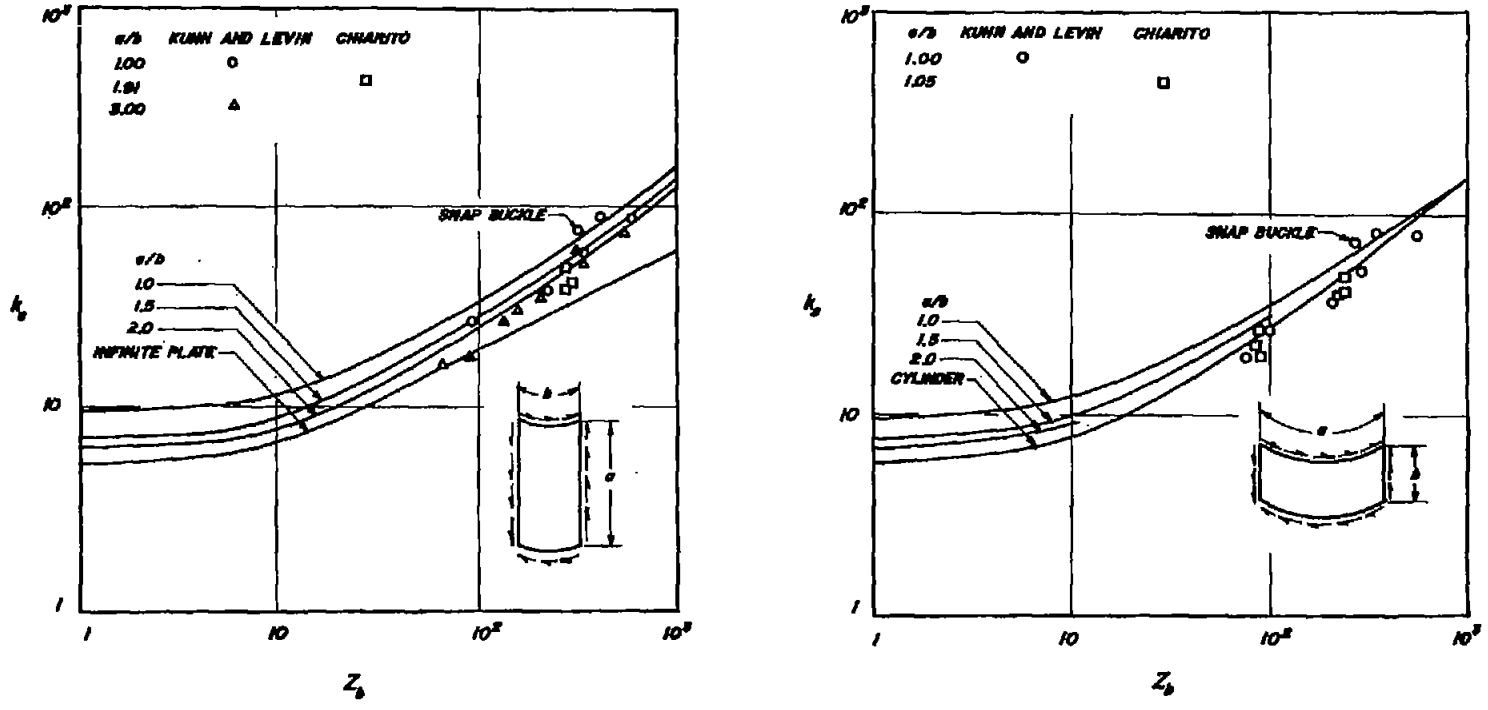

(b) Plates greatly affected by initial eccentricities. Test data from Kuhn and Levine (ref. 81) and Chiarito (ref. 82).

Figure 48.- Concluded.

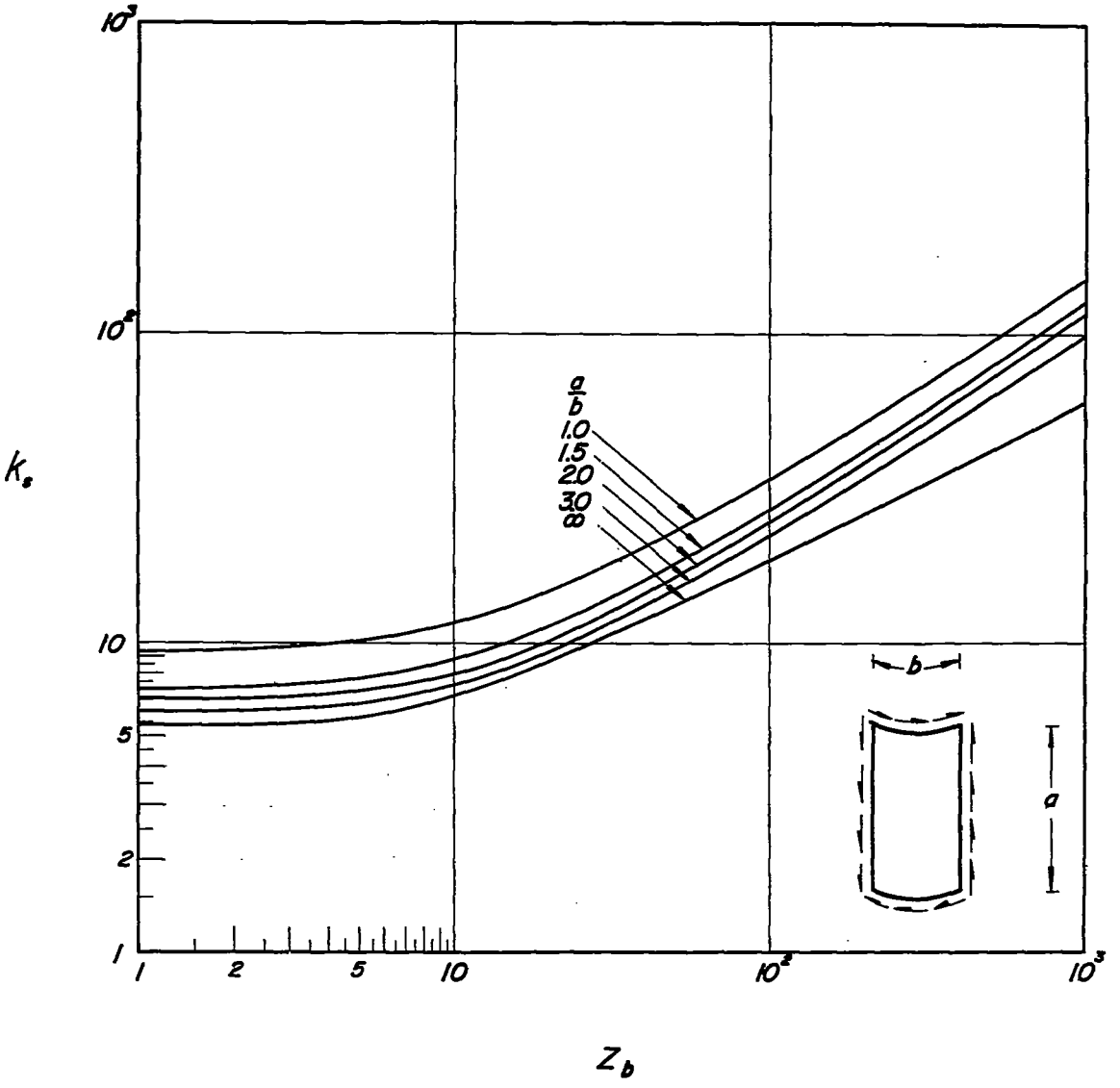

(a) Long simply supported plates.

Figure 49.- Shear buckling coefficients for various curved plates.

$$\tau_{cr} = \frac{k_s \pi^2 E}{12\left(1 - \nu_e^2\right)} \left(\frac{t}{b}\right)^2; \quad Z_b = \frac{b^2}{rt}\left(1 - \nu_e^2\right)^{1/2}.$$

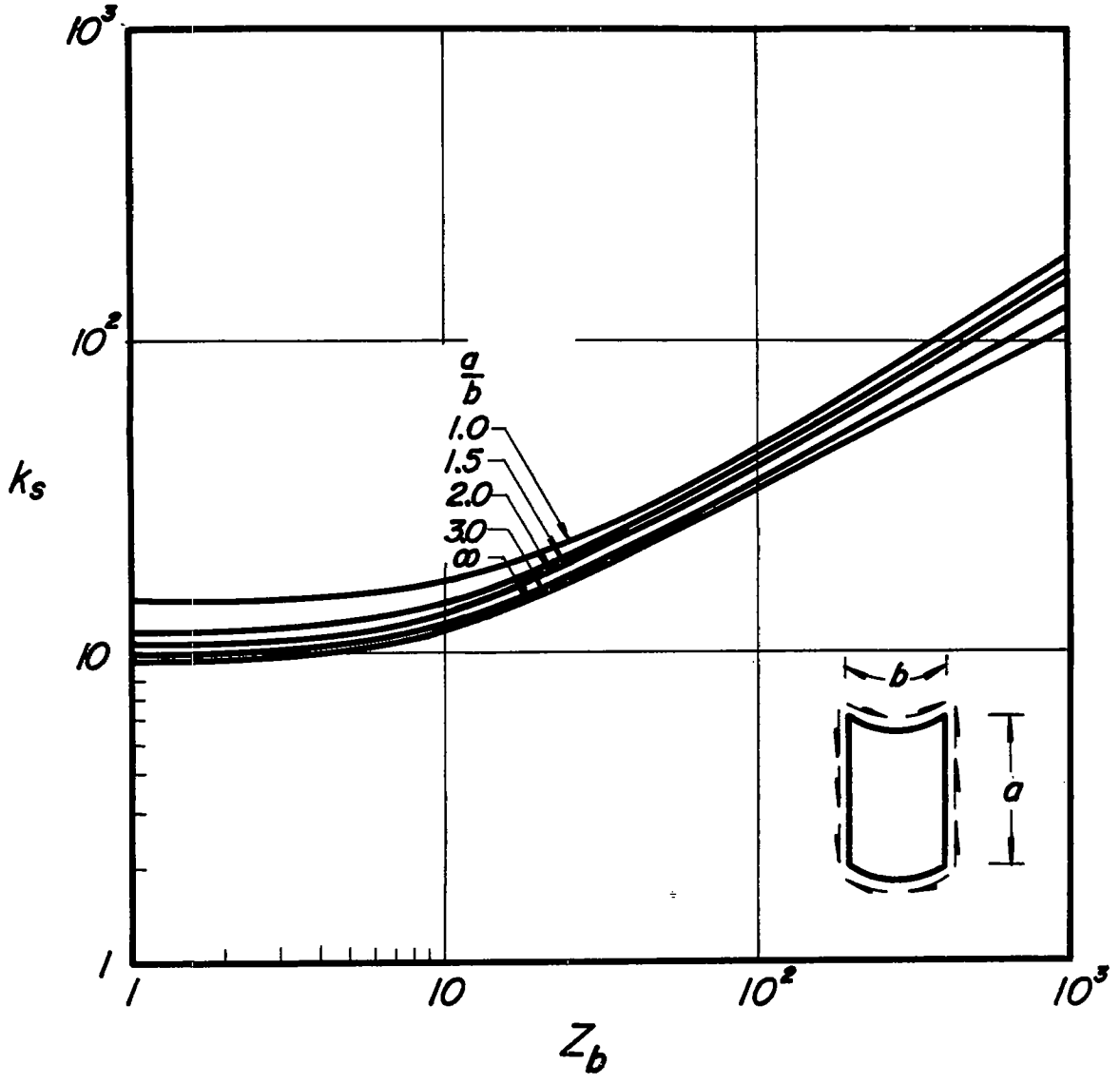

(b) Long clamped plates.

Figure 49.- Continued.

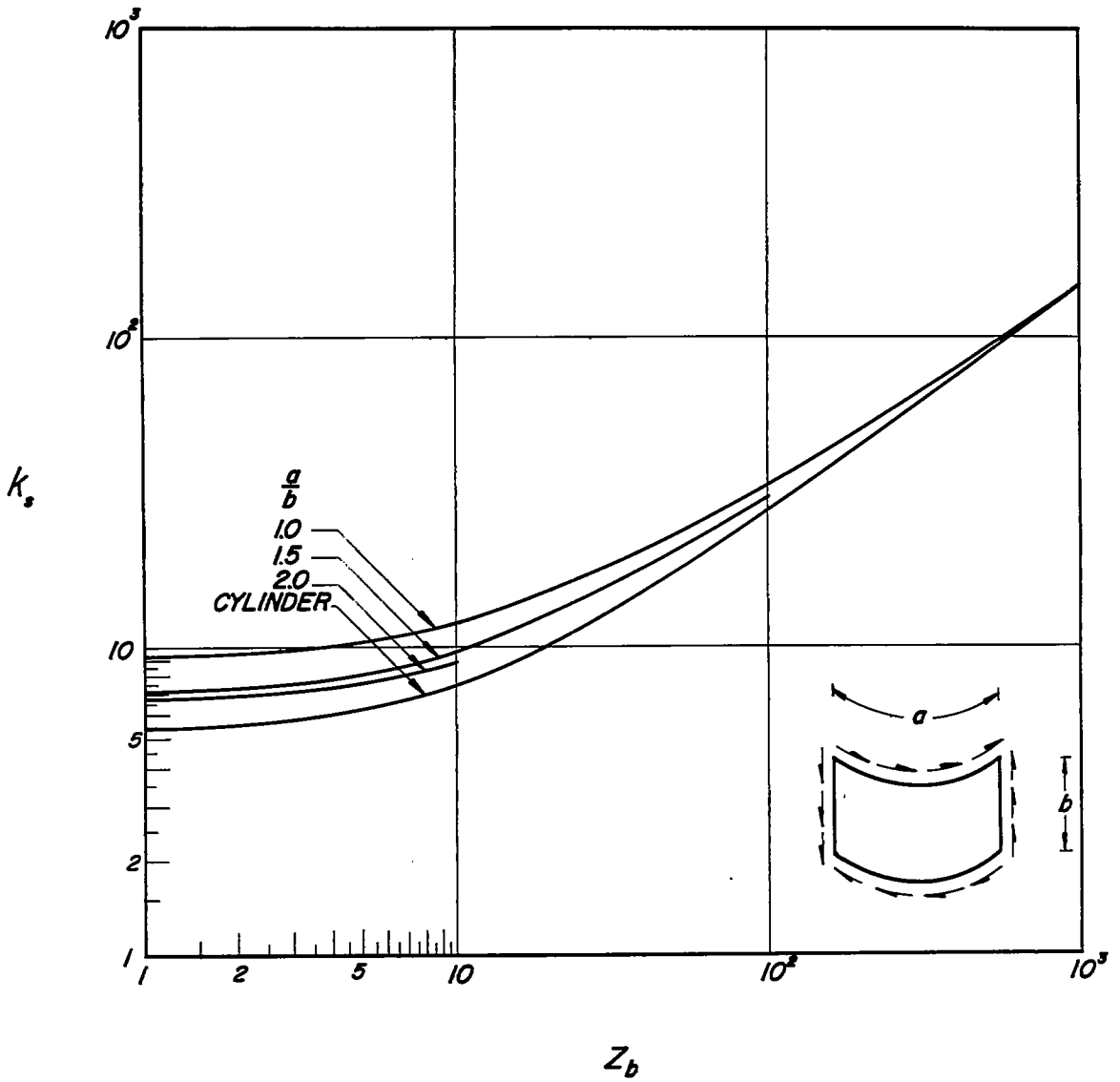

(c) Wide, simply supported plates.

Figure 49.- Continued.

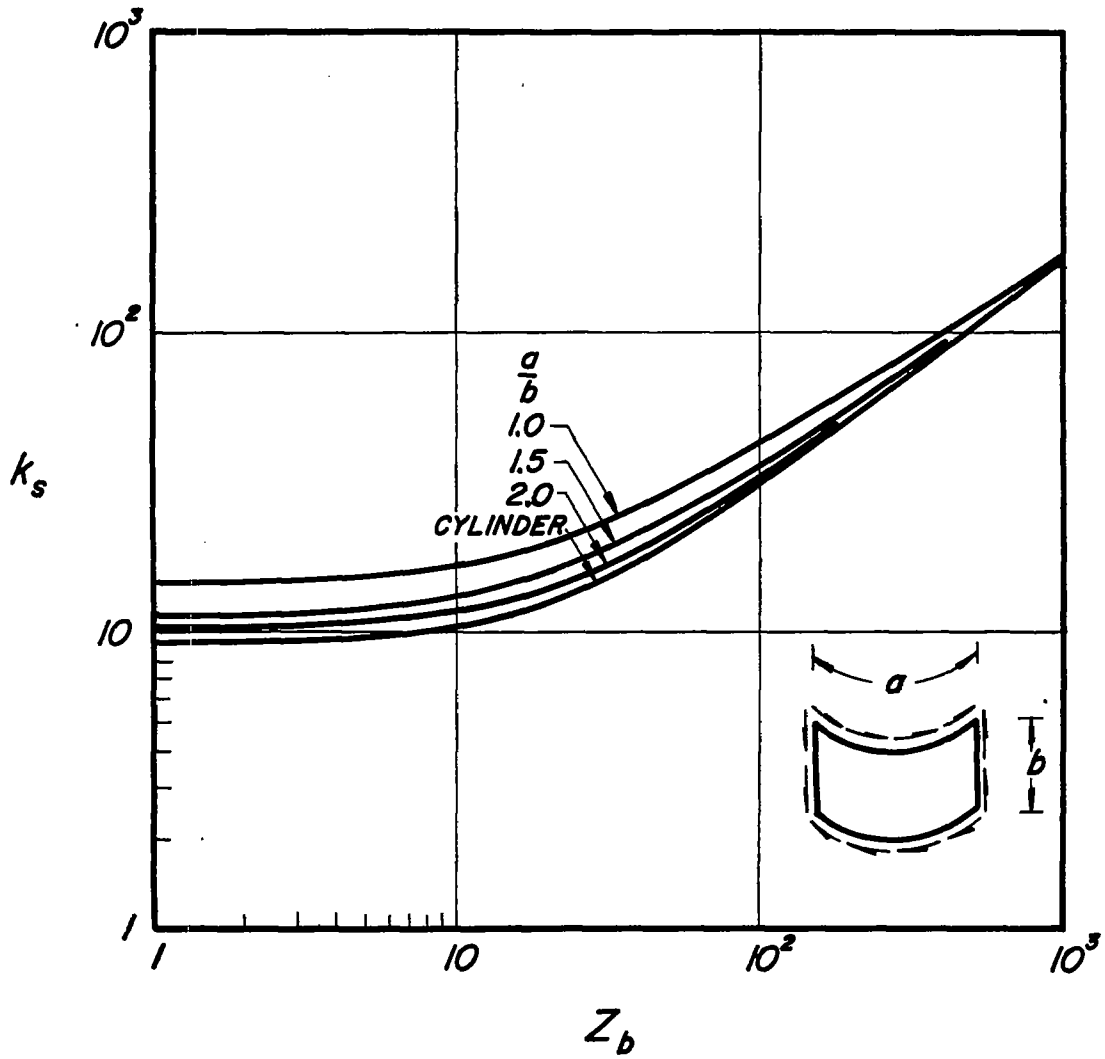

(d) Wide clamped plates.

Figure 49.- Concluded.

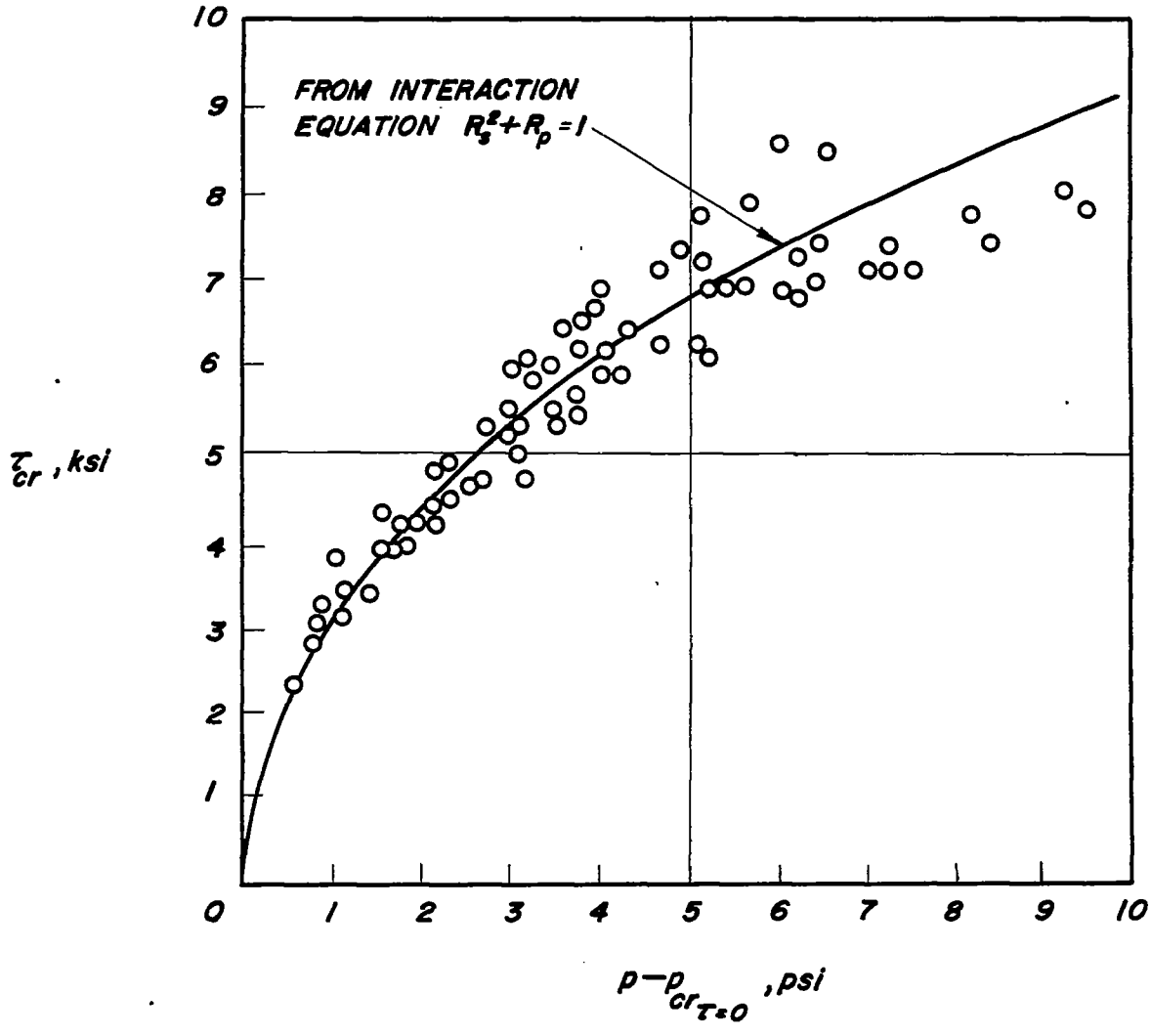

Figure 50.- Effect of internal pressure on buckling of curved plates in shear. Test data from Rafel and Sandlin (ref. 70).

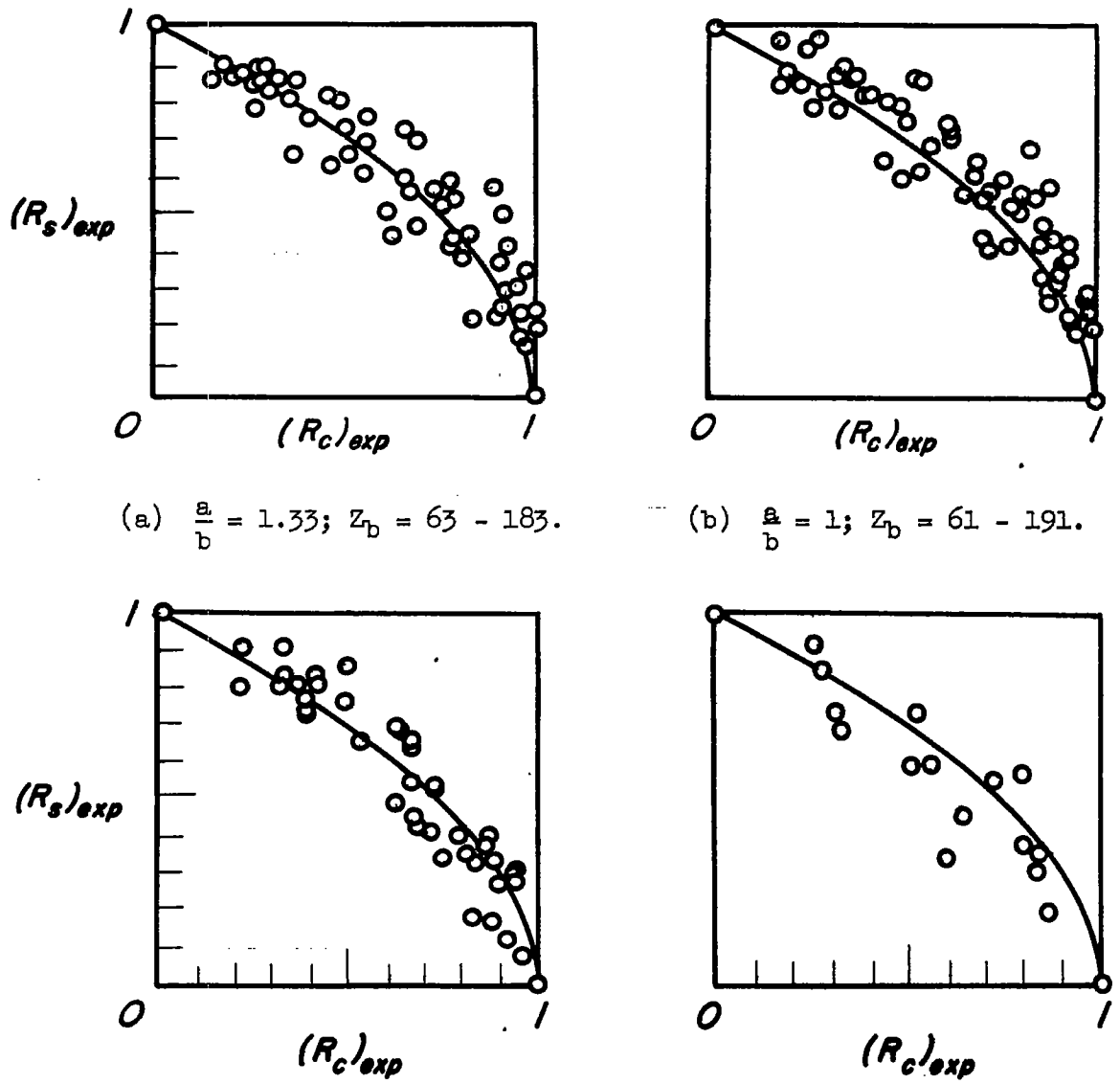

(a) $\frac{a}{b} = 1.33$; $Z_b = 63 - 183$.

(b) $\frac{a}{b} = 1$; $Z_b = 61 - 191$.

(c) $\frac{a}{b} = 1.5$; $Z_b = 27 - 85$.

(d) $\frac{a}{b} = 3$; $Z_b = 11 - 21$.

Figure 51.- Comparison of test data with parabolic interaction curves for simply supported, curved plates under combined shear and axial compression.